X-320-62-193

FINAL REPORT OF THE GODDARD SUMMER WORKSHOP PROGRAM IN SIMULATION OF SPACE ENVIRONMENT

COMPILED BY

ELIAS KLEIN

JUNE 15 TO SEPTEMBER 15, 1962

GODDARD SPACE FLIGHT CENTER

GREENBELT, MD.

FINAL REPORT OF

THE GODDARD SUMMER WORKSHOP PROGRAM IN

SIMULATION OF SPACE EN... MENT

JUNE 15 TO SEPTEMBER 15, 1962

"...We have an infinite amount to learn,
both from Nature and from each other. ..."
--Astronaut John Glenn

Sponsored by

TEST AND EVALUATION DIVISION
OFFICE OF TECHNICAL SERVICES

GODDARD SPACE FLIGHT CENTER
Greenbelt, Maryland

FOREWORD

The great challenge of our time is the exploration and conquest of outer space. To meet this challenge successfully, NASA must have help from educational institutions and from industrial organizations. Such a cooperative enterprise known as the Goddard Summer Workshop was conducted at this Center recently. The results obtained from this interesting experiment are summarized in this volume, which contains the joint efforts of university faculty teams and Goddard Staff members. Certain problems relating to simulation of space environments in the laboratory were investigated for the purpose of advancing our knowledge and understanding of the phenomena involved. Our greatest benefits are derived from this type of study partnership between academic researchers and the NASA family. The relationships are important to our future development and growth.

Harry J. Goett

PREFACE

The Goddard Summer Workshop was born of necessity; in twelve weeks it grew to be a source of hope and promise for a better understanding of space-environment simulation.

In a time of rapid change and unprecedented technology, it is vitally important to increase fundamental knowledge which applies to the reliability of spacecraft. This need for innovations in environmental testing was further emphasized last January by the prospects of Goddard's new space simulators. At that time, the NASA administrator, Dr. James E. Webb, happened to visit Goddard, and the discussion turned to the Buildings 7-10 complex with the diversity of equipments to be housed in them. The thought that by the end of 1962 this complex structure would constitute one of the most advanced facilities of this type in the world was gratifying to all who heard it expressed.

Then there was talk about utilizing these elaborate facilities with maximum effectiveness. What are the various approaches toward achieving such effectiveness? Does the Test and Evaluation Division staff have the time and the in-house capabilities to explore novel ways and means which would provide the applications of new scientific knowledge that is becoming available in this field? Who will specify the test procedures when the new installation is ready for use? The answers to all these questions indicated generally that the projected workload for the newly installed facility would require a large addition to the present staff, just to meet the test schedules. Hence, it appeared very unlikely that there would be available in the Division enough qualified personnel with sufficient time to undertake these studies in the near future. Nevertheless, it was fully recognized that the need for such investigations must be met, and, that prompt action was necessary.

Usually one turns first to a university for help in scientific research and development; that is why this exigency created the idea of a summer workshop. Immediately, attention was focussed upon the possibility of procuring for the summer a number of university professors and graduate students who are specialists in certain disciplines. The Washington area campuses as well as more distant universities were canvassed for available and suitable people. As a result of this search, the academic groups listed in this publication have contributed wholeheartedly to the efforts described herein.

Elias Klein

WORKSHOP PARTICIPANTS

FACULTY MEMBERS

GELLER, Murray, Dr.—Assistant Professor of Physics, Howard University, National Science Foundation, postdoctoral fellow, 1958-59, University of Paris.

GOODWIN, Ralph A., Dr.—Professor, Science Department, United States Naval Academy. Member of various honor and professional societies. Author of several technical publications in optics and spectroscopy.

GUTSCHE, Graham D., Dr.—Associate Professor, Science Department, United States Naval Academy. Member of various honor and professional societies. Author of several technical publications on nuclear reactions. Research experience in nuclear reactions and scattering, nuclear particle accelerators, and Raman spectroscopy.

SHERESHEFSKY, Judah L., Dr.—Professor and formerly Head of Department of Chemistry, Howard University. Specialist in physical chemistry and the physics and chemistry of surfaces. Author of many publications in liquid-vapor equilibrium in capillary and microscopic systems, adsorption of gases and monomolecular films. Exchange professor in chemical thermodynamics and surface chemistry at Israel Institute of Technology, Haifa, Israel. Group head in surface chemistry, Manhattan Project, Columbia University.

THEKAEKARA, Matthew P., Dr.—Professor and Head of Physics Department at Georgetown University. Member of numerous honor and scientific societies. Author of thirteen publications in physics and astrophysics.

WAIDELICH, Donald Long., Dr.—Professor of Electrical Engineering, University of Missouri. Formerly visiting professor at University of New South Wales, Kensington, NSW, Australia, on Fulbright grant. Member and fellow of numerous professional engineering and scientific societies. Many awards and listings in honor societies. Author of numerous scientific publications and co-author of book entitled "Transients in Electrical Circuits."

GRADUATE STUDENTS

CERKANOWICZ, Anthony E.—(Stevens Institute of Technology) Mechanical engineering degree. Working for master's degree in the heat-power field. Assistant instructor in thermodynamics.

CROOKS, J. B.—(Johns Hopkins University) Graduate student in chemical engineering. BES Johns Hopkins, 1962.

FRIEDMAN, Bruce—(Syracuse University) Graduate student and teaching assistant in physics. Working for Ph.D. in physics, New York State Regents Science Scholarship. BS Physics Brooklyn College 1960. Received MS from Syracuse University June 1962.

HASKELL, Donald F.—(University of Buffalo) Lecturer in engineering and completing work for Ph.D. at the University of Buffalo. BES Johns Hopkins, 1955; MES Johns Hopkins, 1957.

HILLIARD, John J.—(Catholic University) Graduate student and assistant in electrical engineering. BEE Catholic University, 1962.

JOHN, James E. A.—(University of Maryland) Graduate student and instructor in mechanical engineering, completing work for Ph.D. in mechanical engineering. BSE Princeton University, 1955; MSE Princeton University, 1956.

PICK, George—(Catholic University) Graduate student and instructor in mechanical engineering. Diploma engineering Technological University of Budapest, 1956. MME Catholic University 1962.

PITTMAN, Michael E.—(University of Maryland) Graduate fellow of NSF in theoretical physics, working for Ph.D. degree. BS Physics Loyola University, 1961.

SCHREIER, Stefan—(University of Maryland) Graduate student in aeronautical engineering and assistant instructor in mathematics. Ph.D. candidate in aeronautical engineering. BA Penn State University, 1953; MSE Princeton University, 1956.

CONTRACT CONSULTANTS

GREENSPON, Joshua, Dr.—Specialist in shell vibrations and structural excitation by high-intensity noise. Author of many publications in this field of dynamics.

STAMBERGER, Paul M., Dr.—Specialist in collidal phenomena and chemistry of rubber. Author of numerous scientific and technical publications.

WILSON, Christopher L., Dr.—Specialist in physical and organic chemical engineering. Author of 100 scientific publications on chemical research.

CONTENTS (Continued)

CONTENTS

PART I

SUMMER WORKSHOP EXPERIMENT

PART I

SUMMER WORKSHOP EXPERIMENT

INTRODUCTION

This final report is prepared to serve a twofold purpose. It provides a means for estimating the value of a summer workshop experiment conducted at Goddard within the confines of a test and evaluation activity. It also records the contributions to several aspects of simulation testing made by a group of university scientists during a twelve-week period. The substantive and tangible results obtained by the academic teams are adaptable to immediate uses and, therefore, may be assessed promptly as they supply needed information.

It is far more difficult to evaluate the long-range assets and benefits which this experiment could eventually bring to Goddard and NASA. To a considerable extent, the future progress of space science and technology depends upon the potential returns from such ventures. This was hopefully expressed by Dr. Goett, the Director of Goddard, at the opening session of the Summer Workshop:

> "I consider the Summer Workshop a very, very interesting experiment, and I re-emphasize that the main product and value of this experiment would hardly appear during the twelve weeks that you will be working here. The more important benefits should come later, from the familiarity with our problems which you people can pick up, and the degree to which you can focus your specialized talents on these problems. We are hopeful that you will be in a position to help us when we come to you. We hope also that as university teachers you will guide your brightest graduates to come here and help us do the job at NASA."

In a sense, this experimental adventure yielded a measure of satisfaction to all who were interested in its undertaking. The Summer Workshop made available some currently needed information for immediate application to environmental testing. It awakened, in the farseeing investigator of space-environment simulation, a keen desire to know why certain procedures and techniques are followed in the evaluation of payloads, and what new ideas could be developed which would prove more useful to test engineers.

The Summer Workshop may have raised more questions than it answered, but it also pointed the way to possible growth and progress for test and evaluation in space activities. Moreover, the Summer Workshop helped to establish fruitful relationships between

academic researchers and practical users of science and technology related to space exploration. Finally, it may be said that a worthwhile mission was accomplished if the academic groups have motivated a few of Goddard's engineers and technicians to learn more about their job and do it better than before.

The more tangible results of the Summer Workshop, produced by the several academic teams, are presented in the six subsequent parts of this report. Each of these parts start with a preliminary statement made at the opening session of the Summer Workshop, suggesting to the different university groups some desirable approaches that might be made toward the solution of a particular problem, and indicating the technical goal to be achieved. These preludes represent a few of Goddard's "voices of experience" requesting help in certain areas of research and development. The results contained and implied in the six articles may be considered as a cooperative response from university faculty members who for three months contributed to the analytical and experimental investigations of the tasks set before them.

GENERAL REMARKS

Success in modern space exploration demands that the flight vehicle be first carefully tested on the ground. Experience has indicated that such an evaluation tends to ensure the performance reliability of the spacecraft. In the words of Dr. Goett, Director of Goddard,

> "If we have learned anything at all during the past three years, we have learned that a tremendously important factor in the reliability of spacecraft is the thoroughness of the testing that is provided on the ground—and this building with all its equipment indicates the importance we place upon this particular part of the job."

Thus, ground testing has become a keystone in the reliability of spacecraft operation, and the need for preflight evaluation is now well recognized. But the procedures and techniques for simulating space environments are by no means fully established, because the knowledge of conditions out there is undergoing rapid changes, and new methods must constantly be devised to meet different situations. A vast amount of outer space information is swiftly unfolding. Consequently, the state-of-the-art in simulation testing is being transformed at an unprecedented rate. By constantly introducing these applied-science innovations into the test procedures, it is possible to do a more thorough job of ensuring spacecraft-performance reliability.

With the shortage of qualified technical manpower in government activities, e.g., Goddard, it is almost impossible for the same group of test and evaluation engineers to carry out all the phases involved in advancing the technology of simulation testing. The background experience and unique skills possessed by the Goddard test group are vital to

the accomplishment of today's routine testing, and must be devoted to it. But the additional responsibilities of keeping pace with new developments in this field, and at the same time putting novel ideas into practical use for ground testing of spacecraft, are beyond the capabilities of this or any other engineering group similarly situated. Present-day simulation involves many disciplines; to integrate the diverse applications of science into a comprehensive set of test procedures requires not only ample time, but also new skills and versatility in several fields. Therefore, to take advantage of the new tools which are becoming available and to utilize them in this effort, it becomes necessary to supplement the available manpower with other professional talents so as to enable GSFC to carry out the job effectively.

There are several ways of procuring the required technical assistance in this effort. It is possible to increase the staff by a few carefully selected specialists who could supply the immediate and future needs of this activity. Such an approach, assuming the procurement of qualified people, would benefit the overall spacecraft testing, and would serve the best interest of the government in its long-range objective. But considerations of manpower ceilings, space limitations, and other temporary handicaps to Federal in-house research preclude the immediate activation of such a program. For prompt action, therefore, other approaches to this problem should be explored, even though the prospects for much greater support of Federal in-house research and development are favorably regarded. In time, the situation will be remedied, because it is recognized that in-house research is likely to add to the government activity's experience and prestige with possible breakthroughs. It builds competence and scientific know-how among its people; it enriches in-house talents and capabilities, and makes for growth and progress of the entire organization.

Still, the job at hand requires immediate technical assistance, and it must be found outside the Center. A common procedure is to contract out government research and development work, and it should be feasible in this case. Perhaps a competent industrial organization would undertake to carry out, jointly with the testing staff on the premises, the different phases of the needed investigations. Another possibility is to invite individual experts or specialists in the technical areas under consideration to work with the permanent staff on the existing facilities to obtain the desired results. To be sure, the effectiveness of such arrangements depends upon careful planning for the use of test equipment and upon precise timing of personnel availabilities; otherwise, the primary objective of the investigation might be vitiated. Another factor which may influence the value of the overall study is the time spent in discussing the various aspects of the investigation and the conditions under which the interchange of ideas must take place. It is rather difficult to assimilate a relationship between theory and experiment while the pressure is on to test a satellite which has an early target date to meet.

In other words, the hiring of consultants and experts to help expand certain phases of engineering and applied science in the test program can be very effective. In general,

however, the busy permanent staff gains little from this temporary relationship, in terms of research experience and training for the future. Unless there is a realistic interchange of pertinent information, and both groups participate in the effort on a mutually contributing basis, the residual benefits to the permanent staff and the government are evanescent in nature. From the long-range viewpoint, the hiring of consultants and experts would prove a huge success if, besides achieving high standards in the current evaluations, the permanent staff gained in its basic understanding of the phenomena involved so as to be encouraged and stimulated to investigate on its own the environmental simulation of outer space.

ORIGIN OF THE SUMMER WORKSHOP

During the past few years fresh information has become available on space-environment simulation. This information is based upon new scientific knowledge of outer space conditions, which has been accumulating rapidly. In attempting to adapt some of these novel ideas to existing test procedures, the Test and Evaluation Division engineers have found that, before certain technological innovations can be put to practical use, they must be subjected to considerable scientific investigation.

For example, in testing the thermal equilibrium of a satellite whose coating does not absorb spectral energy uniformly, it is important that the solar-simulator spectrum should match that of the sun. Hence, before a rational evaluation of this satellite's thermal balance can be made, a careful investigation is necessary to find whether the artificial source is similar to the spectral distribution of the sun. This effort entails an extensive research in spectroscopy, a large departure from the normal function of test and evaluation engineers; yet, many such problems have arisen during the past three years. Solutions to these problems would provide more effective procedures for assessing the reliability of spacecraft, and would also help establish criteria and standards for operating the many varieties of test facilities.

In their desire to update the requirements for reliable spacecraft in orbit, the test and evaluation groups have attempted in spite of obstacles to resolve some of these problems to meet modern testing needs. Several advanced development projects were undertaken in-house, and enough exploratory work was done to indicate the phases of the problems which require attention. Although these efforts, interrupted by high-priority commitments, produced few substantive results, they provided by virtue of experience a number of particular topics which should be investigated promptly. These are:

- Solar Simulation and Albedo Effect on Spacecraft
- Heat Transfer and Cryogenic Pumping in Vacuum Technology
- Corona and Discharge Effects Inside Spacecraft at Low External Pressure
- Magnetic Simulation
- Response of Vehicle Structures to Acoustic Fields

- Relating Damage and Reliability to Environmental Data

Last January the Test and Evaluation Division concluded, that, under existing conditions, there is little probability of conducting in-house one or more of these studies to achieve definitive results; that the solutions to these problems are essential; and that technical assistance for these investigations should be procured from outside Goddard as soon as convenient. A search for qualified scientists was instituted at that time. The competence and talents in the particular disciplines associated with the above topics were not then readily available to assume these studies.

After due consideration of the space availability at Goddard and the timing of the various local personnel who might be involved in this effort, it was decided to tackle the job with university faculty and graduate students. These academic people are usually free for research work during the summer months, about June 15 to September 15, and the Test and Evaluation Division expected to have the facilities in Building 7-10 ready for this purpose by June. That is the immediate practical reason for the Summer Workshop experiment. There is another. It stems from the firm belief that the boundaries of outer space knowledge will be extended by the basic research of academic institutions, and that NASA's greatest benefits will come from its close relationships with universities.

OBJECTIVES AND ORGANIZATION

A primary objective of the Summer Workshop has been to develop methods and techniques for effective utilization of the new facilities in Buildings 7-10. In order to accomplish all that is implied in this statement, full advantage must be taken of the progress which has been made in adapting basic science to test and evaluation engineering. Another aim has been to interest and indoctrinate faculty members from different universities in Goddard's current and future simulation problems. It is believed that goals such as these are attained through a common understanding of the problems involved and the combined efforts of academic scientists and practical engineers. The Summer Workshop was set up with this purpose in mind.

A plan to relate these objectives to the six topics listed on page 1-4 was begun last January, when the Test and Evaluation Division was still huddled in Building 4. From that viewpoint, the prospects of Building 7 becoming available in spring of 1962 seemed most promising, for in this fine structure the Summer Workshop could pursue its studies in a creative atmosphere with ample working space and adequate facilities. At that time, however, the Ad Hoc Committee in charge of this plan urgently needed competent personnel who might use this exquisite laboratory for investigating the existing problems. The plan was to obtain for the summer five or six professors who would act as principal investigators in the different technical areas mentioned, and who could team up with one or more graduate students to tackle a specific problem. This group of university professors, who are specialists in definite scientific disciplines and are experienced in the conduct

of research work, represented the vital part of the Summer Workshop program. It was Goddard's good fortune to be able to procure capable and cooperative professors as well as graduate students. Their wholesome attitudes and unstinting efforts together with the actual results they achieved this summer should stimulate greater accomplishments among those who undertake programs of this type in the future.

Organizational planning and preparation were most important in making effective and optimum use of the time during which the academic groups were to be at Goddard. It was essential to anticipate many of their needs and wants in advance of their arrival in Building 7. First of all, by the end of May, there was hardly a doubt in the mind of any prospective member of the Summer Workshop as to which technical area he would be investigating. The team groupings were arranged either by correspondence, by personal interviews, or by telephone conversation. And it is gratifying to state that the teams, by and large, remained intact and functioned very well as units, even though a large majority of the individuals had not met before coming to Goddard. Then, there were ready for the different teams as they arrived, stacks of pertinent technical material in each of the various subjects to serve as a start for background reading. Thus, every man upon arrival was aware of the general scientific area with which he would be concerned, he was given several publications in his field of study to acquaint him with the problem; and he was furnished a comfortable desk at which to begin his summer's work without loss of time and without feeling at loose ends on a new job.

Another means which proved most helpful to the personnel of the Summer Workshop was the procedure for obtaining urgently needed reference materials for their use. In order to overcome the usual delays in normal government inter-library loans (from one to eight weeks, or more, to obtain a book or a periodical), a more direct approach to the different libraries was pursued in the case of the Workshop project. Inquiry was made directly to the several libraries of the local research institutions as to the availability of the particular book or journal that was needed. If the required reference material was on hand and could be loaned for a couple of weeks, the book was on the desk of the person who asked for it within two days from the date of the request. Indeed, this exceptional service which the Summer Workshop personnel enjoyed was due to a rare set of circumstances, and proper advantage was taken of them. The fact remains, however, that the Workshop efforts were tremendously expedited by this approach; it is estimated that about 15 man-weeks in the overall period were saved by handling the book situation in this manner.

CONCLUSIONS AND RECOMMENDATIONS

The Goddard Summer Workshop experiment has provided some interesting conclusions. To begin with, it has been clearly established that a coordinated interchange of technical information between academic scientists and Goddard staff members can be most valuable to the solution of immediate space problems as well as to the accomplishments

of long-range projects. This conclusion is based on the interest shown by Goddard personnel in the Workshop program and in its technical achievements. Also the comments received, oral and written, indicate that a far better understanding with the university groups has been effected by virtue of the communication channels which have resulted from this experiment. In addition, there is reason to believe that the favorable appraisal of the workshop effort by the Goddard technical people as well as by the visiting participants represents an integrated critical assessment of the situation as a whole. The close association between the academic groups and the permanent Goddard staff provided a procedural flexibility that yielded desired results in less time than ordinarily would be required by contractual means. It is believed that this general environment stimulated new ideas and original thinking.

Now we come to the research findings of the university teams. Some of these are practical and easily recognized as being worthwhile contributions to our problems, while others have given us a good start and are most promising for the future. The workshop studies not only have produced results but they have also encouraged a research spirit and a higher morale factor in Goddard personnel toward scientific approaches and efforts. Because of the Summer Workshop activities here at Goddard, it may be concluded that:

1. At least three of the workshop reports have been or are expected to be submitted for publication in standard scientific journals, and will probably be issued as NASA technical notes.

2. Two local professors associated with the workshop are continuing one or two days per week at Goddard on certain phases of their respective projects. These investigations are conducted in cooperation with and under the control of the Goddard technical staff.

3. Three of the workshop professors have already submitted, or are about to submit, unsolicited proposals to the Director of Grants and Research Contracts, NASA, on certain follow-up studies of the Summer Workshop which they wish to undertake.

4. A number of the graduate students who participated in the various Summer Workshop projects have expressed an interest in coming to Goddard as permanent employees, after completing their work for advanced degrees.

5. One of the investigations carried through this summer was sufficiently definitive and practical to warrant a patent application by Goddard on the idea, product, and technique developed by Messrs. John and Hilliard.

It is therefore recommended that:

1. Plans should be initiated at once to institute a Summer Workshop for the 1963 season.

2. The following improvements should be incorporated in the 1963 Workshop on the basis of experience gained in the 1962 Workshop:

- Start planning and contacting candidates at an early date, preferably before December 1962
- Hold preliminary conferences with team leaders in early spring to discuss programs and arrive at decisions on technical approaches
- Determine what equipment is needed and take timely action to provide it
- Arrange rapid library services to supply references with minimum delay after receipt of requests
- Provide a Goddard permanent staff member to participate full-time with each team
- Solicit and encourage full participation of the Directorates of Tracking and Data Systems and of Space Sciences and Satellite Applications in all scientific phases of the Summer Workshop.

PART II

SOLAR SIMULATION

CONTENTS

ILLUSTRATIONS

TABLES

CONTENTS (Continued)

PART II

SOLAR SIMULATION

PRELIMINARY STATEMENT

(By Milton Schach, Thermal Systems Branch, Spacecraft Technology Division, GSFC)

The general objective of any kind of space simulation is to provide a means for observing the performance of devices or systems on the ground in the laboratory. The space environment (i.e., the atmosphere, the particle flux, and the electromagnetic radiation) is extremely complex and is not readily simulated. Gas composition, particle-energy distribution, and spectral-energy distribution are extremely difficult to simulate, singly or simultaneously.

What are the specific areas which generate an interest in solar simulation? First of all, radiation from the sun is a principal factor in the thermal equilibrium of satellites; solar radiation constitutes at least 75 percent of the average energy incident on the spacecraft. Second, solar radiation is a source of energy for a variety of solar converters, photovoltaic devices, thermoelectric devices, and thermionic devices. Third, the sun is responsible for a variety of photophysical and photochemical effects, which are of interest in the study of materials properties, principally the degradation of materials under solar radiation. The simulation of the ultraviolet spectrum is attracting considerable attention. In addition, solar energy may be used as a means of active temperature control by taking advantage of certain of these photochemical and photophysical properties.

The Summer Workshop will be concerned chiefly with solar radiation and its influence on spacecraft thermal equilibrium. Let us take a quick look at some relevant properties of solar radiation which are reasonably well known.

In the first place, if we talk about solar radiation in the vicinity of the earth, we are talking about an energy of the order of about 130 watts per square foot on a surface normal to the sun's rays. This energy is spread over a spectrum that goes to infinity in both directions. Happily for those of us who are concerned with thermal equilibrium, little more than 1 percent of this energy lies below .3 of a micron in wavelength and slightly more than 3 percent lies above 3 microns in wavelength.

I should point out that the regions both above and below the limits cited are of vital interest in understanding the structure of the sun, and they may be extremely important in understanding materials degradation.

The solar radiation may be described by comparing it to that of a blackbody. In order to match the energy within the bandwidth—from 0.3 to 3 microns—the best fitting blackbody curve would correspond to a temperature of 5800°K.

This energy is remarkably stable, at least in the region with which we are concerned. There is relatively small variation in time. (In practice, there is a variation for those of us who are concerned with earth satellites; namely, the variation that results when the earth moves around in its elliptic orbit. The changing earth–sun distances produces a variation of ±3 percent in the 130 watts during the year.)

Summing up, then, solar radiation at any given distance is uniform in intensity. It is almost parallel, having an angle of collimation of less than one-half degree, and its spectral-intensity distribution curve looks roughly like that of a blackbody at 5800°K.

The external energy sources which contribute to the thermal balance of a spacecraft are two, in addition to direct sunlight: (1) the reflected sunshine that the earth directs towards a satellite, and (2) the earth-emitted radiation. The reflected radiation varies rather widely in intensity, as it is a function of the orbital position and height above the earth's surface. As a result, there may be instantaneous inputs of reflected solar energy up to 50 percent of the direct solar energy. These inputs may be as small as zero when the satellite is over the dark side of the earth. The earth's emitted radiation, too, is a variable quantity, which can achieve values up to 15 percent of the direct solar radiation. The reflected solar energy and earth-emitted energy drop to less than 2 percent of the incident solar energy at a height of 20,000 miles above the earth's surface.

Finally, there is the internal-energy dissipation which must be considered. Most of the spacecraft launched to date dissipate less than 100 watts internally. This source is small compared to solar radiation, but is significant in effect.

What is required in the way of solar simulation for thermal design and for our thermal evaluation studies? First of all, we'd like a source with a good match to the solar spectrum. We would like the radiation to be parallel and uniform over the spacecraft volume. In addition, there are spurious radiation sources which arise as a result of the simulated space geometry, in particular the inter-reflection between the walls of the chamber, the satellite, and the optical elements of the simulator. These spurious sources need to be minimized.

Let us turn briefly to spectral match. The degree of closeness that is required is a function of the optical properties and geometry of the surface of interest. Thus, for example, by using a homogeneous flat plate, the need for spectral match can be eliminated entirely. The objective of simulation is to make certain that the spacecraft will absorb–on every unit area–exactly the same amount of energy in the laboratory as it will in orbit. This requirement can be met by a uniform collimated source of the proper intensity.

It turns out, however, that as soon as simulation is attempted for any elaborate spacecraft whose surface properties vary, this kind of simulation proves quickly inadequate, so that it becomes necessary to achieve an improved spectral match.

The collimation requirement is important, again depending upon the complexity of the satellite. If there is poor collimation–that is to say, if there is divergent sunshine–then parts of the spacecraft which would not normally be illuminated are indeed illuminated, and, conversely, some parts of the satellite will receive less illumination than from a collimated source.

Uniformity is important because of the relationship between incident solar energy and the temperature. It may be worth while to take a moment to indicate what the effects of simulation errors are. All the factors—spectral match, collimation, uniformity, the inter-reflection between the satellites and the simulating source and the walls—act to produce a certain absorbed energy at the surface of the spacecraft. If, for any reason, the energy differs from the true absorbed solar energy, then there is an error in spacecraft temperature. As an example, consider an element of area which is in equilibrium with solar radiation. The equation for equilibrium shows that the temperature varies as the one-fourth power of the absorbed energy. For a surface in equilibrium near room temperature, an error of 10 percent in absorbed energy would result in a maximum temperature uncertainty of 7.5° C.

One general comment may illustrate a point made earlier. Solar simulation is an area that involves more than one discipline; partly because of this, it is an area in which progress is slow. It requires a knowledge of the spectrum of gases and other radiation sources. It requires a knowledge of optical systems. It requires a knowledge of a variety of technologies that go along with these disciplines.

It is therefore our hope that this group can in some measure contribute suggestions and ideas to implementing this technology.

Thank you.

SPECTRAL ENERGY DISTRIBUTION OF A MERCURY–XENON LAMP

by

M. P. Thekaekara

ABSTRACT

This report presents the results of the work done by the Summer Workshop Team A*, Test and Evaluation Division, Goddard Space Flight Center.

A critical analysis has been made of the problems of solar simulation for studying the thermal balance of spacecraft, in particular of the spectral-energy distribution of the high-pressure mercury-xenon arc as compared to that of solar radiation in outer space. The results of previous investigators have been analyzed. A technique has been developed for precision measurement of intensity, using a high-dispersion, high-resolution monochromator. The spectral characteristics of a 2.5-kw mercury-xenon lamp have been studied in the visible region. The data are presented in a series of charts and tables. The applicability of mercury-xenon arcs for solar simulation has been examined with the aid of the relevant experimental data.

INTRODUCTION

The GSFC spacecraft programs at present are the earth-orbiting scientific payloads, in particular, the Nimbus, the Orbiting Geophysical Observatory, and the Orbiting Astronomical Observatory. To test them prior to launching, a space-environment simulator is being constructed. The radiation in the simulator will be that of 127 mercury-xenon lamps. Many interesting and urgent problems are connected with solar simulation, such as the requirements of energy balance, the dependence of thermal balance on the shape of the orbit, the optics of the simulator, etc. Some of these problems are so vast and complex that no attempt at an adequate solution can be made within the brief period allotted to the Summer Workshop.

The spectral distribution of the mercury-xenon lamp is a problem of immediate urgency. There is no longer any question as to the relative merits of the mercury-xenon lamp, the carbon arc, the laser, the plasma jet, and other possible sources; we are committed to the mercury-xenon lamp. Many attempts have been made to determine the

*Members of the Summer Workshop Team "A" were Matthew P. Thekaekara, Ralph A. Goodwin, Graham D. Gutsche, Anthony Cerkanowicz and Bruce Friedman.

spectral-energy distribution of these lamps and the results are highly at variance with each other.

Nor can the question be dismissed as of relatively small importance; the spectral distribution is highly significant for the problem of thermal balance. The total energy received by the test vehicle in the simulator is an integral of the absorption coefficient of the surface coating and of the spectral-energy distribution. If the absorption coefficient is uniform throughout the spectral range, spectral matching is of no importance; it is sufficient that the total energy incident per unit area be equal to that in outer space. However, experiments show that, for practically all types of surface coating, the absorption coefficient varies widely from zero to 100 percent and is highly sensitive to the spectral range. Hence arises the necessity for a spectral match between the solar energy and the energy of the artificial source to be used for the simulator.

The energy due to the sun outside the earth's atmosphere is known to a high degree of accuracy. Its spectral distribution is represented, probably within 1 percent, by the well-known Johnson curve. The planet radiation due to the earth is relatively small and is also sufficiently well-known. The albedo due to the earth is a highly varying factor for which no perfect simulation is possible, but whose spectral characteristics are rather close to those of the solar radiation.

The American Institute of Electrical Engineers has laid down certain specifications for solar simulators: namely, that throughout the 3,000 – 12,000A range, the total energy in any wavelength band shall not deviate from the Johnson solar-distribution curve by more than the following percentages in every square centimeter area of the test region. For 200A band, 20 percent; for 400A band, 15 percent; for 600A band, 10 percent; and for 1,000A band, 5 percent. These specifications are very restrictive and cannot be attempted except for small test areas. In any attempt for spectral match, a compromise must be made between the size of the test area, the cost of the facility, and the spectral match specifications. However, it is important to know what degree of mismatch there will be in any actual simulator.

In problems of thermal balance, the major factor is not the energy distribution but the total amount of energy absorbed by the spacecraft. By adjusting the input wattage of the lamp, it is possible to equalize the energy absorbed per unit area by the test vehicle in the simulator and by the spacecraft in outer space. In doing so, it is essential to know, first, the variation of absorption coefficient with wavelength, and, second, the energy distribution of the mercury-xenon lamp. Extensive studies have been made on the absorption coefficients of surface coatings. The techniques are simple; the results are reproducible. On the other hand, the data concerning the spectral distribution of the mercury-xenon lamp leave a great deal to be desired.

A search through available literature shows that there are five sets of independent data on the spectral-energy distribution of the mercury-xenon lamp. For the sake of convenience these data are designated as lamps 1, 2, 3, 4 and 5.

The most complete data (lamp #1) seem to be those given by the Westinghouse Lamp Division, Westinghouse Electric Corporation, Bloomfield, N. J., in a monograph signed by J.C.H. (1962). The table gives the spectral-energy distribution of the 2.5-kilowatt Hg-Xe short-arc lamp, SAHX-2500B, in watts radiated per 100A band, in the wavelength range $0.2\mu - 2.0\mu$. The total energy radiated in this whole range is 1485.6 watts. It is known that beyond 2.0μ the spectral irradiance decreases exponentially, and becomes practically zero at 5.0μ. Two different methods of extrapolation for the radiant energy in the range $2.0\mu - 5.0\mu$ gave the same value, 243 watts. Thus, the total radiant energy from the 2.5-kw lamp in the whole spectral range $0.2\mu - 5.0\mu$ is 1729 watts. This is taken as a figure to which all other spectral-distribution data are to be normalized.

A second and fairly complete source of information is a paper published by the Hanovia Company on the Hg-Xe lamps and the Xe lamps. The Hg-Xe data (lamp #2) are on a 1000-watt lamp, in the range $0.2\mu - 1.4\mu$, on a percentage basis. The authors state that the energy output in this range is 480 watts. Assuming that the luminous efficiency is the same for the 1-kw and 2.5-kw lamps, the energy from the 2.5-kw lamp in the range $0.2\mu - 1.4\mu$ is found to be 1200 watts = 480×2.5. The energy output of lamp #1 in the same range is 1217.6 watts. The close agreement between these two values shows that a meaningful comparison can be made between lamps #1 and #2. Assuming the output of a 2.5-kw lamp in the range $0.2 - 1.4\mu$ to be 1217.6 watts, the output in watts per 100A band can be calculated from the percentage values supplied by Hanovia.

An independent set of data (lamp #3) is available in a paper published by Mann and Dubey.[1] The authors give a histogram comparing solar radiation and the Hg-Xe lamp radiation, on a percentage basis, for each 500A band in the range $0.3 - 1.3\mu$. Assuming that in this range the total output is the same as that of lamp #1 (namely 1141.8 watts), it is possible to prepare a table of energy output in watts per 500A band for lamp #3.

Minneapolis-Honeywell performed a series of tests on three Hanovia lamps of 2.5-kw rating, operating them under seven different conditions of input wattage and of lamp age. The data are presented in a series of tables, on a percentage basis, for bandwidths of two or more thousands of angstroms. These values have been averaged (normalized to the same output as lamp #2) and values for energy output in watts per 500A band have been calculated. These data are referred to as data on lamp #4.

Minneapolis-Honeywell also made a series of four tests on a 2.5-kw Westinghouse lamp #4-21, operated at 2.5 kw, to determine what change, if any, occurs in spectral distribution due to aging of the lamps. Though the data are not quite conclusive, they seem to indicate that the energy in the range $0.5 - 0.7\mu$ increases with the age of the lamp. Averages of the four tests were made, the totals were normalized to the same output as

lamp #1, and the values of energy output in watts per 500A band were calculated. These data are referred to as data on lamp #5.

In order to compare these data with the solar irradiance, the latter should be normalized to the same total energy. The solar constant (the energy received per cm^2 outside the earth's atmosphere) is 0.140 watts, of which 99.5 percent is in the wavelength range 0.2 – 5μ; therefore, to compare the solar constant with an Hg-Xe lamp of 1729-watt energy output, it is necessary to calculate the energy received from the sun over an area 12,350 cm^2.

(Solar irradiance data available in literature[2] give values at very close intervals in watts per cm^2 of surface per micron-wavelength band. These values multiplied by 123.5 give the solar flux in watts per 100A over an area receiving a total energy of 1729 watts.)

Table 2-1 lists the results of these calculations. The energy values are in watts, integrated over 500A bandwidths. These results are also presented in Figure 2-2. A more detailed comparison of solar irradiance with that of the Hg-Xe lamp is presented in Figure 2-1. The solar irradiance curve in Figure 2-1 is the Johnson curve referred to earlier; the curves for the Hg-Xe lamp are based on data from lamps #1 and #2. The ordinates are energy values integrated over 100A bandwidths.

Table 2-1
Spectral-Energy Distribution of Hg-Xe Lamps:
Comparison of Data Available in Literature.

Wavelengths (Microns)	Energy Radiated in 500 Angstrom Interval by Each Lamp (Watts)					
	Solar	#1	#2	#3	#4	#5
.3 - .35	59.1	442.8	77.5	131.3	33.9	24.9
.35 - .40	75.5	70.5	91.0	154.1	39.8	41.9
.40 - .45	119.2	109.5	97.1	134.7	42.5	63.8
.45 - .50	131.0	26.9	35.1	52.9	13.1	15.7
.50 - .55	120.0	73.5	117.9	94.8	132.1	123.0
.55 - .60	115.5	95.3	146.1	126.7	163.7	159.5
.60 - .65	105.9	36.5	47.4	42.2	53.1	61.1
.65 - .70	95.4	39.7	50.6	50.2	56.6	66.4
.70 - .75	83.5	36.7	49.0	48.0	46.4	22.9
.75 - .80	73.8	37.6	37.3	35.4	35.3	23.4
.80 - .85	65.5	41.6	43.0	28.5	40.7	25.9
.85 - .90	58.5	72.1	45.1	44.5	42.7	44.9
.90 - .95	52.5	76.1	48.2	37.7	45.6	47.4
.95 - 1.00	47.3	85.0	49.7	26.3	97.0	53.0
1.00 - 1.05	42.9	94.6	51.7	30.8	85.1	80.2
1.05 - 1.10	39.2	50.4	26.9	25.1	44.3	31.8
1.10 - 1.15	35.3	50.6	34.9	26.3	57.5	42.9
1.15 - 1.20	32.5	34.5	22.2	18.3	36.6	29.3
1.20 - 1.25	29.8	37.1	23.9	14.8	39.4	31.4
1.25 - 1.30	26.6	30.9	18.8	18.3	31.0	26.2
1.30 - 1.35	24.0	30.5	17.8		29.3	25.9
1.35 - 1.40	21.5	30.7	20.9		34.4	26.0

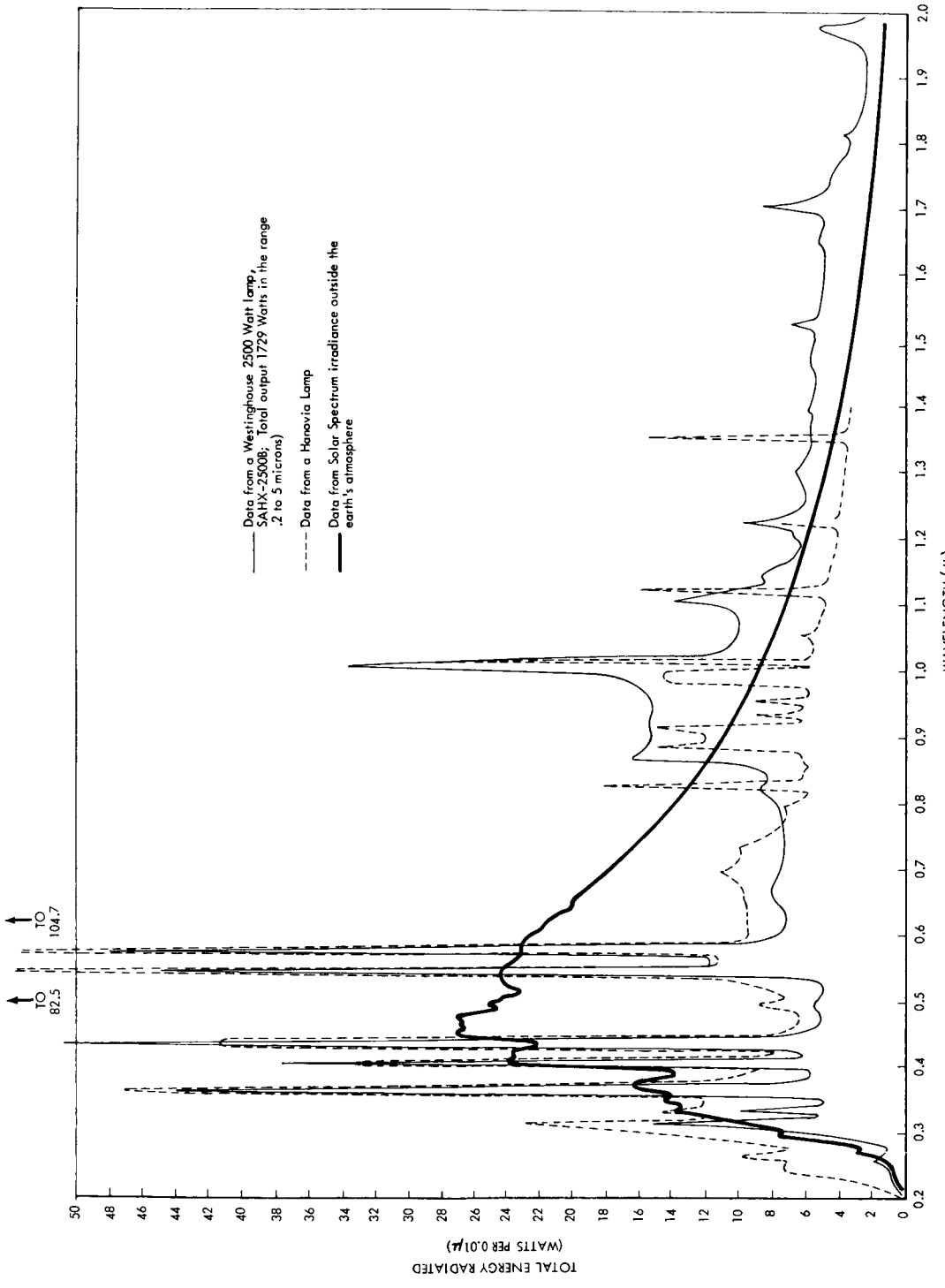

Figure 2-1 - Spectral-energy distribution of typical Hg-Xe lamps vs solar radiation

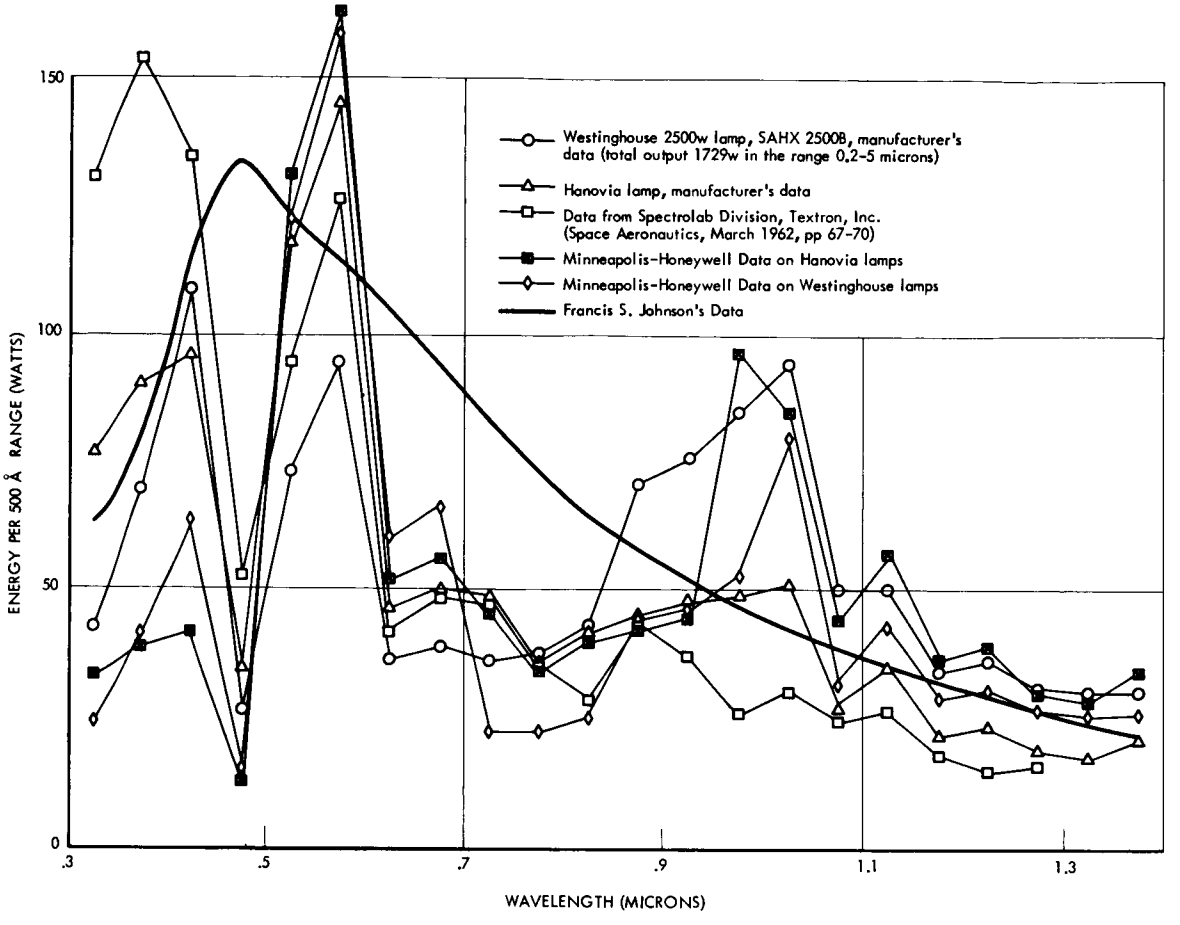

Figure 2-2 - Comparison of spectral-distribution data from different Hg-Xe lamp sources

These five sets of data present considerable variation in the energy values, in particular the wide divergence between lamps #1 and #2, and lamps #4 and #5. In the ultraviolet range the lamps #4 and #5 indicate considerably higher energy. There is an overall agreement between the data on lamps #1 and #2, as shown by the ratio of the energy in the line spectrum to the total energy of the lamp in the range 0.2 – 1.4μ (36 percent from data on lamp #1, and 37 percent from data on lamp #2).

As stated earlier, the AIEE specification on spectral matching for solar energy is that, for any 200A band, the energy shall not deviate from the Johnson curve by more than 20 percent. In ten regions of the spectrum chosen at random, each of 200A width, the Johnson curve was compared to the Westinghouse data (lamp #1) and to the Hanovia data (lamp #2).

The results of this analysis are given in Table 2-2; the average deviation is considerably greater than the AIEE specification (63% for lamp #1 and 95% for lamp #2). A similar comparison made for the 1000A band shows that the average deviation is 41%

according to the Westinghouse data and 44% according to the Hanovia data, compared to the AIEE specification of 5%.

Table 2-2
Comparison of Spectral Irradiance of Hg-Xe Lamps #1 and #2 with the Johnson Curve

Wavelength Range (Microns)	Percentage Deviation from Johnson Curve	
	Westinghouse Data, Lamp #1 (%)	Hanovia Data, Lamp #2 (%)
.21 - .23	+111	+630
.33 - .35	- 48	- 5.3
.4 - .42	- 6.8	- 12
.58 - .60	- 47	- 58
.76 - .78	- 48	- 51
.87 - .89	+ 34	- 8.3
1.00 - 1.02	+240	+ 94
1.12 - 1.14	+ 24	+ 46
1.23 - 1.25	+ 18	- 29
1.36 - 1.38	+ 55	- 19
Average Deviation,	63%	95%

The large differences between the data on lamps #1 through #5 raise an important question for solar simulation. Not only is there a lack of spectral match; there is no reliable information on the extent of the spectral mismatch. The question arises whether the mercury-xenon lamp is something that changes its color every time one looks at it. At any rate, it is important to know the spectral distribution of the energy of these 127 lamps which are going to illumine the test floor of the gigantic simulator.

More than 40 percent of the solar energy is in the visible range from 3500 to 7000A; nearly as much of the mercury-xenon lamp energy is also in the same narrow-wavelength range, where absorption coefficients of materials vary greatly. It is also the range in which the mismatch between the mercury-xenon lamp and the solar radiation is most pronounced. In the long infrared range, the spectral mismatch is less striking. In the ultraviolet range, the energy is relatively small.

Team A of the Summer Workshop decided to measure the spectral energy distribution in this visible range, and to develop a technique of high-precision intensity measurement, using a grating spectrograph rather than a prism spectrograph in order to obtain the necessary high resolving power and spectral dispersion. Very small slitwidths (20 microns) were used, as the spectral range viewed by the instrument at any given time should be small compared to the half-widths of the lines of mercury and xenon.

THEORETICAL CONSIDERATIONS

The essential information needed about the mercury-xenon lamp is the amount of radiant energy falling per unit time per unit area on the test floor of the simulator. If the surface of the spacecraft were an ideal blackbody surface, having an absorption coefficient unity throughout the wavelength range, or an ideal greybody surface, having an absorption coefficient constant and independent of wavelength, it would be sufficient to know the total energy incident on the test floor, per unit area per unit time. The total energy can be expressed as an integral

$$E = \int E_\lambda \, d\lambda. \tag{1}$$

The limits of integration are strictly speaking zero and infinity, but for all practical purposes the limits are 0.2μ to 5.0μ. E is the total energy and is the area under the energy-distribution curve of the monochromatic energy E_λ versus wavelength λ. In wavelength ranges below 0.2μ and above 5.0μ, E_λ is practically zero for both the solar radiation and the mercury-xenon lamp.

For purposes of solar simulation, not only must the total energy be known, but also the energy distribution function E_λ, since the surface coatings vary considerably from the ideal conditions of the perfect black or perfect grey. The absorption coefficient α varies between 0 and 1 and is a function of the wavelength. The total energy absorbed per unit area of the test body is

$$E_t = \int_{0.2\mu}^{5.0\mu} \alpha_\lambda E_\lambda \, d\lambda. \tag{2}$$

In order to draw meaningful results from the solar-simulation tests, the energy E_t absorbed by the test surface should be equal to the energy E_s absorbed by the surface of the spacecraft in outer space.

E_s is the sum of three integrals expressing, respectively, the solar radiation directly from the sun, the solar radiation reflected from the earth, and the planet radiation from the earth.

Assume for the present that E_s (the radiant energy received by the spacecraft) and α (the absorption coefficient of the surface coating) are known to a sufficient degree of accuracy.

A few simple considerations will show how the total energy E_t and the monochromatic radiant energy E_λ on the test floor differ from the same quantities as emitted by the mercury-xenon lamp. The energy emitted by the lamp is collimated and directed to the test floor by a complex optical system, consisting of three quartz lenses and three aluminized reflecting surfaces. Each of these reduces the total available energy by a certain percentage, and also changes the spectral energy distribution to a small extent.

There is in particular a noticeable effect in the wavelength range 0.75 – 0.95μ, where the reflection coefficient of evaporated aluminum drops to about 0.8. In the rest of the spectral range, the reflection coefficient has a practically constant value 0.95. From the known reflection and transmission properties of the optical system, it is possible to calculate the total energy E_t and the monochromatic energy E_λ on the test floor, provided these quantities are known at the source.

Methods suggested for measuring the total energy E_t emitted by the mercury-xenon lamp can be divided into two categories: those which measure the rise in temperature of the liquid in a continuous-flow calorimeter, and those which measure the thermoelectric electromotive force in a thermocouple. All methods call for fairly elaborate calibration procedures for the instruments. The total energy may also be calculated from monochromatic energy distribution, since the total energy is an integral of the energy-distribution function.

The absolute standard of comparison for spectral energy distribution is the ideal blackbody. But an ideal blackbody is impossible to construct, and all practicable approximations to the ideal blackbody are too complex and require experimental procedures which are too elaborate, so that secondary standards of spectral radiance must suffice.

A secondary standard commonly employed is a tungsten-ribbon lamp. The spectral distribution of the tungsten-ribbon lamp can be established in terms of its color-temperature, the spectral emissivity of tungsten, and the absolute radiant-energy output for selected wavelengths in terms of an NBS standard of thermal radiation.

The energy distribution within a blackbody enclosure is given by the Planck equation

$$\psi_\lambda d\lambda = \frac{8\pi ch}{\lambda^5} \frac{1}{e^{ch/\lambda kT} - 1} d\lambda. \tag{3}$$

where $\psi_\lambda d\lambda$ is the energy density per unit volume in the wavelength range λ to $\lambda + d\lambda$; c is the velocity of light; h is the Planck's constant; k is the Boltzman constant; and T is the absolute temperature.

The energy radiated from a small orifice on the side of the blackbody enclosure per unit area of the radiating surface, per unit solid angle, in a direction normal to the surface, is

$$E_\lambda d\lambda = \psi_\lambda d\lambda \times \frac{c}{4\pi}. \tag{4}$$

The values of these functions for different temperatures and wavelengths are available in literature.[3] In using these tables for precision measurement of intensity, it should be noted that several authors (in particular, Pivovonsky and Nagel) base the computations on the following values for the two constants $2hc^2$ and hc/k:

$$2hc^2 = 1.1909 \times 10^{-12} \text{ watt cm}^2 \text{ per steradian.}$$

$$hc/k = 1.4380 \text{ cm } ^\circ\text{K}.$$

If these constants were recalculated from the best available values for h, c and k, a slightly different value would be obtained for hc/k. The value computed from constants h, c and k, given in "American Institute of Physics Handbook" edited by Dwight E. Gray (McGraw Hill Book Company, New York, 1957) p. 7-3, is $hc/k = 1.43885$ cm °K. Another good source for fundamental constants is E. R. Cohen and others in Rev. Mod. Phys. 27, 363 (1955); using this latter source produces very nearly the same value, $hc/k = 1.43879$ cm °K. This difference (nearly ten times the estimated experimental error in the determination of h, c and k) is probably due to a slightly different value of k assumed by Pivovonsky and Nagel.

From the known spectral irradiance of the standard blackbody, the next step is to calculate the spectral irradiance of the secondary standard, the tungsten-ribbon lamp. For this, the temperature of the ribbon for a specified current is determined by comparing the radiation from the tungsten ribbon to that from a blackbody. From the color temperature of the ribbon (the color temperature being defined as that temperature of a blackbody which has the same ratio of spectral radiances as the tungsten ribbon in two intervals λ_1 to $\lambda_1 + d\lambda_1$ and λ_2 to $\lambda_2 + d\lambda_2$) may be derived the true temperature. Next, by employing blackbody data for this temperature and the spectral emissivities of tungsten, a spectral-energy curve for tunsten is calculated. Exhaustive studies are available in literature on the spectral emissivity of tungsten.[4]

In actual practice, it is not necessary to go through this elaborate process of determining the color temperature and evaluating the Planckian functions; calibration charts may be obtained from the Radiometry Section of the National Bureau of Standards for the spectral irradiance of a given lamp at wavelength intervals of 500A or less. The values are quoted to three significant figures, and may have a maximum error of 5 percent.

Calibration charts of the two lamps used in the present investigation are given in Table 2-3.

Values of the spectral irradiance of the tungsten ribbon lamp at intermediate wavelengths are determined by linear interpolation. Since I_W, the spectral irradiance, changes by a factor of 10^4 from one end of the spectral range to the other, it is more convenient to plot $K = \log I_W$ versus λ. Let K_1, K_2 be the values of $\log I_W$ at two wavelengths λ_1, and λ_2.

Values of K_c, where the subscript c denotes that it is a calculated value, are determined from the linear equation

$$\frac{K_c - K_1}{\lambda - \lambda_1} = \frac{K_2 - K_1}{\lambda_2 - \lambda_1} . \tag{5}$$

where λ_1, and λ_2 are 4000A and 6000A, and λ takes successively the values in column 1 of Table 2-3.

Table 2-3
Spectral Irradiance of Lamps U-187 and U-21 at 35 Amperes
(in microwatts per steradian per nanometer per mm^2 of source)

	Lamp U-187	Lamp U-21
2500	3.76×10^{-3}	5.87×10^{-3}
2600	8.71×10^{-3}	1.31×10^{-2}
2700	1.68×10^{-2}	2.47×10^{-2}
2800	3.09×10^{-2}	4.49×10^{-2}
2900	5.35×10^{-2}	7.61×10^{-2}
3000	8.81×10^{-2}	1.24×10^{-1}
3200	2.11×10^{-1}	2.96×10^{-1}
3500	6.37×10^{-1}	8.59×10^{-1}
3700	1.18	1.55
4000	2.55	3.30
4500	6.84	8.69
5000	1.47×10	1.80×10
5500	2.54×10	3.05×10
6000	3.86×10	4.55×10
6500	5.32×10	6.25×10
7000	6.82×10	7.86×10
7500	8.16×10	9.21×10

At each of these values is found the difference $\Delta K = K_c - K_s$, where $K_s = \log I_w$ is the standard value from the log of I_w in Table 2-3. A graph is drawn for ΔK versus λ, which permits calculation of log I_w at wavelength intervals as close as are needed for the problem on hand, by applying the correction ΔK to the linearly interpolated value of K_c as given by equation (5).

The spectral energy distribution of the mercury-xenon lamp can be determined by comparing its energy output in a given spectral range to that of the standard tungsten-ribbon lamp. It is essential that the energy output from the two sources be measured under identical conditions, and that the response of the recording device be strictly linear.

The spectrum of the mercury-xenon lamp shows a large number of lines superposed on the continuum. Since the tube operates under a high pressure of about 20 atmospheres, all the lines show considerable broadening. If the spectral range covered by the photomultiplier tube for any given setting of the spectrograph is of a bandwidth comparable to the halfwidth of the spectral lines, we are essentially comparing a line spectrum of mercury-xenon with a continuous spectrum of tungsten. In such a case, the response of the photomultiplier tube is not strictly linear to the intensity, and a correction factor must be introduced; this correction factor depends on the wavelength range, the slit width, and other constants involving the geometry of the spectrograph.

On the other hand, if the slit width used is sufficiently small, and the spectral range covered at a given setting is therefore very small compared to the halfwidth of the lines,

we are essentially comparing one continuous spectrum with another. If the response of the recording electronics is linear, the ratio of the two spectral irradiances is equal to the ratio of the corresponding signals. Thus the basic equation for absolute intensity measurement may be written

$$\frac{I_H}{I_W} = \frac{s_H}{s_W}. \tag{6}$$

where I signifies the spectral irradiance and s a corresponding signal, and the subscripts H and W refer respectively to the two sources, mercury-xenon and tungsten.

It will be helpful to recall a few basic ideas about a plane-grating monochromator in Ebert mounting:

The theoretical resolving power of a grating is

$$\frac{\lambda}{d\lambda} = nm. \tag{7}$$

where n is the total number of rulings on the grating and m is the order of the spectrum. In our case we have the first order spectrum; the grating has a ruled area of 52×52 mm^2, and the number of rulings is 30,000 per inch. Hence n = 61,400 lines and for λ = 4000A, $d\lambda$ = .065A. The theoretical resolving power is such that two lines .065A apart from each other will be just resolved, and an infinitely narrow line of wavelength 4000A will have a half-width of .065A.

The theoretical resolving power is rarely achieved because of imperfections in the grating, or lack of alignment.

Another factor that contributes to the observed line width is the finite width of the slit. Let the grating be set for a particular wavelength in the neighborhood of λ = 4000A in the first order. From the grating equation is derived

$$\lambda = d(\sin\alpha + \sin\beta). \tag{8}$$

where d is the grating spacing, and α and β are the angles of incidence and diffraction. Assume that the normal to the grating is inclined towards the exit slit and away from the entrance slit.

From the known values of λ and d, it is readily seen that $(\sin\alpha + \sin\beta) = 0.472$.

Values of α and β can be calculated as follows: Let ϵ be the angle which the bisector between the incident and diffracted beams makes to either of the two beams, and let γ be the angle which the same bisector makes with the grating normal. Thus

$$\alpha = \gamma + \epsilon \text{ and } \beta = \gamma - \epsilon; \text{ and,} \tag{9}$$

$$\sin\alpha + \sin\beta = \sin(\gamma + \epsilon) + \sin(\gamma - \epsilon)$$

$$= 2 \sin\gamma \cos\epsilon.$$

The value of ϵ is known from the geometry of the Ebert mounting spectrograph. Take for example a pencil of rays which enters the spectrograph through the geometrical center of the entrance slit and reaches (after reflection, diffraction, and reflection) the geometrical center of the exit slit. From the entrance slit to the mirror the rays form a divergent cone, and from the mirror to the exit slit they form a convergent cone. The axes of these two cones are parallel, and the distance between the points where the axes meet the mirror is equal to the distance, D, between the two slits. Thus

$$2\epsilon = \frac{D}{F}, \quad \text{where } F = 50 \text{ cm}$$

$$\text{Hence } \epsilon = .1032 \text{ radian} = 5^\circ - 55'.$$

$$\gamma = 13^\circ - 43'; \ \alpha = 19^\circ - 21' \text{ and } \beta = 7^\circ - 48'.$$

These equations hold strictly for the limiting case where both the slits are geometrical points. In the actual case of finite slit widths, corresponding to every point on the entrance slit there is a point on the exit slit which satisfies the grating equation (8) for the same wavelength λ. This is the special advantage of the curved slit in the Ebert mounting.[5]

Differentiating equation (8) with respect to β, $d\lambda = d \cos \beta d\beta$. The broadening of the spectral line due to the exit slit only is given by $d\lambda$, which for a slit of 25 microns width is

$$d\lambda = 8.47 \times 10^{-5} \times 0.9441 \times 5 \times 10^{-5} \text{ cm} = 0.4\text{A}.$$

The entrance slit contributes about the same linewidth which is superposed on the width due to the exit slit, so that the instrumental linewidth due to the slits alone is of the order of 0.4A.

The emission lines of the mercury-xenon lamp have a halfwidth considerably greater than this, so that the present set-up is essentially comparing one continuous spectrum with another, and equation (6) can be applied without any elaborate correction factors.

EXPERIMENTAL ARRANGEMENT

The spectrograph as was stated earlier is a plane-grating monochromator in Ebert mounting. The experimental arrangement is shown in Figure 2-3. The light enters the instrument through a straight slit 25 microns wide and passes to a concave mirror, where it is collimated and reflected to the grating. The grating ruled on a 58×58 mm^2 blank, has 30,000 grooves per inch on a ruled area 52×52 mm^2. The diffracted light, still parallel, but with separate wavelengths diverging, is reflected back to the mirror, where it is again reflected and focussed on the exit slit.

The wavelength of the light reaching the exit slit is changed by rotating the grating about its center. The grating is rotated by action of an 8-inch lever arm mounted on the

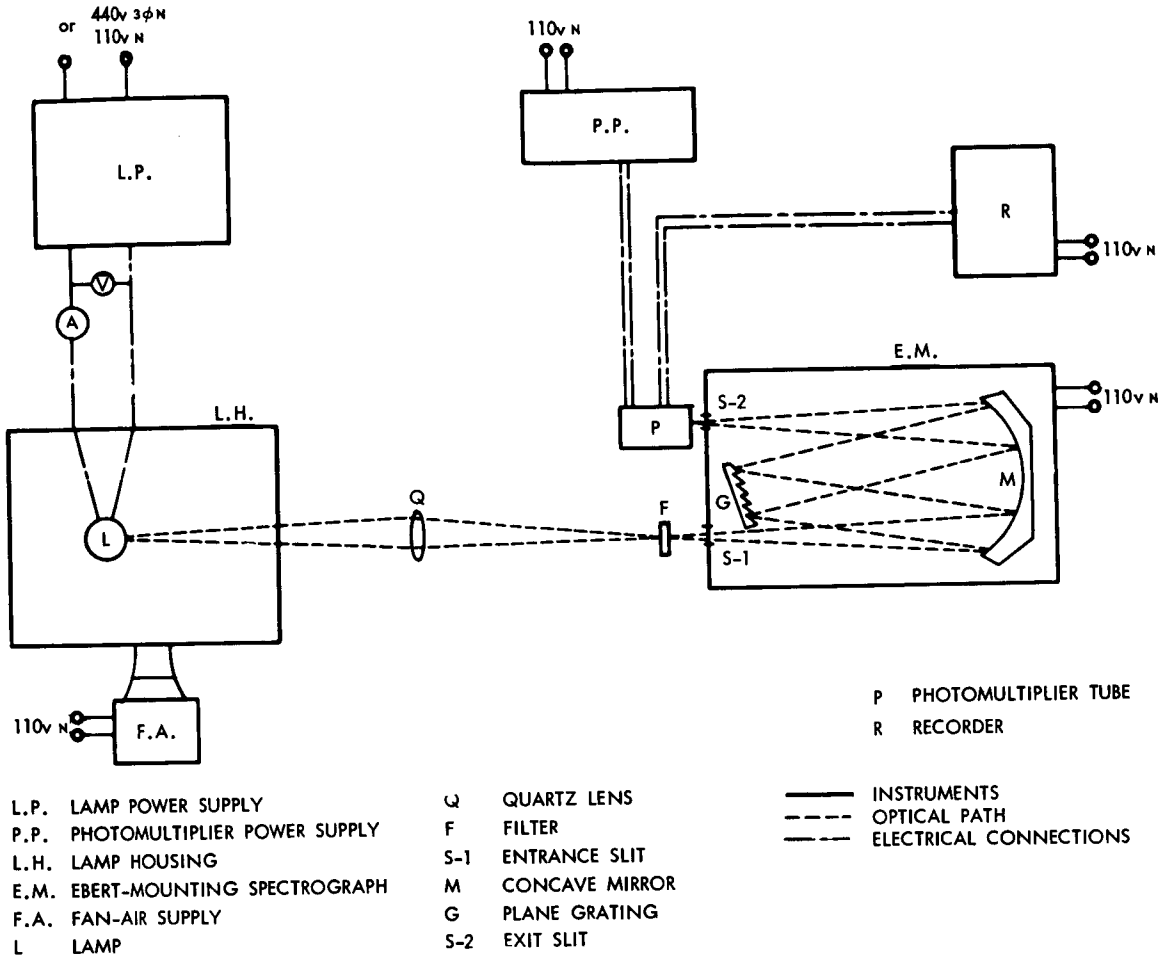

Figure 2-3 - Experimental arrangement for the measurement of intensity

pivot shaft and driven by a split nut on a precision screw. The linkage is designed to provide a linear motion directly proportional to the sine of the angle of rotation, so that the screw rotation remains proportional to the wavelength. A simple system of gears permits the operator to select any of eight different speeds of rotation on the automatic drive or four different speeds on the manual drive. Both the manual and automatic drives are reversible. A Veeder-Root counter attached to rotating gear reads the wavelength correct to 2A. The eight automatic speeds available are 500, 250, 125, 50, 20, 10, 5, and 2A per minute.

Light is focussed on the slit by a quartz double-convex lens having an effective aperture of about F:8.5, the same as that of the spectrograph; in this way the full light-gathering power of the spectrograph is utilized, without letting too much stray light into the instrument. Care must be taken in aligning the source and the lens along the optic axis of the instrument. Once the exact position of the lens was found, it is rigidly fixed; as different sources are interchanged one for another, the only precaution to be taken is

that a well-focussed image of the source must be formed at the center of the entrance slit. The lens, with a diameter of 3.24 cm, is at a distance of 51.3 cm from the slit and 74.8 cm from the source.

The light from the exit slit enters a photomultiplier tube. Two different types of photomultiplier tubes were used during the experiments, GE tube 1P28 and EMI tube 9592B, having spectral responses S-5 and S-10, respectively. The 1P28 tube has a relatively higher gain and narrower spectral-band response than the 9592B tube. Power for the phototubes is obtained from a standard phototube power supply. The output of the phototube is fed through a 1-megohm resistor to a recording device.

Two types of recording device were used. In the earlier phase of the experiment, the voltage across the megohm resistor was led to a vacuum-tube digital voltmeter. The voltmeter, supplied by the Hewlett Packard Co., had an input impedance of 11 megohms; response time, less than 1 second; ranging time, 0.2 to 2 sec.; accuracy, within 0.2 percent; variable sampling rate, between 5 printouts per second and one printout every 5 seconds. The instantaneous voltage across the megohm resistor was displayed on a lighted panel, and the value was printed out on a strip chart at any desired rate. The main advantages of this recording technique over the conventional pen-recorder technique were that it eliminated the need for reading out the recorder signals from a roll of paper, and that during any single scanning of the spectrum the output signals were recorded over a range of several decades with an accuracy ranging between 1 and 0.1 percent. The digitizer automatically adjusted the decimal point in the voltage and had a range from 999 volts to .001 volt. However, if the relay for changing the decimal point tripped at the same time as the relay for the printout tripped, the printout was skipped. Thus, quite frequently during the scan of the mercury-xenon spectrum, printouts in the vicinity of the strong emission lines were missing from the strip chart and it is precisely here that the values are most significant. Another disadvantage was that a great deal of information concerning the fine structure of the emission lines was omitted from the strip charts. These disadvantages could of course be overcome by scanning the spectrum at a very slow speed in the vicinity of the emission lines. There was also some uncertainty about the wavelength corresponding to any given printout; this defect was later corrected by adding a clock printer unit (561A clock printer) to the digitizer-printout rack. On the same line as the printout of the voltage, the printout of the time was also given, in hours, minutes and seconds. This constituted a fairly accurate recording of the wavelength corresponding to each printout.

In the later phases of the experiment, the more conventional device was used of a pen continuously recording the changing voltages over a slowly moving strip of ruled paper. The voltage across the megohm resistor was applied to a decade voltage divider (type 1454A–Serial 3411, General Radio Corp.), which permitted the full-scale deflection of the recorder to be set at different values, 50, 25, or 5 millivolts, etc. Through the voltage

divider the signal was fed to a Brown Electronic strip chart recorder (model KSY 153 × 18 (VAH) 163-26). The chart drive speed of 1 inch per minute along with a grating drive of 50 angstroms per minute was fully adequate for displaying the profiles of all the strong lines.

The light source used for the initial alignment of the spectrograph was a small high-pressure mercury-arc lamp (Central Scientific Company, Serial No. 26830 Type SH). The power supply for this lamp consisted of a simple transformer (Hanovia type 7606, catalog number 5043). The lamp, which is compact and easily mounted in position, proved to be extremely useful for all routine calibration procedures, for testing the linearity of response of the phototube and associated electronics, for measuring the transmission coefficients of the filters, for checking the accuracy of the wavelength counter, etc.

Two tungsten-ribbon lamps manufactured by the General Electric Company (Type 30A/T24/3) were used as intensity standards. The lamps are designated U-21 and U-187 in the calibration charts supplied by the Radiometry Section, Atomic Physics Division of the National Bureau of Standards. The values of spectral radiance given in the calibration charts can be assumed to hold true for at least 40 hours of operation, provided the operating current never exceeds the rated value. Both the lamps were fairly new, and the glass walls and quartz window of the lamp showed no signs of darkening through tungsten sputtering, so that the NBS values of spectral radiance could be accepted with confidence.

The power supply for the standard lamp was a variac transformer shown in Figure 2-4b. The standard lamp operates at 6 volts, 35 amp. The current was read by a sensitive ammeter connected in series with the transformer output through a calibrated shunt. The least division of the ammeter was one ampere and a rough estimate had to be made for fractions of an ampere. This was not considered satisfactory; for further work, a more precise method of measuring and stabilizing the current should be devised. The conventional arrangement is to balance on a precision potentiometer the lamp-input current with a known current, the latter being determined by a standard cell and a standard ohm.

The mercury-xenon lamp used in these experiments was a 2500-watt lamp supplied by the Westinghouse Corporation, type SAHX – 2500B, referred to in the records of the Test and Evaluation Division, GSFC, as Lamp #R137. A summary of its hours of operation is given in Table 2-4. The lamp was enclosed in a large rectangular box of aluminum, 46 × 35 × 27 inches.

The lamp is held in position by two clamps rigidly attached to the back side of the box. The light issues from a circular opening on the front side of the box, which is restricted by a diaphragm so that only a narrow pencil of rays emerges from the box, just sufficient

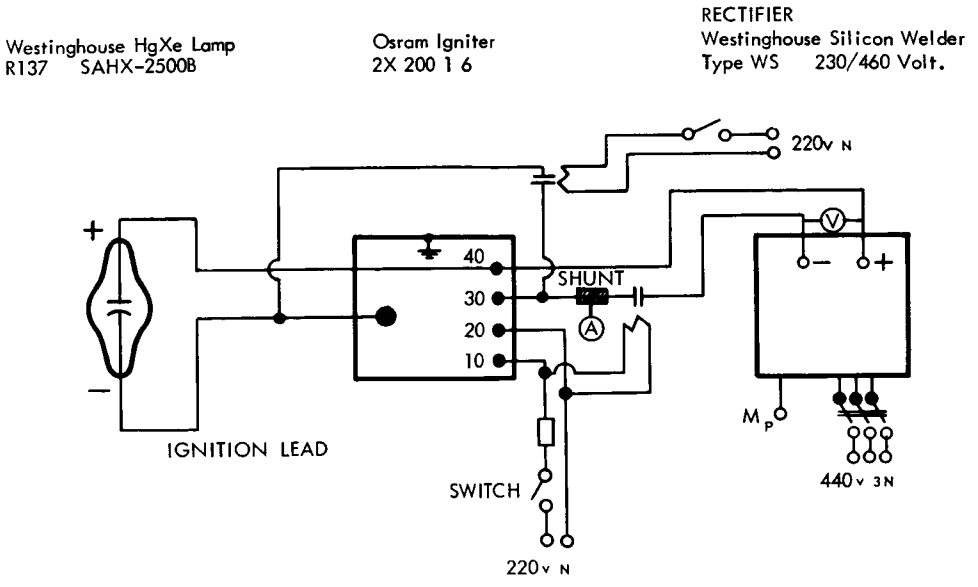

Figure 2-4a - Power supply for Hg-Xe lamp, schematic diagram

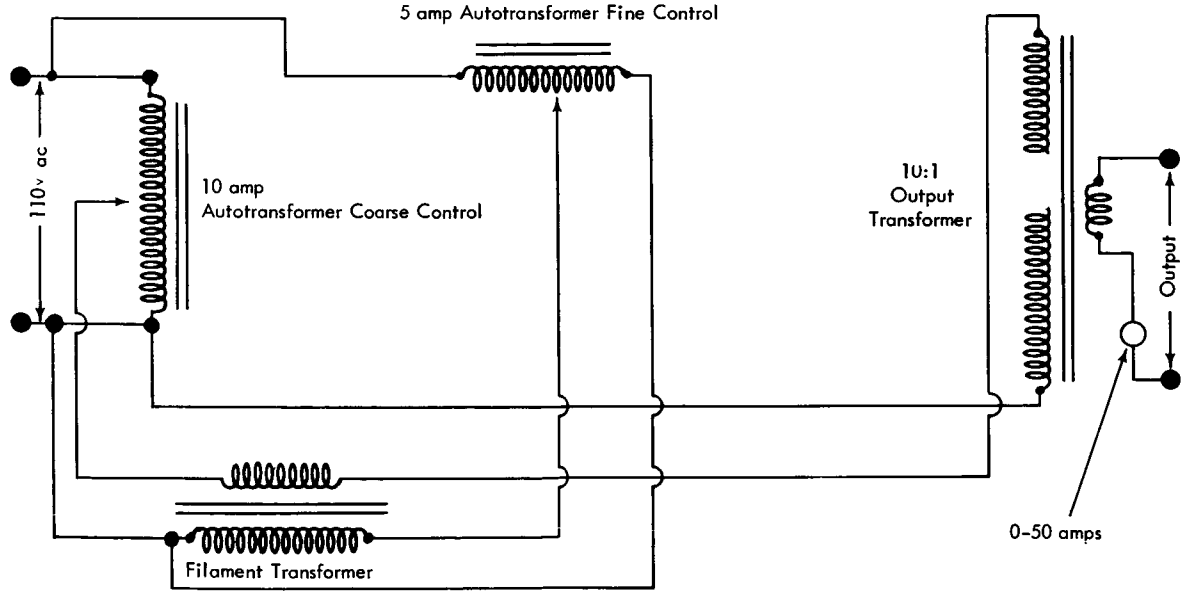

Figure 2-4b - Power supply for standard lamp, schematic diagram

Table 2-4
Operating History, Hg-Xe Lamp #R137
(Westinghouse type SAHX-2500B)

Date	Average			Operation Hours	Cumulative Operation Hours
	Volts	Amps	Watts		
7/19/62	38	65.5	2490	1.00	1.00
7/31/62	37-38.7	65.5	-	4.75	4.75
8/1/62	Lamp ignited and shut off for brief periods during the morning				
8/1/62	40	64.0	2520	3.00	8.75
8/10/62	36.9	65.5	2420	2.00	10.75
8/15/62	-	65.3	-	0.67	11.42
8/15/62	38.0	65.5	2490	1.67	13.09
8/15/62	38.0	65.5	2490	1.22	14.31
8/17/62	37.5	65.5	2460	1.00	15.31
8/17/62	38.2	65.5	2500	2.17	17.48
8/20/62	38	65.5	2490	1.45	18.93
8/21/62	38	65.5	2490	1.08	20.01
8/21/62	38	65.5	2490	0.58	20.59
8/23/62	38	65.5	2490	1.83	22.42
	27	56.2	1515	1.50	23.92
8/28/62	38	65.5	2490	2.33	26.25
9/5/62	38	65.5	2490	6.63	32.88

to cover the collimating lens, reducing to a minimum the hazard due to the strong ultraviolet radiation. Excessive heating within the lamp enclosure is avoided by allowing a strong air supply from below, provided by a motor-driven air blower, 0.1 hp, 1600 rpm. The hot air escapes through an opening above the enclosure.

The temperature inside the enclosure was measured by two copper-constantan thermocouples, one located very close to the lamp at the power lead and the other located about 3 inches behind the lamp. The current output of the thermocouples, calibrated in terms of the temperatures within the enclosure, was continuously recorded by a Minneapolis-Honeywell strip-chart recorder whenever the lamp was in operation. If the temperature showed a tendency to rise or fall, it was stabilized by the simple device of lowering or raising a shutter held against the intake of the air blower. By adjusting the rate of cooling, a steady state was attained, with no tendency to drift either in the temperatures recorded by the thermocouples or in the current and voltage supplied to the lamp.

The power supply for the mercury-xenon lamp is shown in Figure 2-4a. The input is 440 volts, 3-phase ac, stepped down and rectified by a Westinghouse silicon welder type WS rectifier unit. The rectified current is led to the lamp through an Osram igniter, Siemens-Schuckert, type ZX-200-1b. The input wattage of the lamp is determined by measuring separately the current and the voltage.

In the experimental setup described above, there are several different components, each supposed to be adequate for a precision measurement of intensity. However, the degree of reliability of each component and the percentage error that might be introduced by each had to be separately determined. The spectral radiance of the tungsten-ribbon lamp is known at the calibrated wavelength with a percentage error less than 5 percent; for most of the values, the error is presumably much less than 5 percent. On the other hand, because of the aging of the lamp or due to an inaccurate reading of the current input, larger and systematic errors might possibly be introduced, whose magnitude would be difficult to assess. The current input is a very significant factor, since the C^2R heating which controls the temperature of the ribbon is proportional to the square of the current, and the total radiant-energy output is proportional to the fourth power of the temperature. Hence, there is a degree of uncertainty about the standard of comparison, and the experiment should be set up so that the probable error due to any of the other sources is considerably less than that due to the standard.

The output of the photomultiplier tube is measured by a vacuum-tube voltmeter in the digitizer-printout unit. A calibration of this voltmeter seemed desirable and was performed by using a standard voltage-input unit, which can change the input from 1000 volts to .001 volt in stages of .01 volt, with a rated accuracy of 0.1 percent. In the ranges 0–1 volt and 10–900 volts, the reading of the digitizer was exactly that of the input. In the range 2–10 volts, the readings of the digitizer were about 0.5 percent lower; in the range 900–990 volts the values were 0.5 percent higher. In the range 990–999 volts, the values were 1 percent higher. As the digitizer readings during the scanning of a spectrum were well below 100 volts, this small difference could be totally ignored.

A wavelength calibration of the monochromator was made with the aid of a type SH mercury-arc lamp. The Veeder-Root counter of the spectrograph had been set accurately by the manufacturers to read the wavelength within 1 or 2 angstroms; however, the aluminum casing of the spectrograph and the lever arm controlling the grating drive are both subject to small changes in length, caused by fluctuations in ambient temperature, and for this reason the calibration would not necessarily remain constant. The mercury-arc lamp was focussed on the entrance slit and the reading of the digitizer was noted. The grating, manually rotated from the long-wavelength end to the short-wavelength end of the spectrum, was set successively on the peaks of the strong mercury lines, and the counter reading was noted for each line. The actual wavelength of the line appeared higher than the counter reading by about 3A; in no case was the difference greater than 4A or less than 2A. This correction factor is of some importance in measuring the signal for various wavelength settings of the tungsten-ribbon lamp. For the mercury-xenon lamp, however, the number of emission lines is sufficiently large to serve as an internal calibration of the spectrum chart, so that the counter readings are less significant.

The phototube signals from the mercury-xenon lamp are considerably stronger throughout the spectral range than those from the tungsten lamp. The ratio of the signals

varies from about 50 at 6500A to about 5000 at the short-wavelength end of the spectrum, 3500A, and at the peaks of the mercury lines. Thus, a relatively small error in the data from the standard lamp would introduce a very large error in the intensity of the Hg-Xe spectrum. The error can be minimized by reducing the Hg-Xe illumination on the entrance slit by a known constant ratio, through the use of a wire-gauze filter, a rotating sector, or any other type of achromatic filter. The present experiment used neutral filters, manufactured by Bausch and Lomb, which consist of thin aluminum films deposited on glass plates. Three grades of filters were available which reduce the intensity by a factor of 25, 10, and 5. These filters are respectively marked 1.4, 1.0 and 0.7, which are the logarithm to the base 10 of the intensity-reduction factor. By interposing one or more of these filters in front of the entrance slit, the signal from the phototube can be brought to a value very close to that given by the standard lamp in the same region. Several measurements were made on the transmission coefficients of the filters; most of the filters were found to have a transmission coefficient very close to the rated value. All tests for any dependence of the transmission coefficient on the wavelength were negative. In a particular case (filter #1 which was most used in these experiments), the average value of the ratio of the voltage output without filter and with filter was 9.93; the value was recorded at 9 wavelengths between 4000A and 6500A. The average deviation of the values about the mean was 0.18, which corresponds to about 2 percent.

The aluminum-film filters also gave a ready means of checking whether the voltage output on the digitizer or the recorder is directly proportional to the light input at the entrance. The linearity of response of the photomultiplier and the associated electronics is a necessary condition for absolute-intensity measurements, in terms of the tungsten-standard lamp. The tests showed that, within the limits of accuracy of the digitizer unit, the response was linear and independent of wavelength, except for very small and very large output signals. For very small output signals, the percentage error in the millivolt reading is too high; thus, a reading of 4 millivolts signifies any value between 4.5 and 3.5 millivolts and has a possible maximum error of 12 percent. At very high voltages, say 20 volts and above, the current through the megohm resistor is 20 microamps. This photoelectric current is generated by light incident on an area 25 microns $\times$ 4 mm of the cathode surface. If the whole cathode surface of 25 mm $\times$ 8 mm were equally illumined, the total current output would be about 40 milliamps, which is considerably above the maximum rated output of the phototube. Hence, at such high values of the signal, the linearity law of the phototube response breaks down completely. Below 10 or 15 volts the output of the phototube is strictly linear with light input. The dark current remained at zero most of the time and at one millivolt occasionally.

Several sets of measurements were made on signal strengths from both the standard tungsten lamps, U-21 and U-137, using both the phototubes 1P28 and 9592B. The wavelengths were set manually, with due corrections for the counter readings. The set of values for signal strengths showed a good consistency even though the measurements

were made at intervals of several days. The average deviation between different sets of readings was of the order of 1 percent.

The earlier recordings of the signal strength from the tungsten lamp were made with the image of the tungsten ribbon focussed on the full height of the entrance slit. When the tungsten lamp was replaced later by the mercury-xenon lamp, it was found that the image of the mercury-xenon arc had a height of only about 4 mm, considerably less than the height of the slit. The entrance slit was therefore masked to less than 4-mm height. Table 2-5 shows how the signal strengths are changed by masking the slit: columns 2 and 3 give the signal strengths (average of over ten printouts at each wavelength) for the full slit and masked slit respectively; and column 4, the ratio of the two values. The ratio is fairly constant. The average of the ratio is .2412, and the average deviation is .00236, about 1 percent. The logarithm of this value is a correction factor to be subtracted from the values of log s_W.

For all later recordings of the signal strengths from the standard tungsten lamp, the masked entrance slit of height less than 4 mm was used, so that no correction factor was needed.

Table 2-5
Comparison of Signal Strengths for Masked Slit and Full Slit, Using U-21 Tungsten Lamp and 1P28 Phototube

Wavelength	S_1 Full Slit	S_2 Masked Slit	S_2/S_1
6075A	.6994	.1656	.237
5825	1.189	.2816	.237
5575	1.491	.3575	.239
5325	2.196	.5355	.244
5075	1.774	.4290	.242
4825	1.332	.3250	.244
4575	.9486	.2275	.240
4325	.5888	.1428	.243
4075	.3179	.0775	.244
3825	.1453	.0352	.242

RESULTS

The spectral distribution of energy of the mercury-xenon lamp as obtained from one series of experiments is given in Table 2-6. The intensity values are on the logarithmic scale. The value of log I_H was obtained from the expression

$$\log I_H = \log s_H + (\log I_W - \log s_W).$$

Values of log I_W, for the standard lamp for wavelengths at 25A intervals, were obtained from the NBS calibration table, using the method of linear interpolation. The signals s_W were measured at intervals of 125A; values log s_W for wavelengths at smaller intervals

Table 2-6
Spectral Irradiance of Hg-Xe Lamp U-187 with Photomultiplier Tube 1P28
(I_H in microwatts per steradian, per manometer, per mm^2 of source, in a direction normal to the axis of the lamp)

λ	log I_H	λ	log I_H	λ	log I_H	λ	log I_H	λ	log I_H	λ	log I_H	λ	log I_H
3603	3.37	3807	3.31	4011	3.16	4216	3.18	4420	3.34	4624	3.17	4828	3.11
3607	3.44	3811	3.24	4016	3.19	4220	3.10	4424	3.32	4628	3.13	4832	3.12
3611	3.55	3816	3.33	4020	3.27	4224	3.10	4428	3.30	4632	3.18	4836	3.17
3616	3.64	3820	3.45	4024	3.36	4228	3.10	4432	3.28	4636	3.16	4841	3.10
3620	3.71	3824	3.26	4028	3.41	4232	3.10	4436	3.25	4641	3.10	4845	3.10
3624	3.79	3828	3.22	4032	3.47	4236	3.10	4441	3.23	4645	3.10	4849	3.10
3628	3.93	3832	3.19	4036	4.05	4241	3.11	4445	3.22	4649	3.10	4853	3.18
3632	4.12	3836	3.19	4041	4.41	4245	3.12	4449	3.21	4653	3.00	4857	3.11
3636	4.47	3841	3.12	4045	4.62	4249	3.12	4453	3.20	4657	3.10	4861	3.10
3641	4.71	3845	3.12	4049	4.63	4253	3.13	4457	3.20	4661	3.10	4866	3.10
3645	4.75	3849	3.22	4053	4.16	4257	3.14	4461	3.20	4666	3.10	4870	3.18
3649	4.06	3853	3.29	4057	4.01	4261	3.15	4466	3.18	4670	3.25	4874	3.18
3653	4.72	3857	3.50	4061	3.81	4266	3.16	4470	3.17	4674	3.28	4878	3.10
3657	4.83	3861	3.35	4066	3.61	4270	3.17	4474	3.17	4678	3.17	4882	3.19
3661	4.76	3866	3.18	4070	3.49	4274	3.19	4478	3.16	4682	3.12	4886	3.19
3666	4.59	3870	3.21	4074	3.93	4278	3.21	4482	3.15	4686	3.17	4891	3.19
3670	4.36	3874	3.22	4078	4.35	4282	3.24	4486	3.14	4691	3.17	4895	3.18
3674	4.21	3875	3.23	4082	3.86	4286	3.26	4491	3.13	4695	3.18	4899	3.10
3678	4.29	3882	3.24	4086	3.39	4291	3.30	4495	3.13	4699	3.10	4903	3.13
3682	4.38	3886	3.26	4091	3.31	4295	3.34	4499	3.21	4703	3.10	4907	3.18
3686	4.20	3891	3.31	4095	3.29	4299	3.39	4503	3.13	4707	3.15	4911	3.41
3691	4.06	3895	3.35	4099	3.26	4303	3.44	4507	3.11	4711	3.15	4916	3.87
3695	3.89	3899	3.40	4103	3.25	4307	3.50	4511	3.10	4716	3.14	4920	3.83
3699	3.84	3903	3.45	4107	3.32	4311	3.51	4516	3.17	4720	3.14	4924	3.35
3703	3.81	3907	3.48	4111	3.33	4316	3.49	4520	3.10	4724	3.14	4928	3.24
3707	3.77	3911	3.58	4116	3.28	4320	3.47	4524	3.12	4728	3.10	4932	3.18
3711	3.72	3916	3.42	4120	3.26	4324	3.49	4528	3.16	4732	3.19	4936	3.15
3716	3.66	3920	3.37	4124	3.22	4330	3.62	4532	3.10	4736	3.00	4941	3.16
3720	3.57	3924	3.32	4128	3.20	4332	3.73	4536	3.10	4741	3.16	4945	3.13
3724	3.57	3925	3.27	4132	3.17	4336	3.93	4541	3.10	4745	3.11	4949	3.17
3728	3.53	3932	3.24	4136	3.16	4341	4.11	4545	3.12	4749	3.10	4953	3.34
3732	3.50	3936	3.20	4141	3.14	4345	4.31	4549	3.12	4753	3.01	4957	3.76
3736	3.47	3941	3.18	4145	3.12	4349	4.39	4553	3.16	4757	3.05	4961	3.57
3741	3.43	3945	3.16	4149	3.10	4353	4.67	4557	3.10	4761	3.05	4966	3.16
3745	3.44	3949	3.15	4153	3.08	4357	4.74	4561	3.18	4766	3.04	4970	3.18
3749	3.57	3953	3.15	4157	3.07	4361	4.87	4566	3.17	4770	2.95	4974	3.18
3753	3.56	3957	3.13	4161	3.06	4366	4.70	4570	3.18	4774	3.04	4978	3.10
3757	3.36	3961	3.12	4166	3.06	4370	4.74	4574	3.10	4778	3.05	4982	3.19
3761	3.32	3966	3.12	4170	3.06	4374	4.26	4578	3.19	4782	3.04	4986	3.18
3766	3.39	3970	3.12	4174	3.05	4378	4.03	4582	3.11	4786	3.05	4991	3.14
3770	3.50	3974	3.12	4178	3.11	4382	3.84	4586	3.16	4791	3.05	4995	3.17
3774	3.31	3978	3.13	4182	3.10	4386	3.74	4591	3.00	4795	3.05	4999	3.12
3778	3.29	3982	3.32	4186	3.10	4391	3.68	4595	3.14	4799	3.05	5003	3.17
3782	3.38	3986	3.12	4191	3.18	4395	3.62	4599	3.11	4803	3.16	5007	3.16
3786	3.64	3991	3.12	4195	3.10	4399	3.55	4603	3.10	4807	3.15	5011	3.15
3791	3.54	3995	3.13	4199	3.16	4403	3.50	4607	3.10	4811	3.16	5016	3.16
3795	3.36	3999	3.14	4203	3.11	4407	3.45	4611	3.15	4816	3.13	5020	3.16
3799	3.28	4003	3.14	4217	3.11	4411	3.41	4616	3.16	4820	3.56	5024	3.19
3803	3.29	4007	3.15	4219	3.11	4416	3.38	4620	3.18	4824	3.16	5028	3.10

Table 2-6 (Continued)

λ	log I_H	λ	log I_H	λ	log I_H	λ	log I_H	λ	log I_H	λ	log I_H	λ	log I_H
5032	3.18	5245	3.17	5457	4.58	5670	3.32	5878	3.49	6086	3.20	6295	3.28
5036	3.19	5249	3.16	5461	4.79	5674	3.34	5882	3.58	6091	3.19	6299	3.29
5041	3.03	5253	3.16	5466	4.86	5678	3.34	5886	3.56	6095	3.19	6303	3.29
5045	3.27	5257	3.17	5470	4.72	5682	3.35	5891	3.62	6099	3.19	6307	3.30
5049	3.13	5261	3.16	5474	4.34	5686	3.37	5895	3.46	6103	3.19	6311	3.30
5053	3.19	5266	3.17	5478	4.36	5691	3.38	5899	3.31	6107	3.19	6316	3.30
5057	3.16	5270	3.17	5482	4.22	5695	3.40	5903	3.82	6111	3.19	6320	3.30
5061	3.15	5274	3.17	5486	3.98	5699	3.42	5907	3.37	6116	3.21	6324	3.29
5066	3.15	5278	3.17	5491	3.84	5703	3.44	5911	3.35	6120	3.29	6328	3.30
5070	3.14	5282	3.17	5495	3.71	5707	3.46	5916	3.34	6124	3.26	6332	3.31
5074	3.05	5286	3.17	5499	3.64	5711	3.52	5920	3.33	6128	3.19	6336	3.30
5078	3.05	5291	3.18	5503	3.58	5716	3.57	5924	3.33	6132	3.18	6341	3.31
5082	3.05	5295	3.18	5507	3.59	5720	3.61	5928	3.32	6136	3.19	6345	3.31
5086	3.05	5299	3.18	5511	3.50	5724	3.66	5932	3.32	6141	3.19	6349	3.31
5091	3.05	5303	3.18	5516	3.50	5728	3.72	5936	3.30	6145	3.19	6353	3.31
5095	3.04	5307	3.18	5520	3.46	5732	3.79	5941	3.30	6149	3.20	6357	3.32
5099	3.04	5311	3.12	5524	3.43	5736	3.86	5945	3.29	6153	3.20	6361	3.33
5103	3.04	5316	3.11	5528	3.41	5741	3.96	5949	3.29	6157	3.20	6366	3.33
5107	3.05	5320	3.11	5532	3.40	5745	3.80	5953	3.28	6161	3.10	6370	3.32
5111	3.05	5324	3.12	5536	3.37	5749	4.18	5957	3.27	6166	3.21	6374	3.33
5116	3.05	5328	3.13	5541	3.36	5753	4.34	5961	3.20	6170	3.21	6378	3.34
5120	3.04	5332	3.13	5545	3.34	5757	4.51	5966	3.26	6174	3.21	6382	3.34
5124	3.15	5336	3.19	5549	3.34	5761	4.71	5970	3.26	6178	3.23	6386	3.34
5128	3.26	5341	3.15	5553	3.21	5766	4.87	5974	3.25	6182	3.23	6391	3.34
5132	3.15	5345	3.16	5557	3.21	5770	4.87	5978	3.24	6186	3.23	6395	3.33
5136	3.17	5349	3.18	5561	3.30	5774	4.70	5982	3.24	6191	3.24	6399	3.35
5141	3.16	5353	3.20	5566	3.29	5778	4.52	5986	3.24	6195	3.24	6403	3.37
5145	3.16	5357	3.26	5570	3.28	5782	4.61	5991	3.23	6199	3.25	6407	3.37
5149	3.16	5361	3.42	5574	3.27	5786	4.84	5995	2.95	6203	3.24	6411	3.38
5153	3.15	5366	3.47	5578	3.27	5791	4.84	5999	2.13	6207	3.24	6416	3.38
5157	3.15	5370	3.34	5582	3.26	5795	4.67	6003	3.21	6211	3.25	6420	3.37
5161	3.15	5374	3.26	5586	3.26	5799	4.49	6007	3.20	6216	3.24	6424	3.38
5166	3.15	5378	3.26	5591	3.27	5803	4.41	6011	3.20	6220	3.26	6428	3.38
5170	3.16	5382	3.26	5595	3.26	5807	4.37	6016	3.20	6224	3.26	6432	3.39
5174	3.02	5386	3.26	5599	3.59	5811	4.30	6020	3.20	6228	3.27	6436	3.39
5178	3.17	5391	3.28	5603	3.26	5816	4.21	6024	3.19	6232	3.27	6441	3.30
5182	3.17	5395	3.39	5607	3.26	5820	4.13	6028	3.19	6236	3.28	6445	3.41
5186	3.02	5399	3.33	5611	3.26	5824	3.99	6032	3.19	6241	3.27	6449	3.41
5191	3.15	5403	3.35	5616	3.26	5828	3.94	6036	3.20	6245	3.17	6453	3.41
5195	3.15	5407	3.34	5620	3.27	5832	3.88	6041	3.21	6249	3.25	6457	3.42
5199	3.18	5411	3.34	5624	3.26	5836	3.82	6045	3.21	6253	3.26	6461	3.43
5203	3.03	5416	3.45	5628	3.26	5841	3.76	6049	3.21	6257	3.26	6466	3.43
5207	3.14	5420	3.49	5632	3.26	5845	3.71	6053	3.21	6261	3.27	6470	3.44
5211	3.15	5424	3.44	5636	3.36	5849	3.66	6057	3.21	6266	3.26	6474	3.44
5216	3.14	5428	3.47	5641	3.27	5853	3.62	6061	3.21	6270	3.26	6478	3.46
5220	3.14	5432	3.53	5645	3.27	5857	3.58	6066	3.21	6274	3.27	6482	3.44
5224	3.15	5436	3.62	5649	3.28	5861	3.55	6070	3.23	6278	3.27	6486	3.54
5228	3.15	5441	3.74	5653	3.28	5866	3.53	6074	3.24	6282	3.28	6491	3.48
5232	3.17	5445	3.91	5657	3.28	5870	3.51	6078	3.21	6286	3.28	6495	3.46
5236	3.15	5449	3.98	5661	3.29	5874	3.48	6082	3.21	6291	3.28	6499	3.46
5241	3.16	5453	4.38	5666	3.30								

of 25A were also obtained by the method of linear interpolation. A graph was plotted for $\log I_W - \log s_W$ versus wavelength. This graph served as the calibration curve for any given set of measurements on the mercury-xenon lamp, for conversion of the digitizer voltages into absolute intensity values.

The values for s_H were printed out for approximately every 2A; two successive printouts were averaged on each of two different runs, and the average of both runs was taken. Printouts which were skipped because of hunting decimals were supplied by interpolation. The wavelengths were calculated from the time indicated by the clock printer. The values of s_H thus represent the average over a small-wavelength range of 4A in most cases, and 5A in a few cases.

The units for I_H are the same as those of I_W, namely, microwatts per steradian per nanometer per mm^2 of source.

The series of experiments whose results are presented in Table 2-6 was made with the photomultiplier tube 1P28, and with the standard lamp U-187. Another series of experiments was made with the same standard lamp, but with the phototube 9592B. Two more series of runs were made using the same two phototubes but a different standard lamp, U-21. Extensive tabulations have been made of the results of these three additional series of runs; these lengthy tables have not been included in the present report, because they do not add significantly to the foregoing analysis of the spectrum. Their main value is that they serve as a check on the internal consistency of the results.

Upon comparison of the four series of runs, or different runs in the same series, the total light output of the mercury-xenon lamp is seen to change considerably. A small increase in the wattage input of the lamp does not necessarily mean an increase in the light output. The lamp operates steadily for long intervals of time and there is no indication of the energy distribution shifting from the line spectrum to the continuum and vice versa, or from one spectral range to another. In other words, the total intensity goes up or down without any noticeable change in the relative spectral distribution of energy.

This result is significant in the use of these lamps for solar simulation. Once the spectral distribution of the lamp has been carefully determined, for matching absorption of energy on the test floor to that in outer space, it will be sufficient to monitor the total irradiance of energy on the test floor. On the other hand, the total irradiance should be directly measured and cannot be computed as a function of the wattage input of the lamps. These two conclusions should, however, be considered tentative for the present, and should be tested by more rigorous methods.

As a check on the internal consistency of the measurements, the data from two series of runs with the two phototubes, and with the same U-21 tungsten lamp, were compared. The values of $\log I_H$ from phototube 1P28 were on an average higher than those

from phototube 9592B, meaning that the total light output of the lamp was higher in the former case. The average of the difference calculated from 83 pairs of values was 0.030. Most of these values were taken from the continuum of the spectrum, because the sampling of printouts around the peaks did not permit matching of wavelengths. The mean deviation of the differences around 0.03 was 0.024. Thus we conclude that during the runs with the 1P28 tube the lamp was burning 7.2 percent more brightly (log 1.072 = .030), and that the average deviation in the intensity values on a relative scale is 5.7 percent. Since wavelength assignments for the printouts were highly uncertain, it appears that a major part of the 5.7 percent deviation is spurious. Comparison of successive runs with the pen recorder shows that on the relative scale the average error is of the order of 1 or 2 percent.

The charts made by the pen recorder showed several interesting features: There is a strong continuum whose energy is practically the same for every 100A band throughout the spectral range. Superposed on the continuum are the strong emission lines, many of which are obviously due to atomic mercury and xenon. A listing of all the spectral lines clearly distinguishable from the continuum is given in Table 2-7. Lines whose wavelengths are listed only to four significant figures are unclassified, and the wavelengths are estimates from the relative positions of the lines with respect to the known lines of mercury and xenon. The unclassified lines are of intensity comparable to the lines of xenon. The xenon lines are on the average of intensity about one-tenth that of the five groups of strong mercury lines. The intensities of the lines in Table 2-7 are in arbitrary units: I_1, quoted from the "Handbook of Chemistry and Physics," and I_2, measured approximately from the pen-recorder charts of the mercury-xenon lamp.

The profiles of the mercury lines are shown in Figure 2-5. All the strong mercury lines show clearly the self-reversal effect. The line which originates in the high-temperature plasma between the electrodes is very intense. It has also a large halfwidth of about 10 or 20A. The profile of the line is highly asymmetric, and is intermediate between the Holtsmark profile due to statistical broadening and the Weisskopf profile due to collision broadening. There is also a considerable amount of Doppler broadening, characteristic of the high temperature of the plasma. Surrounding the plasma is mercury vapor at a lower temperature which absorbs a part of the energy from the central part of the emission line. A dip appears in the middle of the line; the wavelength of the lowest point of the dip is very close to that of the sharp emission line of a low-pressure discharge.

A comparison between the results of these measurements and the data reported earlier from Westinghouse and Hanovia would be instructive. A direct comparison is not possible because the earlier data do not give the spectral distribution within wavelength ranges smaller than 100A; the present data, on the other hand, cover a limited range (3500 to 6500A) and give the spectral irradiance in one particular direction, and of only that part of the source which is focussed on the slit. The earlier data cover the

Table 2-7
Emission Lines in the Spectrum of the Hg-Xe Lamp
(I_1 intensity from literature; I_2, intensity from the photoelectric recording. In arbitrary units.)

λ	I_1	I_2	Element
3341.48	100	550	Hg
3350		20	
3385.25	200	70	Hg
3349		40	
3516		20	
3542		300	
3543.08	40	50	Hg
3559		250	
3578.75	40	30	Hg
3604.09	50	50	Hg
3605.80	200	500	Hg
3650.15	500	3000	Hg
3662.88	400	1700	Hg
3663.28	400	1700	Hg
3750		350	
3753		50	
3769		100	
3789		400	
3806.38	200	20	Hg II
3819		250	
3858		120	
3897		40	
3902		60	
3908		100	
3914.29	100	20	Hg
3918.92	200	10	
3983.98	400	900	Hg II
4008		20	
4046.56	200	3000	Hg
4077.81	150	2000	Hg
4094		10	
4110		60	
4140.38	200	10	Hg
4193.15	200	20	Xe
4193.53	150	10	Xe
4339.23	150	400	Hg
4347.50	200	1000	Hg
4358.35	3000	6000	Hg
4500.98	500	150	Xe
4524.21	400	100	Xe
4582.75	300	20	Xe
4624.28	1000	70	Xe
4671.23	2000	250	Xe
4690.97	100	10	Xe
4697.02	300	30	Xe
4734.15	600	250	Xe
4792.62	150	10	Xe
4807.02	500	100	Xe
4829.71	400	50	Xe
4843.29	300	20	Xe
4916		1200	
4916.51	500		Xe
4916.04	50		Hg
4960		700	
5028.28	200	40	Xe
5047		30	
5368.07	100	150	Xe II
5405		30	
5460.74	2000	6000	Hg
5769.59	600	5000	Hg
5789.66	500	5000	Hg
5790.65	1000	5000	Hg
5889		100	
6123		30	

whole spectral range and give the integrated result of the radiation from the whole source in all directions.

However, a meaningful comparison may be attempted in the following way: The antilogarithm of the values in Table 2-6 gives the intensity I_H in microwatts per steradian per mm^2 of the source for a 10A range. To find the total energy radiated in the spectral range covered by the data, multiply I_H by 0.4 or 0.5 (depending on whether the wavelength intervals are 4A or 5A) and add all the values together. The results from the tube 9592B

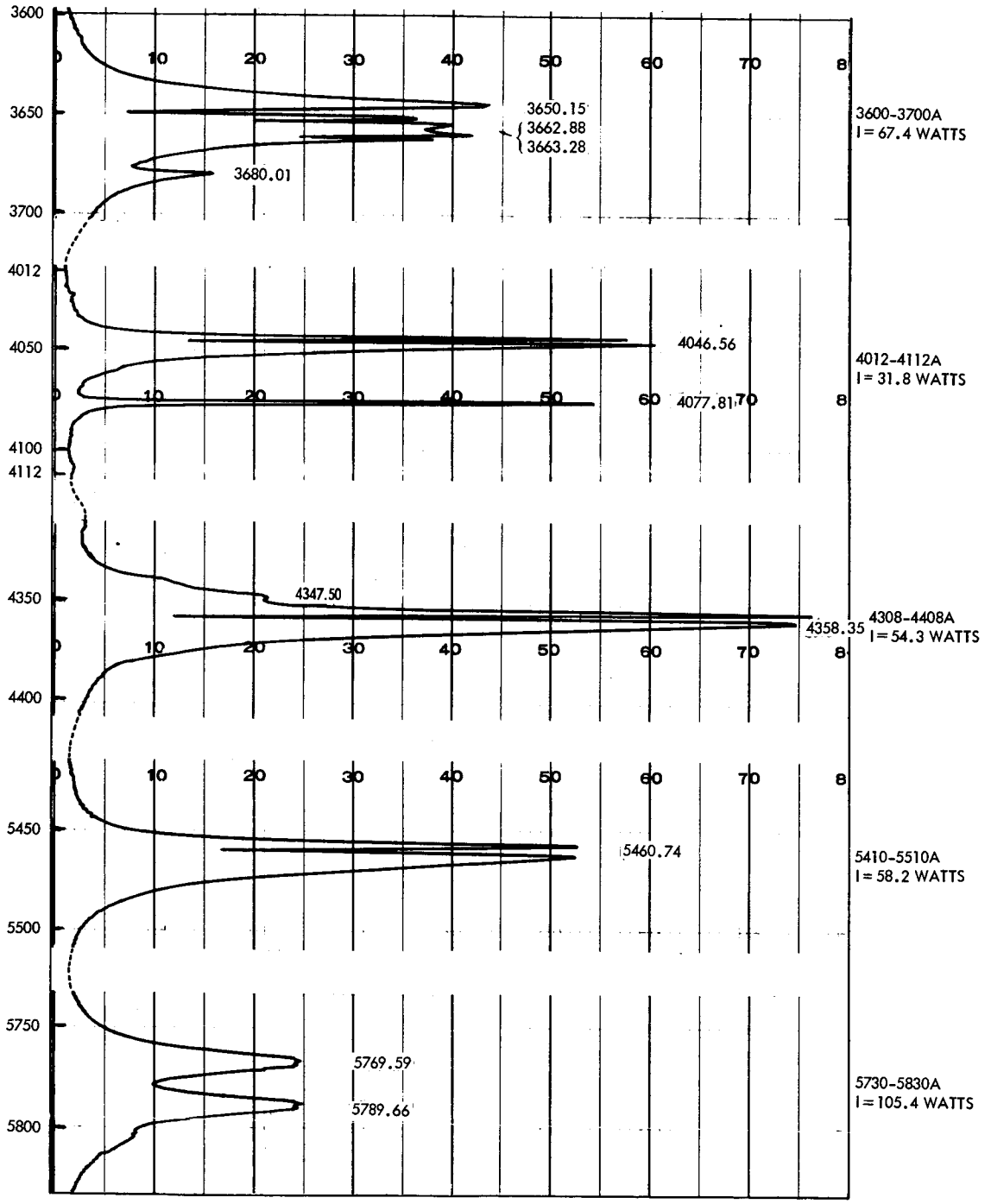

Figure 2-5 - Profiles of strong mercury lines, Hg-Xe lamp

do not cover the range 3500 to 3600A; therefore, the total for 3600 to 6500A must be considered. If the values from the two sets of data (for 1P28 tube and 9592B tube) are averaged, the lamp is found to emit 1.2295 watts in the spectral range 3600–6500A per mm^2 of the surface of the source per unit solid angle in a direction normal to the axis of the tube.

Now consider an idealized source, uniformly bright sphere which radiates the same amount of energy in all directions. In the actual source, these assumptions are only approximately valid, because the irradiance along the axis of the tube is less than that along the normal, and the irradiance from the periphery of the plasma is less than that from the center. Let r be the radius and A ($= \pi r^2$) the area of cross section of the idealized source. The total radiant energy in all directions from the whole source = 1.2295 watts/ $mm^2 \times 4\pi \times$ A watts.

From the Westinghouse data, the energy radiated in the range 3500 to 6500A is 412.2 watts; the Hanovia data for the same range gives the value 534.6 watts. The average of the two is 473.4 watts; deducting from this 10 watts (the average of the two sets of data for 3500 to 3600A), the result is 463.4 watts.

It seems reasonable to assume that the relative spectral distribution is independent of the power level at which the tube is operated. The total radiation in these measurements could well be made equal to 463.4 watts by a slight adjustment of the power level. This produces the equation

$$1.2295 \ \frac{\text{watts}}{mm^2} \times 4\pi A = 463.4 \text{ watts}$$

Whence $A = 29.99 \ mm^2$ or $r = 2.9$ mm.

This value is of the right order of magnitude.

To obtain from the present data a set of values normalized to the same total energy as the Hanovia-Westinghouse data, all values of I_H should be multiplied by $29.933 \times 4\pi / 10 = 37.69$. This would give the energy radiated in microwatts by the whole lamp in all directions per spectral range of 1 angstrom.

This procedure of normalization leads to certain other significant results.

Of the total energy of 463.4 watts in the range 3600 to 6500A, a major part is concentrated in five short spectral ranges around the strong emission lines of mercury. These ranges are shown in Figure 2-5 mentioned earlier. For purposes of comparison with the Westinghouse-Hanovia data, a wavelength band of 100A was chosen for each line or group of lines, and the total energy emitted in each band was calculated. The results are presented in Table 2-8 along with those interpolated from the Westinghouse and Hanovia data.

Table 2-8
Energy Due to the Line Spectrum

Wavelength Band A	Strong Hg Lines A	Spectral Radiance in Walls		
		Ours	Westinghouse	Hanovia
3600 - 3700	3650, 3662, 3663	67.4	43.8	46.9
4012 - 4112	4046, 4077	31.8	37.6	33.1
4308 - 4408	4347, 4358	54.3	50.6	41.2
5410 - 5510	5460	58.2	44.9	82.5
5730 - 5830	5770, 5790	105.4	47.9	104.7

The energy in these five wavelength ranges combined is 317.1 watts, about 68 percent of the total energy in the range 3600 to 6500A. The rest of the energy, 32 percent, is distributed over the continuum. Over most of the continuum the energy in each 100A range is the same. It varies between 0.8 percent and 1.4 percent of the total energy. The average energy per 100A range is 1.1% of the total, that is, 5.1 watts. The spectral distribution curve of the solar energy, normalized to the same total output as the 2.5-kw mercury-xenon lamp, gives for the region between 4000 and 6500A an average irradiance of 23.7 watts per 100A range. Thus it is seen that, if the total radiant energy from the mercury-xenon lamp is adjusted to be the same as that due to solar radiation in outer space, the energy input on the test floor of a solar simulator is only one-fifth that of the solar energy over a large part of the spectral continuum, while it is 25 times greater than the solar energy over five narrow wavebands each of about 10 or 20A. This significant difference between the spectral distributions of the solar radiation and the Hg-Xe lamp radiation clearly shows the necessity for accurate determination of the spectral quality of the radiation incident on the test floor of the simulator.

REFERENCES

1. Solar Simulators, A. E. Mann and Michael Dubey, Technical Staff, Spectrolab Division, Textron, Inc. Space Aeronautics, March 1962.

2. Johnson, Francis S., "Satellite Environment Handbook," Stanford University Press, 1961, p. 69, where references to earlier literature are given.

3. Pivovonsky and Nagel, "Tables of Blackbody Radiation Functions," McMillan Company, New York, 1961.

4. J. C. DeVos, "A new determination of the emissivity of tungsten ribbon," Physica, 20, 690 and 715 (1954).

   Robert D. Larrabee, "Spectral emissivity of tungsten," J. Opt. Soc. Am. 49, 619 (1959).

   R. D. Allen, L. F. Glasier, and P. L. Jordan, "Spectral emissivity, total emissivity, and thermal conductivity of molybdenum, tantalum and tungsten above 2300°K," J. Applied Physics, 31, 1382 (1960).

5. Fastie, W. G., "Image-forming properties of the Ebert monochromator," J. Opt. Soc. Am. 42, 647 (1952).

Fastie, W. G., "Experimental performance of curved slits," J. Opt. Soc. Am. 43, 1174 (1953).

PART III

HEAT TRANSFER AND CRYOGENIC PUMPING IN SPACE SIMULATION

CONTENTS

III Heat Transfer and Cryogenic Pumping in Space Simulation

ILLUSTRATIONS

TABLES

PART III

HEAT TRANSFER AND CRYOGENIC PUMPING IN SPACE SIMULATION

PRELIMINARY STATEMENT

(J. H. Boeckel, Associate Chief, Test and Evaluation Division, GSFC)

While there is a good deal of glamor attached to the space program and our contribution to it, our work in the end is largely the application and extension of basic engineering diciplines. I would like to discuss two such areas in which I feel the Summer Workshop could make a fruitful contribution.

First, simulation of the space environment requires that the test object "see" the blackness of space while subjected to a very low pressure. To simulate black space, the temperature of the chamber walls needs to be below 100°K; Liquid Nitrogen (LN_2) provides an excellent heat-transfer medium at these temperatures. Once an extended area of LN_2 surface has been introduced into the chamber, one soon realizes that water vapor, the bete noir of high vacuum, will condense on these panels and will in effect be pumped from the system. Further, with LN_2 available as a thermal shield, it becomes practical to operate a gaseous helium (GHe) system at a temperature of about 20°K to condense nearly all the remaining gases.

Cryogenic pumping in this manner has received a good deal of attention. However, logical design of a system depends heavily on the actual gases which must be removed. I feel that identification of the constituents of the atmosphere within a space simulator is a matter of great importance. When this has been accomplished, the study can then be extended to cover the manner in which these gases are best pumped.

Second, simulation of the space environment requires the provision of a source of thermal radiation which simulates the input from the sun. We now have what we believe to be a good optical design for a solar simulator; however, the engineering practicality of the system remains in question. In particular, the energy balance in a system which dissipates some 800 kilowatts in a confined area deserves careful analysis. Optical tolerances, vacuum seals, material properties may all depend heavily on how the excess energy is channeled. This analysis clearly leads to many other problems in the engineering design of the solar simulator.

Although I have cited two specific questions whose study I believe would be rewarding, we hope for a greater benefit from this program than the generation of two isolated pieces of information. In our group we are very close to the turmoil of last-minute operations in getting a satellite ready for launching. Thus we are somewhat concerned that, in our evaluation of our needs, we have in the press of circumstances overlooked important unresolved problems. We believe that the Summer Workshop may well uncover some of these for us.

Last, as Dr. Goett said earlier, we feel that contact with the local scientific community can be of great mutual benefit over a long period of time. The Summer Workshop gives us an excellent opportunity to get to know each other, our capabilities, and our goals, so that both groups can expect quick and effective response in the future when either has a problem and turns to the other for help.

SECTION A

CRYOGENIC PUMPING AND VACUUM TECHNOLOGY

by

J. L. Shereshefsky, Murray Geller,
George Pick, and J. B. Crooks

ABSTRACT

This report includes a study of the vapor pressures of ice, water, solid and liquid CO_2, liquid Hg, and liquid CO at moderate and low temperatures. It is shown that Antoine's equation $\log P = A - B/(C + T)$ fits the data exceedingly well, and lends itself to more confident extrapolation.

The report contains an account of a cryosorption experiment at liquid-nitrogen and helium-vapor temperatures, with coconut charcoal as adsorbent. The pressures obtained at liquid-nitrogen temperature were 20 times lower than without the adsorbent, and about 200 times lower at the helium-vapor temperature.

It also includes an account of a new method of calibration of an ionization gauge; a discussion of several problems related to cryogenic pumping; and a review and bibliography of adsorption of common gases on steel and related metals.

INTRODUCTION

Within the broad frame of reference of "heat transfer and cryogenic pumping" which was the area of its concern, Team B has chosen to devote itself mainly to study and investigation of the following subjects:

- Vapor pressure and temperature relations of residual gases
- Cryosorption as a method of cryogenic pumping
- A method of calibration of ionization gauges in high vacuum
- A survey of the literature on adsorption of common gases on steel and other metals

It has also considered various problems related to analysis of residual gases, measurement of contamination on the surfaces of spacecraft, location of leaks in cryoliners at liquid-nitrogen temperature, and orientation of vacuum sensors in a space simulator.

VAPOR PRESSURE AND TEMPERATURE RELATIONS FOR RESIDUAL GASES

The purpose of this study was to assess the validity of existing equations for vapor pressure at low temperatures of the common gases and vapors occurring in the atmosphere and evolved by the various components of a vacuum chamber. Time limitations did not allow an extensive investigation. However, as shown in the following analysis, the Antoine equation when applied to liquid and solid H_2O and CO_2, liquid CO, and liquid Hg gives an extremely good fit over a wide range of temperatures and can be extrapolated with greater confidence than can the equations containing five constants which are presently in use.

Theoretically, one can start from the Clapeyron equation (which is exact)

$$\frac{dP}{dT} = \frac{\Delta H}{T\Delta V} \tag{1}$$

where

P = pressure
T = temperature
ΔH = enthalpy of phase change from solid→gas or liquid→gas
ΔV = change in volume from solid→gas or liquid→gas,

or

$$\frac{dP}{dT} = \frac{\Delta H}{T}\left(V_{gas} - V_{con}\right) \qquad \text{con. = condensed phase} \tag{2}$$

and since $V_{con} << V_{gas}$

$$\frac{dP}{dT} = \frac{\Delta H}{TV_{gas}} \sum_{i=0}^{\infty} \left(\frac{V_{con}}{V_{gas}}\right)^i \tag{3}$$

For the V_{gas}, we can use a virial expansion

$$PV_{gas} = \left(\sum_{i=0}^{\infty} b_i P^i\right) RT \tag{4}$$

where R = gas constant, b_i = virial coefficient.

Substituting (4) in (3) for V gas we obtain:

$$\frac{dP}{P} \sum_{i=0}^{\infty} b_i P^i = \frac{\Delta H}{RT^2}\, dT \sum_{i=0}^{\infty} \left(\frac{V_{con}}{V_{gas}}\right)^i . \tag{5}$$

A usual and extremely valid (except near critical point) assumption is to let

$$\frac{V_{con}}{V_{gas}} \simeq 0$$

so that the only major stumbling block to integration of Equation (5) is to find an expression (analytical or otherwise) for ΔH. A first approximation is to let ΔH = constant and $b_i = 0$ ($i=1, \ldots, 00$) and $b_o = 1$ so that we can integrate to obtain

$$\ln P = -\frac{\Delta H}{RT} + \text{Constant} \tag{6}$$

This is the celebrated Clausius - Clapeyron equation:
Instead of assuming ΔH= Constant, an exact expression is

$$\Delta H = \Delta Ho + \int_0^T \left(Cp_{gas} - Cp_{con}\right) dT \tag{7}$$

where

Cp = heat capacity

ΔHo = Constant of integration-enthalpy at absolute zero.

This produces (within the approximation of $V_{con}/V_{gas} = 0$) an exact expression for P vs T:

$$\ln P + b_i P + b_2 p^2 + \ldots = K - \frac{\Delta Ho}{RT} + \frac{1}{R}\int \frac{dT}{T^2}\left(\int_0^T \left(C_{P_{gas}} - C_{P_{con}}\right) dT\right) \tag{8}$$

Thus, an accurate determination of vapor pressures is possible at all temperatures, if the heat capacities are known well.

Using empirical expressions for heat capacities (see any standard thermodynamic text) as

$$Cp = A + BT + CT^2 \tag{9}$$

$$Cp = A^1 + B^1 T + C^1/T^2$$

or others (and this is a dangerous procedure for the range of validity is limited), an empirical expression for the vapor pressure vs temperature can be obtained in any of the forms:

$$\log P = A - \frac{B}{T} \tag{10}$$

$$\log P = A - \frac{B}{T} + C \log T$$

$$\log P = A - \frac{B}{T} + CT$$

$$\log P = A - \frac{B}{T} + C \log T + DT + FT^2 + \frac{G}{T^2}$$

The disadvantage of most (if not all) of these equations is that they are strictly limited to the range in which the empirical constants are evaluated, and cannot be extrapolated to lower temperatures (which is the case of interest to us!)

An empirical equation with the advantage that it can be extrapolated out of the region of determination of the constants is the Antoine equation

$$\log P = A - \frac{B}{C + T} \tag{11}$$

Rossini* claims that it is the best empirical equation for vapor pressure and is the most reliably extrapolated. What follows is an attempt to evaluate the constants for H_2O, CO_2, and CO, and to compare the calculated pressures with experimental values in other regions of the scale.

H_2O: Liquid-vapor pressure

$$\log P = 5.12146 - \frac{1696.7}{T - 42} \tag{12}$$

T (°K)	P (atm) predicted	P (atm) - exper.	% error
275	.006909	.006883	.38
300	.035081	.034844	.68
325	.13361	.13329	.24
350	.40988	.41069	.20
375	1.0623	1.0675	.49
400	2.4102	2.4232	.54
425	4.9137	4.9337	.41
450	9.1804	9.1968	.18
475	15.958	15.947	.07
500	26.113	26.050	.24
525	40.607	40.490	.29
550	60.461	60.387	.12
575	86.724	87.014	.33
600	120.44	121.88	1.18
625	162.62	166.93	2.58

.53 average % deviation

(Experimental data NBS Circular 564 (1955))

Solid - vapor pressure

$$\log P = 7.83158 - \frac{2792.5}{T + 5} \tag{13}$$

*Rossini-Chemical Thermodynamics

T (°K)	P (atm) predicted	P (atm) - exper.
270	$.0_2 4754$	$.0_2 4633$
260	$.0_2 1967$	$.0_2 1933$
250	$.0_3 7596$	$.0_3 751$
240	$.0_3 2714$	$.0_3 2696$
230	$.0_4 8884$	$.0_4 883$
220	$.0_4 2633$	$.0_4 262$
210	$.0_5 697$	$.0_5 687$
200	$.0_5 162$	$.0_5 158$
190	$.0_6 324$	$.0_6 32$
180	$.0_7 546$	$.0_7 5$
170	$.0_8 749$	$.0_8 7$
160	$.0_4 808$	$.0_4 8$
155	$.0_4 239$	$.0_4 3$

Empirical constants evaluated from 210-260;
rest of values are extrapolated
(Experimental data NBS Circular 564 (1955))

Using the same equation and changing units to mm

$$\log P\,mm = 10.71239 - \frac{2792.5}{t + 278.1} \qquad (14)$$

T (°C)	P mm predicted	P exper.	P. K. Kelley
-20	.7815	.776	.779
-30	.2863	.2859	.2931
-40	.09641	.0966	.0994
-50	.02951	.02955	.02985
-60	.008103	.00808	.00840
-70	.001965	.00194	.00198
-80	.000413	.00040	.000413
-90	$.0_4 736$	$.0_4 70$	$.0_4 745$
-100	$.0_4 108$		$.0_4 110$
-110	$.0_5 126$		$.0_5 125$
-120	$.0_6 112$		$.0_6 113$
-130	$.0_8 719$		$.0_8 698$
-140	$.0_9 310$		$.0_9 293$
-150	$.0_{11} 819$		$.0_{14} 74$
-183	$.0_{18} 223$		$.0_{21} 16$

The experimental values are taken from Handbook of Chemistry and Physics (&I.C.T.). Experimental values go down to -98°C, and in that range the predicted values agree exceedingly well (using Antoine-type equation). The column marked Kelley* is <u>not</u> experimental but based on the <u>accepted empirical</u> equation

$$\log P\,mm = 1.207 + 3.857 \log T + 3.41.10^{-3} T + 4.875.10^{-8} T2 - \frac{2461}{T} \qquad (15)$$

*Dushman-Vacuum Tech.

derived from ΔF expressions. Thus, although Kelley uses a five-constants expression, the values are less sure than the three-term empirical Antoine equation. Though both empirical equations may not be highly valid below -120°C, the Kelley expression yields much smaller values than the Antoine equation.

Preliminary calculations on solid CO_2 seem to indicate the same general results. The Antoine equation (16) gives an extremely good fit over a wide range and can be extrapolated, whereas the Kelley empirical equation (17)

$$\log P_{mm} = 9.4364 - \frac{1217.4}{t + 264.1} \tag{16}$$

$$\log P_{mm} = 8.882 + 0.8702 \log T - 3.891.10^{-3} T - \frac{1408}{T} \tag{17}$$

gives much too small values at low temperatures.

The results for solid CO_2 are as follows:

$$\log P_{mm} = 9.4364 - \frac{1217.4}{T - 9} \tag{18a}$$

T °K	P(pred.) mm	P(exp.) mm	% error
135	.595	.59	-
145	3.054	3.05	-
155	12.53	12.53	-
165	42.90	42.91	-
175	126.67	126.62	-
185	330.65	330.8	-
195	778.47	782.4	.5
200	1155.0	1165.8	1.18
205	1679.5	1706.4	1.58
210	2397.1	2457.9	2.47
215	3362.8	3491.4	3.68

Data from NBS-Circular 564 (1955).

Agreement is very good until the critical temperature 217°K is approached. Using the same equation, but putting it in the form of °C, produces

$$\log P_{mm} = 9.4364 - \frac{1217.4}{t + 264.2} \tag{18b}$$

Its application to the data of Meyers and Van Dusen is given in the following table.

T°C	P(pred.) mm	P (exp.) mm	% error	P (pred.) Kelley
-60	2982.6	3073.1	3.03	
-70	1471.0	1486.1	1.03	
-80	671.87	672.2	.05	
-90	280.48	279.5	.36	
-100	105.26	104.81	.43	
-110	34.791	34.63	.46	
-120	9.862	9.81	.53	
-130	2.317	2.31	.30	
-140	.4310	.431	-	
-150	.05973	.0605	1.29	.06194
-160	$.0_2 5664$	$.0_2 59$	4.00	$.0_2 730$
-170	$.0_3 326$	$.0_3 37$		$.0_3 382$
-180	$.0_4 0951$	$.0_4 13$		
-185	$.0_5 1162$	$.0_5 17$		
-189	$.0_6 18$	$.0_6 3$		

(Data from Meyers and Van Dusen, J. Res. NBS 10, 381 (1933))

Kelley uses the expression

$$\log P\,\text{mm} = 8.882 + .8702 \log T - 3.891.10^{-3} T - \frac{1408}{T} \tag{19}$$

derived from ΔF data, but this equation gives a very poor fit.

For liquid CO_2, the best Antoine constant is actually zero, which produces:

$$\log P\,\text{mm} = 7.57368 - \frac{861.7}{T} \tag{20}$$

This equation gives an average deviation of ±.33 percent over the liquid range from 216°K to 304°K, as shown in the table below.

T°K	P mm (pred)	P mm (exp.)	% error
220	4,538	4,500	.84
230	6,717	6,705	.18
240	9,622	9,625	.03
250	13,393	13,393	-
260	18,174	18,143	.17
270	24,110	24,023	.36
280	31,346	31,196	.48
290	40,022	39,865	.39
300	50,274	50,329	.11

(Data from NBS Circular 564 (1955))

The data for Hg (liquid) can best be represented by an Antoine equation:

$$\log P\,\text{mm.} = 7.70536 - \frac{2975.3}{t + 260} \tag{21}$$

t°C	P (pred) mm	P (exp) mm	% error
400	1575.2	1574.1	.06
370	960.86	960.66	.02
340	557.86	557.90	-
310	305.87	305.89	-
280	156.87	156.87	-
250	74.377	74.375	-
220	32.123	32.133	.03
190	12.405	12.423	.15
160	4.1813	4.189	.19
130	1.1923	1.186	.53
100	.2758	.2729	1.06
70	.04890	.04825	1.35
40	$.0_26133$	$.0_26079$	.90
20	$.0_21200$	$.0_21201$	-
0	$.0_31828$	$.0_3185$	1.19
-20	$.0_4203$	$.0_4181$	
-38.9	$.0_5177$	$.0_5124$	

Kelley gives an expression for liquid Hg:

$$\log P\,\text{mm} = 10.377 - .8254 \log T - \frac{3285}{T} \tag{22}$$

This expression gives very poor results, in comparison with the Antoine equation which holds extremely well over 9 decades of pressure.

The results for liquid CO, using the Antoine equation,

$$\log P\,\text{mm} = 6.74265 - \frac{303.57}{T - 3} \tag{23}$$

are given below:

	T (°K)	P (pred) mm	P (exp) mm	% error
Triple point	68.09	11.99	11.53	3.99
	70	162.85	158	3.07
	75	336.07	332	1.23
	80	631.26	629	.36
Boiling point	81.62	761.1	760	.15
	85	1,098.0	1,098	-
	90	1,792	1,796	.22
	95	2,773	2,780	.25
	100	4,103	4,110	.17
	105	5,841	5,840	.02
	110	8,046	8,040	.08
	115	10,770	10,770	-
	120	14,062	14,110	.34
	125	17,963	18,140	.97
	130	22,509	22,990	2.14
Critical point	132.88	25,430	26,242	3.10

Summary of constants in the Antoine equation for the several substances investigated:

$$\log P_{mm} = A - \frac{B}{T + C} \qquad (23a)$$

System	A	B	C
H_2O - liquid	5.12146	1696.7	-42
H_2O - ice	7.83158	2792.5	+5
CO_2 - liquid	7.57368	861.7	0
CO_2 - solid	9.4364	1217.4	-9
Hg - liquid	7.70536	2975.3	-13.2
CO - liquid	6.74265	303.57	- 3

SECTION B

CRYOSORPTION AS A METHOD OF CRYOGENIC PUMPING

INTRODUCTION

The cryopanels presently used in vacuum chambers and simulators are of limited surface area, adequate only for condensing the vapors in the residual gases. For condensing the noncondensible gases, the chambers must be equipped with active adsorbents having large specific surfaces. At low temperatues, these materials also tend to lower the vapor pressure of the condensible gases. The condensation process, whether of vapors by lowering the temperature, or of gases by adsorption, is nearly instantaneous under proper conditions and is in any case much faster than a diffusion pump. These materials can be easily incorporated in existing cryopanels, or cryopanels with surface properties of active adsorbents can be developed.

To demonstrate the applicability and effectiveness of cryosorption in cryogenic pumping, an inner shroud was designed and built into an existing vacuum chamber, and an experiment carried out as described below. It should be pointed out that the design and form of the shroud are far from ideal, and were conditioned by considerations of time, availability of material, and ready fabrication facilities.

DESCRIPTION OF EXPERIMENT

EXPERIMENTAL FACILITY. The experimental apparatus is shown in Figures 3-1 and 3-2. Testing was conducted in a stainless steel cylindrical vacuum chamber 22 inches in diameter, and 30 inches in height. It was equipped with an oil-vapor diffusion pump, type PMC-4100, backed by a mechanical pump, and included an aluminum cryopanel. The oil diffusion pump was equipped with a liquid nitrogen-cooled trap to prevent the oil vapors from diffusing into the test chamber.

The cryogenic fluid used in the cryopanel was liquid nitrogen, which entered under 3-4 lb/in^2 pressure from a pressurized container. The liquid nitrogen evaporated in the cryopanel and the vapor was vented out. No attempt was made to recover the nitrogen vapor.

TEST ARRANGEMENT. The experimental shroud assembly, mounted within the aluminum cryopanel as shown in Figure 3-3, was made of copper and consisted of 18

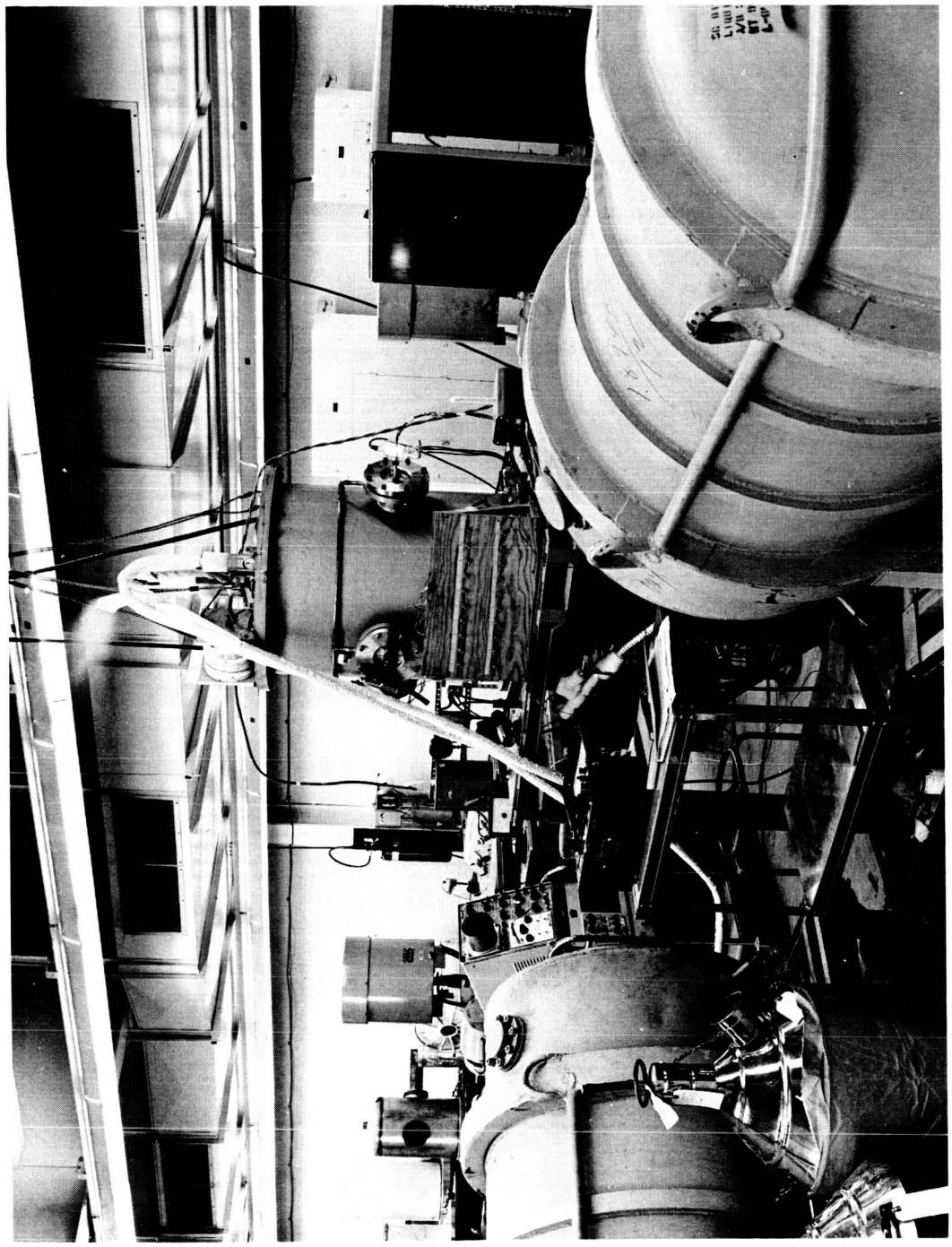

Figure 3-1 - Experimental apparatus, stainless steel vacuum test chamber

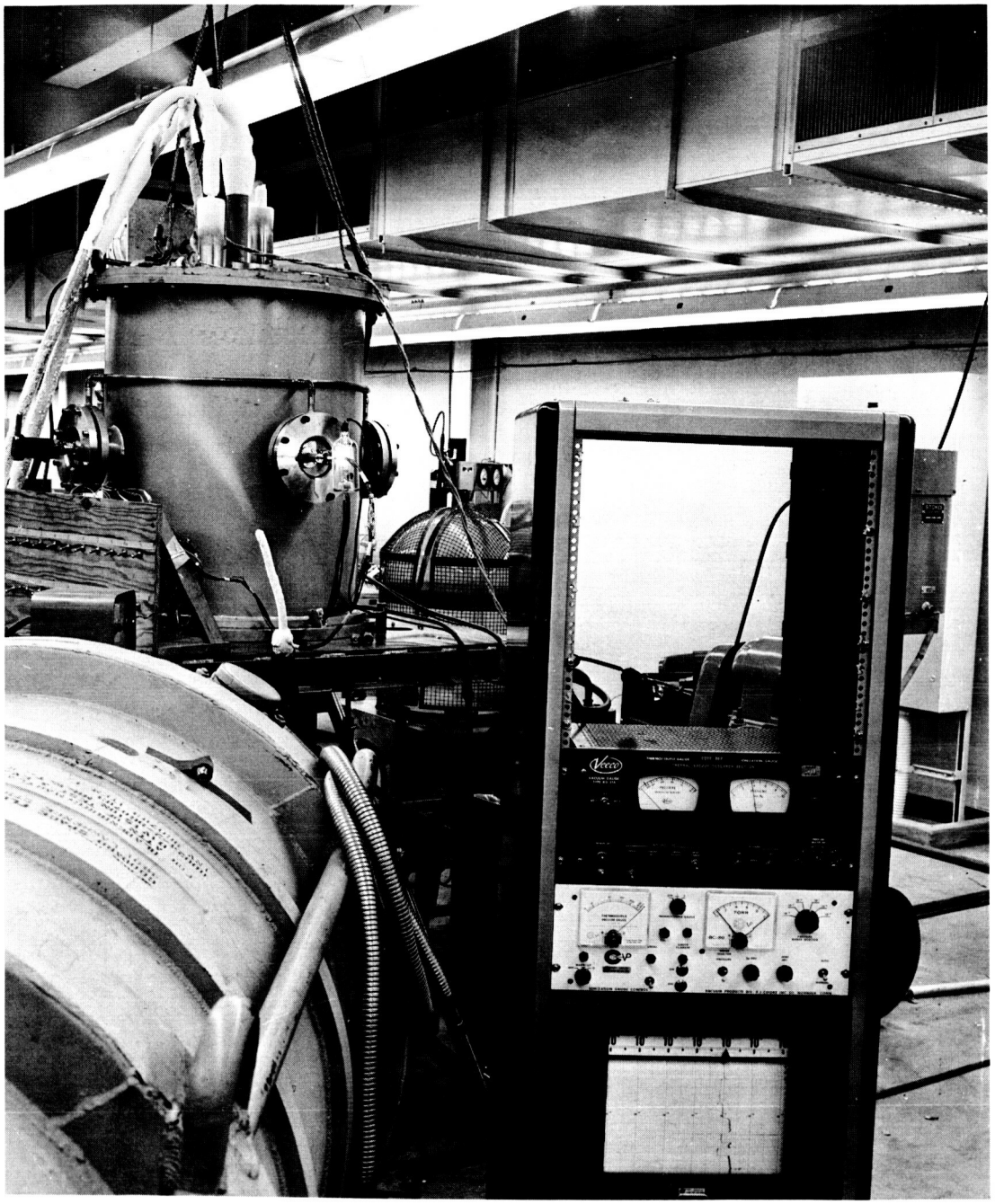

Figure 3-2 - Experimental apparatus, stainless steel vacuum test chamber

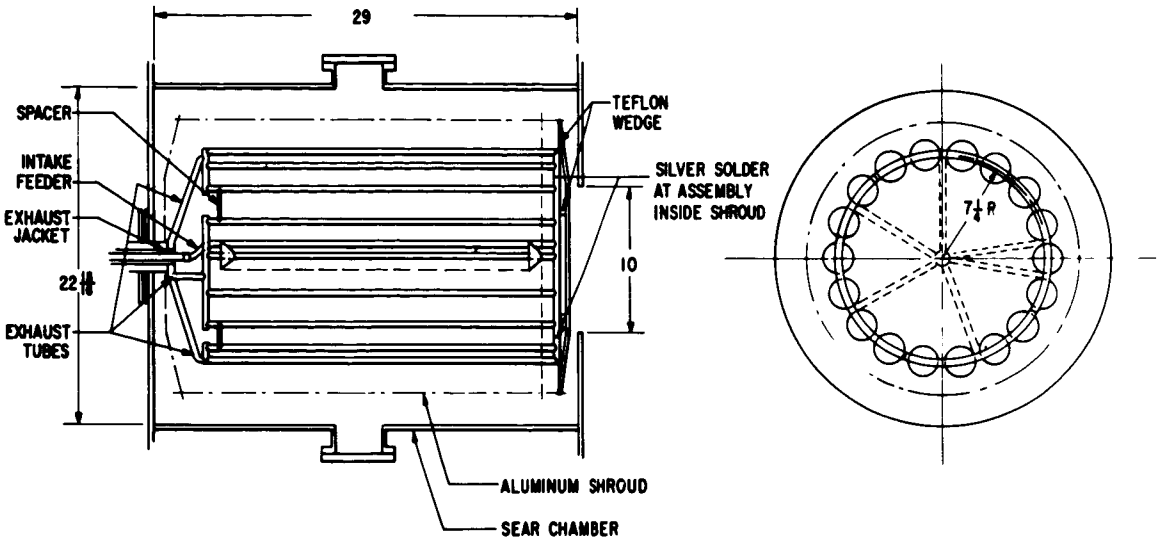

Figure 3-3 - Assembly of experimental shroud, diagram

vertical 3/8" O.D. tubes. The tubes formed five sections connected at the bottom of the assembly, approximating a cylindrical array. Total length of the tubes was approximately 35 feet.

Each tube was equipped with 29 cone-shaped cups which were silver-soldered at equal intervals along the length of the tube surface. Total number of cups was 532. The cups (13/16-inch deep, and 2 inches base diameter) were fabricated from 0.020-inch thick copper sheet material, and were formed on the lathe, using a die. Figure 3-4 shows the experimental shroud before installation, and Figure 3-5 is a detailed drawing of one section.

Deposited in the cups was a total amount of 2300 gm of activated coconut charcoal having a potential specific surface of 890 m^2/gm. To obtain low surface temperatures, liquid nitrogen was introduced in the tubes as a coolant (77°K); helium vapor was also used, providing an even lower temperature (~25°K). No attempt was made to recover the nitrogen or helium vapors.

INSTRUMENTATION. Pressure and temperature sensors were installed to provide information about the pressure and temperature distribution. Five pressure gauges provided pressure data in different locations. One thermocouple gauge measured the forepressure in the mechanical pump, and a similar gauge registered the pressure in the diffusion pump. In the test chamber, one thermocouple gauge registered the pressure from 1 mm to 1×10^{-3} mm/Hg. Below this pressure range, a Veeco tubular ionization gauge (in connection with a Veeco type RG-31A control panel) registered the pressure in the vicinity of the vacuum-chamber wall. In the middle of the test chamber, a nude gauge

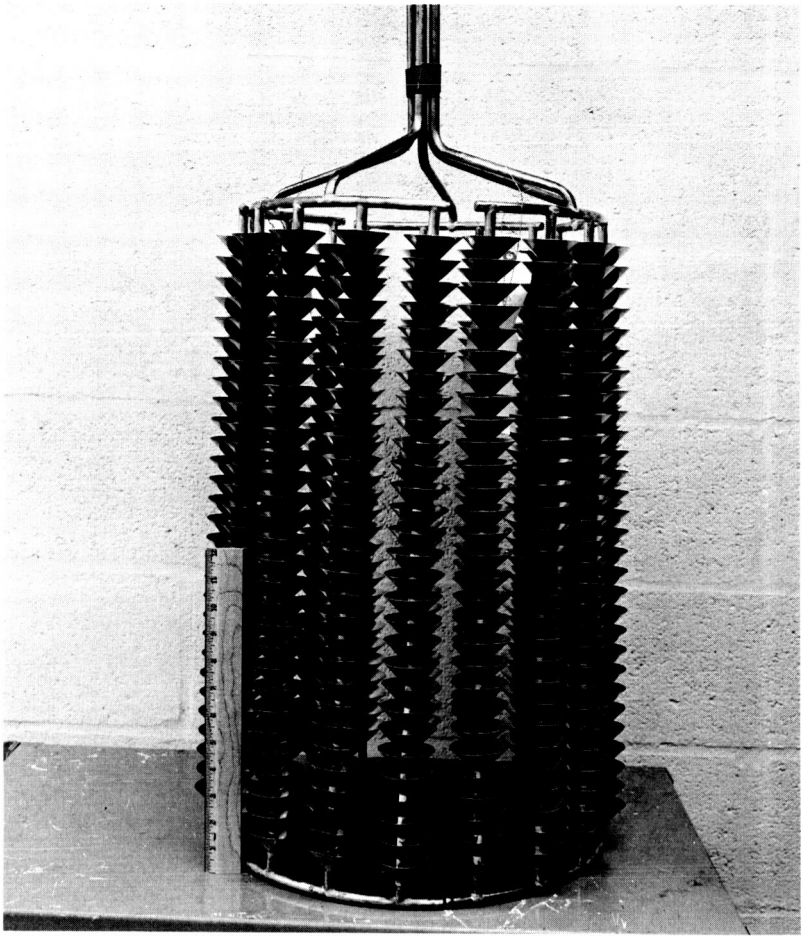

Figure 3-4 - Experimental shroud
before installation

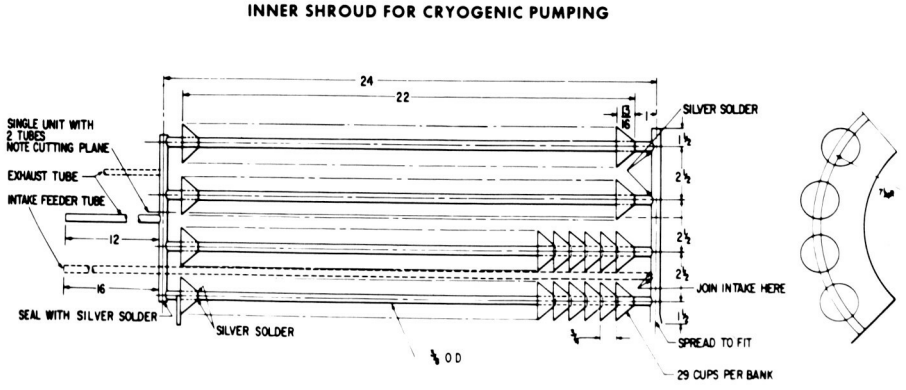

Figure 3-5 - Section of inner shroud, detailed drawing

was installed in connection with a Cooke ionization-gauge control panel. Both gauges were capable of measuring pressures between 10^{-4} to 10^{-9} mm/Hg.

The temperature distribution of the experimental shroud and of the cryopanel was observed by using 15 copper-constantan thermocouples (30 gauge) in connection with a switchboard, an ice junction, and a Minneapolis-Honeywell Model No. 2733 potentiometer. The measuring range of the potentiometer was between 0.005 to 100 mv, with the smallest division being 0.005 mv.

The thermocouples registering surface temperatures were fastened to the surfaces by means of a special Scotch brand aluminum tape with adhesive on one side.* The thermocouple wires were protected by radiation shields. The thermocouple location chart is shown in Figure 3-6.

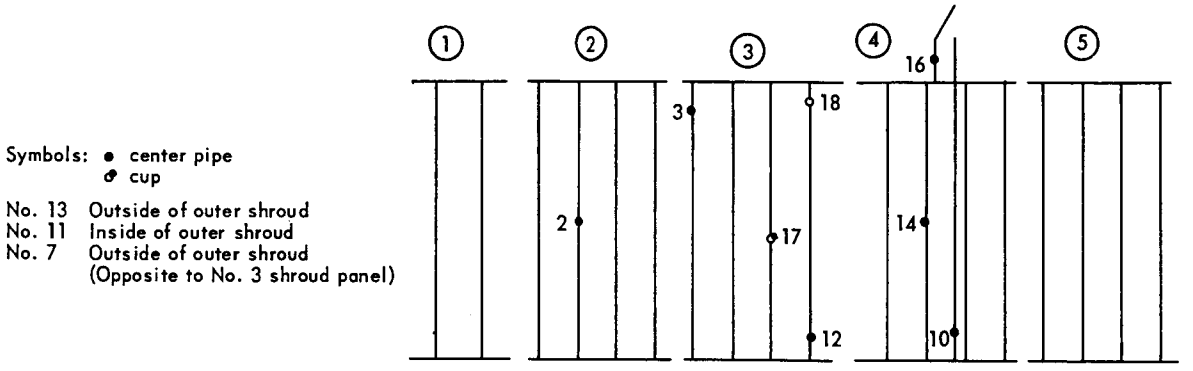

Figure 3-6 - Thermocouple location chart

EXPERIMENTAL PROCEDURE AND RESULTS

The pump-down procedure was designed to minimize oil contamination and build-up of condensate upon the surfaces of the test assembly. Immediately after the vacuum reached 2.5×10^{-2} mm/Hg pressure, obtained with the mechanical pump, the cooldown of the liquid nitrogen trap was begun and continued concurrently with the warm-up of the diffusion pump. When the diffusion pump became effective, chamber pressure dropped to 7×10^{-5} mm/Hg, and the bakeout of the coconut charcoal was begun.

The baking of the charcoal was done by means of hot dry nitrogen gas. The gas, pressurized at about 2 psi, was forced through an electrically heated coil where it warmed up to 220°C. The hot gas was then introduced into the inner shroud to heat the charcoal.

* The adhesive material did not endure the severe thermal cyclings sufficiently, and three thermocouples were lost in the course of the experiment; however, the tape material did not show evidence of extensive outgassing.

Table 3-1 contains selected parameters related to the baking period.

Table 3-1

Temperature drop of nitrogen gas	70°C
Temperature drop between gas and tube-wall surface	20°C
Average temperature drop in a vertical tube	47°C
Average temperature difference between tube and cup surface	3.5°C
Temperature drop between the shroud and the cryopanel	53°C
Temperature uniformity at the same elevation	4%
Pressure ratio between inner and outer gauge	3.4

Figure 3-7 contains the pressure- and temperature-time history of the bake-out period. The bake-out period lasted 4 hours, of which the first 35 minutes took to reach a temperature of 98°C. After this, the temperature dropped slightly. Parallel with this process, the pressure increased sharply in the first hour and then dropped very sharply in the next hour. The gas flow was adjusted and a higher gas temperature level was obtained; concurrently, the pressure increased again and reached in the next hour a peak which was very much smaller than the first peak. The pressure dropped rapidly afterward. It is interesting to note the parallel behavior of the pressure-time curve of the inner and outer gauges; the general behavior of the curves is largely the same, but the ordinate differs by a nearly constant factor.

After the baking was completed, 30 minutes was required to cool down the assembly to room temperature. Dry cold nitrogen gas was used for this purpose.

Upon completion of the pumping, liquid nitrogen was introduced into the shroud, and in one-half hour the pressure in the middle of the vacuum chamber dropped 2 decades; in the next hour it dropped nearly another decade. The difference of pressure readings between the inner and the outer gauges increased roughly to a decade.

On reaching a steady state after 8 hours, the cryopanel was cooled with liquid nitrogen and the inner shroud was warmed with gaseous nitrogen to clear it of liquid nitrogen. After this, liquid helium was introduced at a pressure of about 4 ounces and with an approximate rate of 1/2 liter/minute. In 10 minutes, the pressure in the inner portion of the chamber dropped 2 decades to 3.2×10^{-9} mm/Hg. In the next 10 minutes, the pressure dropped by a factor of 2 to its lowest value. Doubling the liquid helium rate did not affect the pressure.

The pressure registered by the outer gauge after reaching its lowest value remained approximately 2 decades above the pressure registered by the inner gauge.

It should be noted that, in the middle of the experiment, a change of helium tanks was made which took 5 minutes; during this period, the inner pressure gauge registered a three-decade increase in pressure. This phenomenon shows that the pressure is extremely sensitive to temperature variations, and that the response is fast.

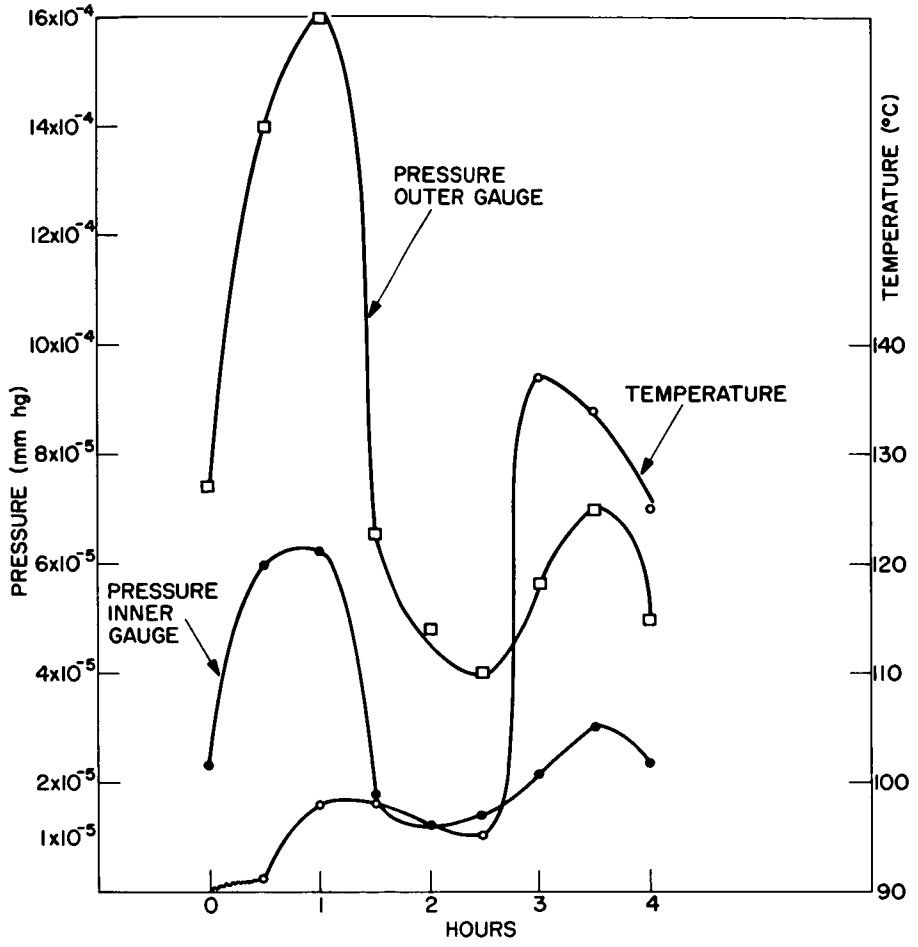

Figure 3-7 - Pressure- and temperature-time history of bakeout period

Figure 3-8 is the pressure-time history of the cooling period of the experiment, and Figure 3-9 is the temperature-time history. Table 3-2 contains selected data pertinent to the cooling period with liquid nitrogen used as coolant; Table 3-3 contains selected information pertinent to the cooling period when liquid helium was used as coolant.

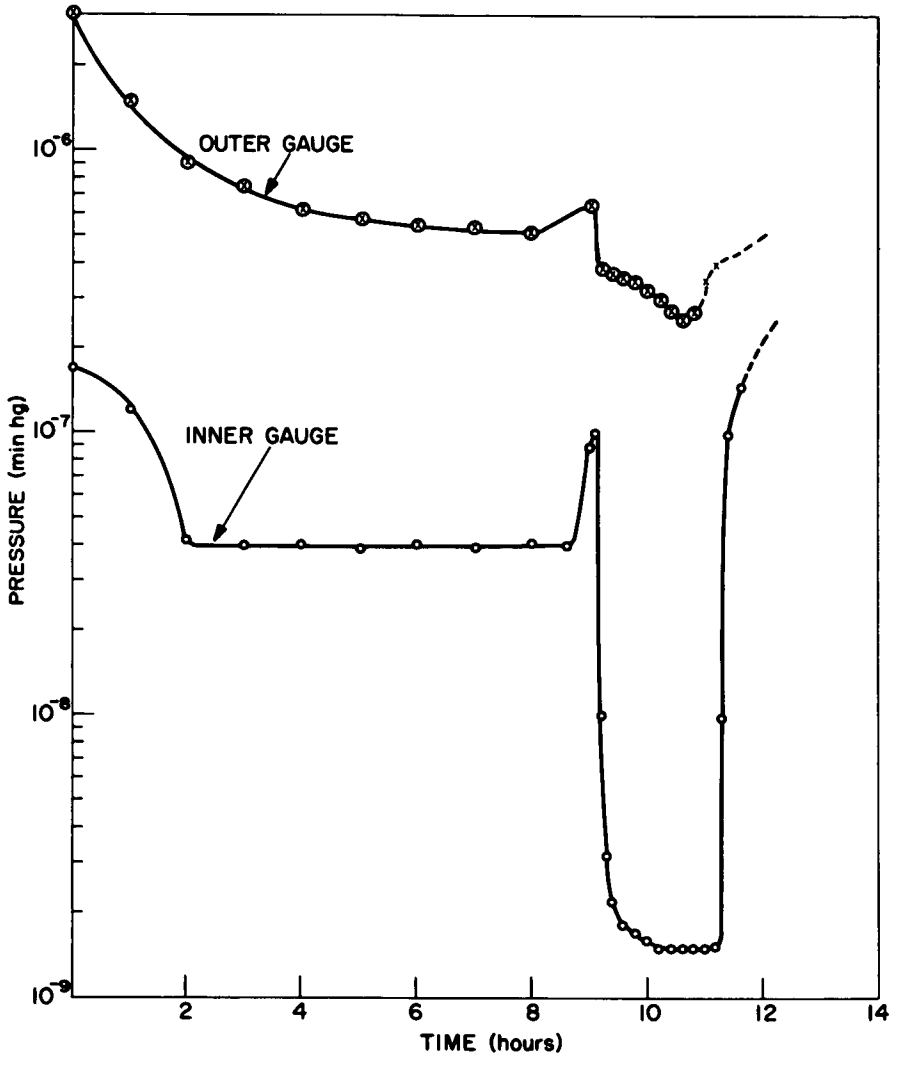

Figure 3-8 - Pressure-time history of cooling period

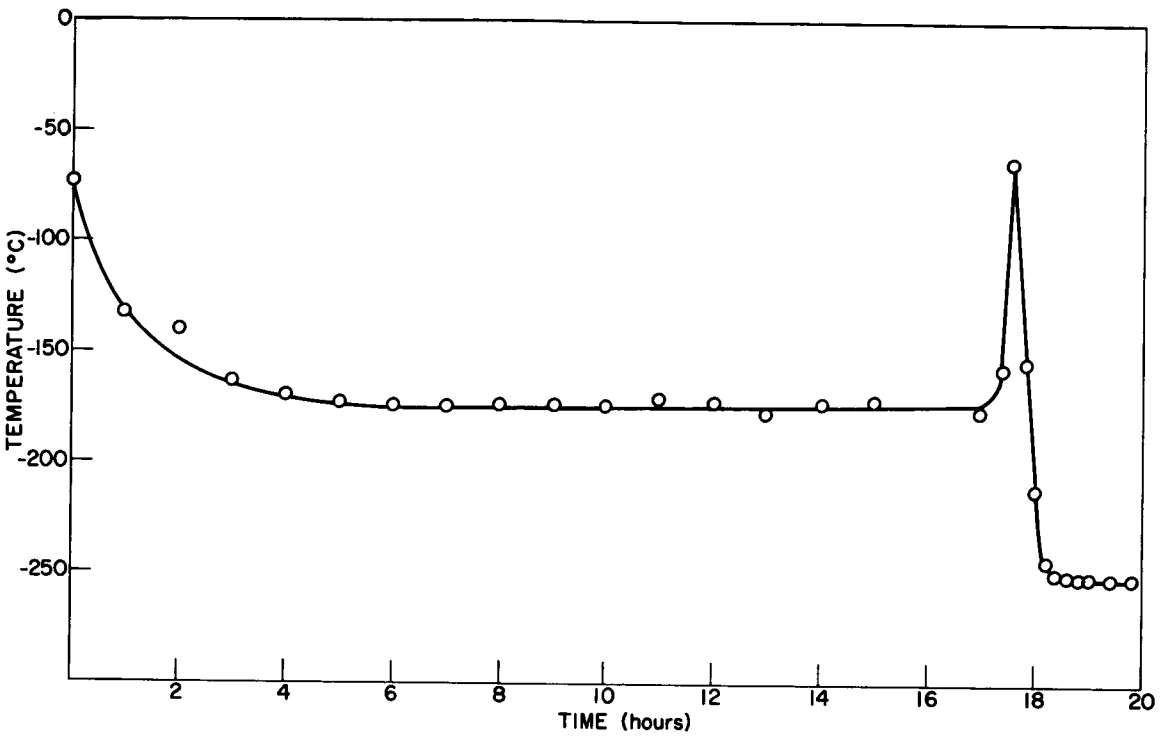

Figure 3-9 - Temperature-time history

Table 3-2

Average temperature of the vertical tube	-175°C
Average temperature rise in vertical tube	23°C
Maximum temperature rise between inlet and outlet	30°C
Temperature rise between the LN_2 and the tube wall	3-5°C
Temperature difference between the inner shroud and the cryopanel	143°C
Average temperature difference between the cup surface and the tube	21°C
Temperature uniformity of the same elevation	2%
Temperature fluctuations in the same location	1%
Corr. pressure ratio between the inner and outer gauge	10.6

Table 3-3

Average temperature in the vertical tube	-253°C
Average temperature rise in a verticle tube	9°C
Maximum temperature rise between inlet and outlet	22°C
Temperature difference between the cup surface and tube	20°C
Temperature uniformity at the same elevation	8%
Temperature fluctuations in the same location	1%
Corr. pressure ratio between the inner and outer gauge	85
Temperature of cryopanel	-186°C

INTERPRETATION OF RESULTS

THE ANNULAR AND CENTRAL CYLINDERS. Assuming that the ionization gauges reflect the pressures prevailing in the portions of the vacuum chamber with which they

directly communicate–and there are no valid reasons for assuming otherwise–the striking facts of this experiment are: in the liquid-nitrogen experiment, the corrected steady-state pressure registered by the outer gauge is 10 times higher than the pressure registered by the inner gauge; in the helium-vapor experiment, the disparity between the two gauges is even greater, namely 85 times.

This is readily explained by the following facts: a) at low surface coverage the adsorption process is almost instantaneous and the equilibrium pressure is practically constant; b) the transport of matter from a region of higher pressure to one of lower pressure by molecular flow is much slower than by mass flow, and is equivalent to a restrictive connection between the two regions; c) evolution of gas from the chamber walls and inleakage through O-rings represent a source of gas supply in the annular cylinder of the vacuum chamber.

It thus seems that the vacuum system consists of an annular cylinder delineated by the chamber walls and the cryopanel, characterized by a high pressure, and an inner cylinder delineated by the inner walls of the cryopanel, including the inner shroud with the adsorbent. The pressure in the latter is determined by the "vapor pressure" of the adsorbed gases on the charcoal at the prevailing temperature, while the pressure in the former is determined by the efficiency of the pumping system.

TRANSPORT OF MATTER FROM ANNULAR CYLINDER TO INNER CYLINDER. The steady state observed in this experiment cannot be explained on the basis of equilibrium established by transpiration, because of the temperature difference between the two compartments; such an equilibrium would require that the ratio of the temperatures of the two sections of the chamber be about 110 for the liquid-nitrogen experiment, to about 6400 in the helium-vapor experiment. The steady state must, therefore, be explained on the basis of a process involving mass transport, due to net molecular flow from the high-pressure to the low-pressure compartments, and immediate uptake of the transported gas by the adsorbent. As will be shown, because of the large area of adsorbent, the surface coverage remains very low, even after hours of gas flow. The low coverage accounts for the constancy of the pressure in the inner cylinder.

The area through which the mass transport takes place is confined to two circular openings in the cryopanel, 3 inches in diameter and at right angles to each other, and an area between the cryopanel and the base plate described approximately by the surface of a cylinder 10 inches in diameter and 1.5 inches in height, the total being approximately 400 cm^2. The opening on top of the cryopanel is neglected.

The rate of transport can be calculated from the equation for the rate of molecular collisions with a surface

$$z = \frac{1}{4} An\bar{c}, \qquad (1)$$

where A is the area, n is the molecular density and $\bar{c}$ is the average molecular velocity. Substituting for n and $\bar{c}$ the equivalent kinetic terms, z is given by

$$z = \frac{A}{(2\pi mk)^{1/2}} \cdot \frac{P}{T^{1/2}} , \tag{2}$$

where P is the pressure, T is the absolute temperature, m is the molecular mass, and k is the Boltzmann constant. This equation is also applicable to the evaluation of the backward molecular flow from the low- to the high-pressure compartments, the net flow being the difference between the flows in the opposite directions. Thus the net flow in the direction of low pressure is given by

$$\Delta z = \frac{A}{(2\pi mk)^{1/2}} \left(\frac{P_1}{T_1^{1/2}} - \frac{P_2}{T_2^{1/2}} \right) , \tag{3}$$

where P_1 and T_1 are the pressure and temperature of the annular cylinder, and P_2 and T_2 are the pressure and temperature of the inner cylinder.

As shown in Table 3-4, the net rate of molecular flow is approximately 9×10^{16} molecules, or 3.36×10^{-3} cc of gas at STP, per second, in the liquid-nitrogen experiment, and 3.44×10^{16} molecules, or 1.29×10^{-3} cc at STP per second, in the helium-vapor experiment. The backward molecular flow is appreciable, about 15 percent in the latter case and about 10 percent in the former case. The composition of the gas is assumed to be equivalent to that of air.

Table 3-4
Parameters of the Experiment Involved in the Calculations

Volume of chamber	197 liters
Volume of cryopanel	134 liters
Volume of annular cylinder	63 liters
Surface area of chamber walls	1.83 sq. m.
Transport area	396 sq. cm.
Specific surface of charcoal (assumed)	400 sq. m./gm
Temperature of charcoal in LN_2 experiment	120°K
Temperature of charcoal in He-vapor experiment	40°K
Temperature of cryopanel in LN_2 experiment	241°K
Temperature of cryopanel in He-vapor experiment	91°K
Time average pressure in annular cylinder in LN_2 experiment	5.95×10^{-7} Torr
Pressure in annular cylinder in He-vapor experiment	1.5×10^{-7} Torr
Temperature of tubular gauge	350°K
Rate of transport of gas in LN_2 experiment	8.97×10^{16} $\frac{\text{molec}}{\text{sec}}$
Rate of transport of gas in He-vapor experiment	3.44×10^{16} $\frac{\text{molec}}{\text{sec}}$

The pressure values for the annular cylinder used in these calculations were corrected and time-averaged, the corrections being made on the basis of transpiration equilibrium between the tubular gauge at an estimated temperature of 77°C and the measured temperature of the cryopanel facing the gauge. This corrected pressure reflects the pressure of gases at the cryopanel. The equation used is given by

$$P_1 = P_2(T_1/T_2)^{1/2}, \qquad (4)$$

where P_1 is the corrected pressure, P_2 is the pressure registered by the tubular gauge, T_1 is the temperature of the cryopanel, and T_2 is the temperature of the glass envelope of the gauge.

FRACTION OF ADSORBENT SURFACE COVERED WITH ADSORBED GAS MOLECULES. The calculations of coverage are based on an assumed value of specific surface area for the coconut charcoal, of 400 m^2 per gram. This value is about 45 percent of the value given for the material, when activated at about 350°C. Also involved is the value of 13.47 sq.Å for the area of an "air-molecule," obtained from the given values of nitrogen and oxygen at -253°C.

The coverage, that is, the fraction of surface covered, after nine hours (the duration of the liquid-nitrogen phase of the experiment) is 4.3×10^{-4}; at the end of the helium-vapor phase of the experiment, (after 10 hours and 45 minutes) the coverage is about 4.6×10^{-4}. It is of interest to point out that, at the average rate of coverage of 4×10^{-5} per hour, it would take about 2.5×10^4 hours, or 2 years and 9 months, to form a monolayer. This leads to the possibility of either decreasing the quantity of adsorbent, or lowering the temperature of activation, which is preferable, or both. It should be pointed out, however, that the equilibrium pressure tends to rise with increase of coverage. A desirable limiting coverage can be obtained from a study of adsorption vs equilibrium pressure. As pointed out elsewhere in this report, the adsorption literature seems not to include information of this type in high-vacuum systems.

SOURCES OF ADSORBED GASES. According to the calculations in section 2, at least 3.36 microliters of gas, or 9×10^{16} molecules, had to be supplied from somewhere to the annular cylinder of the chamber each second. If the walls of the chamber (which are at a temperature not much below that of the room) are the source of this gas, it seems that 5×10^{12} molecules, or approximately 2×10^4 microliters/cm^2, would be evolved each second, and a monolayer of adsorbed gas would be depleted in 2.5 minutes. Although many monolayers of gas would be supplied by the chamber wall, which was not baked out, it is quite certain, in view of the duration of the experiment, that the major source of the gas supply is due to in-leakage.

CONCLUSIONS AND RECOMMENDATIONS

This experiment and the interpretation of its results show that cryosorption (a) is a highly efficient method of cryopumping; (b) is at least 8 times as fast as the 10-inch diffusion pump used in the experiment; (c) has a high potential for coping with inleakage; and (d) produces higher vacua than the diffusion pump capability, 20 times in LN_2 experiment and about 200 times in the He experiment.

It is recommended that further studies be made with respect to:

a. Cryosorption efficiency of different adsorbents

b. Cryosorption efficiency of given adsorbents, with respect to different gases and to binary gas mixtures

c. Cryosorption efficiency of adsorbent activated at different temperatures

d. Design and fabrication of cryopanels that would incorporate efficient cryosorbing surfaces

SECTION C

A METHOD OF CALIBRATION OF IONIZATION GAUGES

INTRODUCTION

The calibration of ionization gauges is frequently made by establishing the value of the constant, K, in equation

$$P = K\left(\frac{I_+}{I_-}\right) \tag{1}$$

by comparing the ratio of the ion current I_+ to the electron current I_- of the ionization gauge with the pressure reading, P, of a McLeod gauge in the pressure range of 10^{-4} to 10^{-5} mm/Hg. This procedure assumes the constancy of K in the higher decades of vacuum. However, it has been shown by Nottingham and Torney[1] that in the regions of pressure 10^{-3} to 10^{-4} mm Hg, that the constant, K, depends on the pressure and the electron current I_-. To test the constancy of K at pressures less than 10^{-5} with the McLeod gauge is not reliable, for reasons connected with the reproducibility of McLeod gauge readings.

THEORY OF NEW METHOD

Since the McLeod gauge is not precise at pressures less than 1×10^{-5} mm/Hg, and the ionization gauges are most useful at these very pressures, it was considered feasible to compare the ratio I_+/I_- of an ionization gauge with the pressure calculated from a known quantity of gas in a known volume at constant temperature.

This method based on Boyle's law could be made very precise, if it were not complicated by the phenomenon of adsorption and desorption. With the expansion of the gas into a baked-out chamber which is provided with an ionization gauge, at pressure less than 10^{-6} mm/Hg, the amount of gas adsorbed on the surface of the chamber can be an appreciable fraction of the total.

To account for the gas removed from the gas phase by adsorption, a small vessel containing chamber-wall material in a finely divided state and of known geometric surface

area may be brought into contact with the gas in the expansion chamber. From the ratio of the readings of the ionization gauge, the adsorption coefficient may be calculated.

Let p_1 be the pressure of the gas confined in the small vessel of volume v_1 at the constant temperature T, and let V be the volume and S the geometric surface of the chamber at temperature T. The quantity of gas in moles, n, is given by

$$n = p_1 v_1 / RT \tag{2}$$

This quantity of gas on expanding into the chamber of volume V is given by

$$n = \frac{PV}{RT} + A, \tag{3}$$

where P is the pressure and A is the number of moles of gas adsorbed on surface S. On expanding the surface to S_1', the gas quantity is now given by

$$n = \frac{P'V}{RT} + A', \tag{4}$$

where p' is the gas pressure and A' is the quantity of gas adsorbed. If A' differs from A, then p' is different from P.

At low pressure and in a narrow region of pressure, it is reasonable to assume (on the basis of the Langmuir adsorption isotherm) that

$$A = KSP \tag{5a}$$

and

$$A' = KS'P' \tag{5b}$$

where S and S′ are the respective geometric surfaces, P and P′ are the gas pressures, and K is the adsorption coefficient per unit surface and unit pressure.

Equating (2) and (3) and combining with (5a) and (5b), we obtain

$$\frac{V}{RT}(P - P') = K(S'P' - SP) \tag{6a}$$

or

$$\frac{V}{RT}\left(1 - \frac{P'}{P}\right) = K\left(S'\frac{P'}{P} - S\right) \tag{6b}$$

Now, assuming that in a narrow region of pressure the constant K in equation (1) is independent of pressure, therefore at a given emission current I_-, the ratio P'/P is given by the ratio of ion corresponding currents of the ionization gauge

$$P'/P = \frac{I'_+}{I_+} \quad . \tag{7}$$

Combining (7) with (6b), and substituting r for S'/S, produces

$$\frac{V}{RT}\left(1 - \frac{I'_+}{I_+}\right) = KS\left(r\frac{I'_+}{I_+} - 1\right) \tag{8}$$

From this equation, the value of K, the adsorption coefficient, can be evaluated, when it is combined with equations (3) and (5a). In order to compute the gas pressure P'_1, equation (8) may be combined with equations (4) and (5b).

APPARATUS

The apparatus made of pyrex glass, shown in Figures 3-10 and 3-11, includes three pressure gauges, a mercury manometer for measuring pressures of 20 mm/Hg and above, a small McLeod gauge for pressures of 10^{-4} to 1 mm/Hg, and a large Consolidated Vacuum Corporation McLeod gauge for pressures of 10^{-6} to 10^{-4} mm/Hg. It also includes a calibrated capillary for introducing desired quantities of gas, and a flask of calibrated volume containing a known number of glass spheres of known diameter. The flask, prior to the introduction of the glass spheres, was used for the calibration of the volume of the system. Two ionization gauges, a Veeco and a NRC, were sealed to the apparatus for calibration. The apparatus was evacuated by means of a mechanical pump and a Varian ion pump. The ion pump and the ionization gauges were protected from Hg vapor by liquid-nitrogen traps.

The parameters of the apparatus are given in Table 3-5.

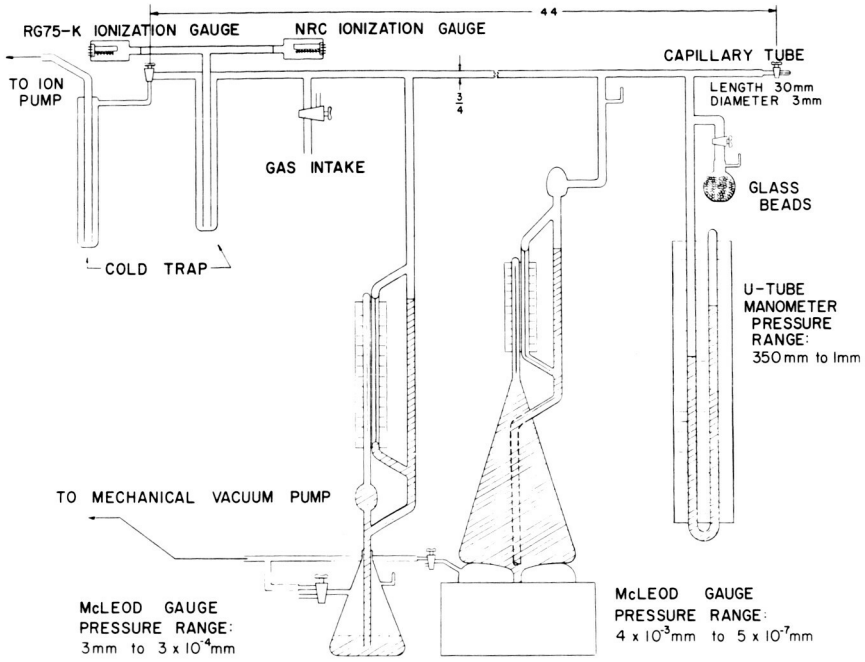

Figure 3-10 - Ionization-gauge calibration apparatus, diagram

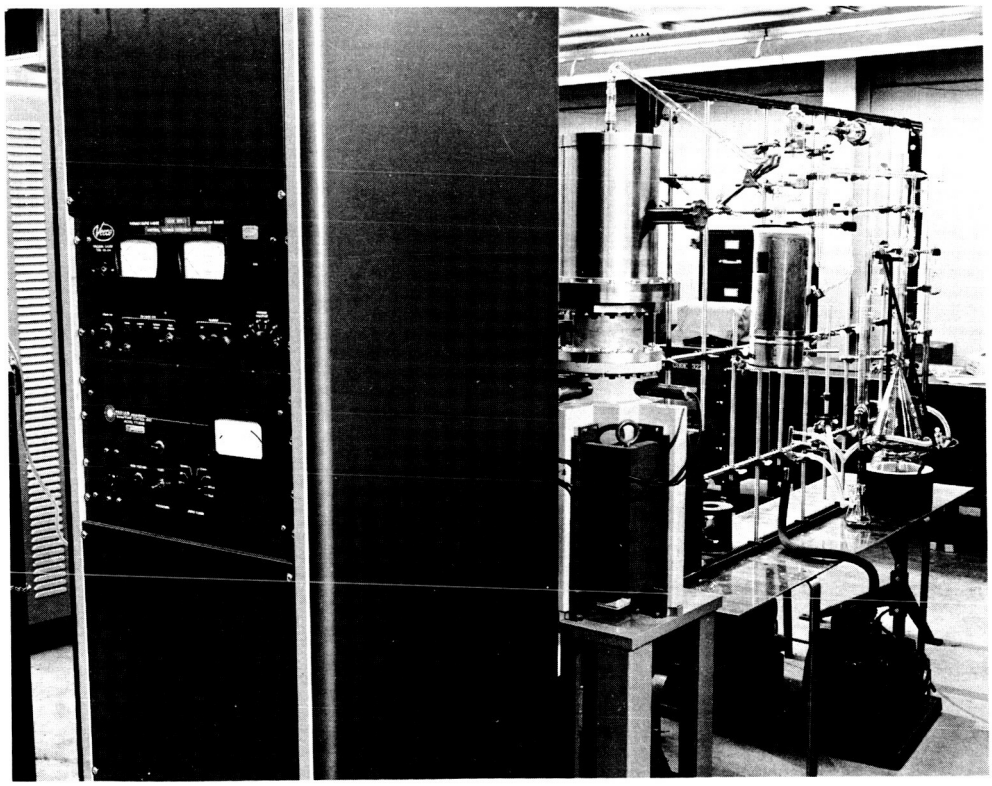

Figure 3-11 - Ionization-gauge calibration apparatus

Table 3-5

Capillary diameter	~ 3 mm
Capillary volume	0.1187 cc.
Flask volume	116.54 cc.
Diameter of capillary in small McLeod Gauge	2.635 mm.
Diameter of glass sphere, average	2.962 mm.
Weight of spheres in flask	131.25 gm.
Number of spheres	3806.
Surface area of spheres	1057 sq. cm.
Surface area of apparatus	1594 sq. cm.
Volume of apparatus (exclusive of ion pump)	3.473 liters

PROCEDURES

CALIBRATION OF VOLUME OF APPARATUS. Helium is introduced into the apparatus through the intake stopcock to a desired pressure, read on the manometer; the stopcock to the flask is then closed, and the apparatus evacuated to at least 10^{-5} mm/Hg. The gas is allowed to expand into the apparatus (exclusive of the ion pump) and the pressure is read again, either on the manometer or on the small McLeod gauge. The volume is calculated from the known volume of the flask and the pressure readings, using Boyle's law.

CALIBRATION OF ION GAUGE. The ionization gauges and the glass spheres are baked (the former at about 400°C, and the latter at about 275°C) for six to ten hours, while the ion pump is evacuating the system to about 2×10^{-8} Torr as indicated by the ion vac pump gauge, or until a sticking vacuum is reached on the CVC McLeod gauge.

The connecting tubes and the McLeod gauges are flamed while the baking and pumping is in process. The ionization gauge to be calibrated is allowed to degas and stabilize to a constant reading.

The gas taken for calibration purposes and stored prior to the baking process in the calibrated capillary at a known pressure (from 0.01 to 0.2 mm/Hg) is allowed to expand into the apparatus, exclusive of the flask of spheres. Readings at different emission settings are taken on the ionization gauge, and also on the CVC McLeod gauge, if the pressure is within the reliable range.

The stopcock to the flask of spheres is now opened, and readings are taken periodically on the ionization gauge at different settings of emission current, and if possible on the McLeod gauge, until constancy of reading is obtained.

RESULTS OF DISCUSSION

Regretably, the time remaining after completing construction of apparatus, and eliminating unforeseen difficulties, was inadequate for a full test of the method and its limitations.

Only one experiment was carried out, on which it is not possible to base any evaluation.

The data are as follows:

Pressure of nitrogen in capillary: 12.6×10^{-2} mm Hg (1)

PV of nitrogen: 14.95×10^{-3} cc - mm Hg (2)

Veeco reading prior to introduction of gas: (3)

emission, ma	10	8	6	4	2
Reading, Torr $\times 10^7$	10.5	8.2	5.4	3.4	1.6

Veeco reading after introduction of nitrogen: (4)

emission, ma	10	8	6	4	2
Reading, Torr $\times 10^6$	2.5	2.0	1.5	1.0	0.57

Veeco reading after opening stopcock to spheres: (5)

emission, ma	10	8	6	4	2
Reading, Torr $\times 10^6$	2.5	2.0	1.5	1.0	0.62

The background pressure recorded by the Veeco gauge and given under (3) is too high, and is evidently due to insufficient degassing of the apparatus. The difficulty of baking the several sections of the apparatus simultaneously is the weakest aspect of the apparatus design; the sections of the apparatus which require baking should be brought together to make possible enclosing it by an oven.

The reading in (4) and (5) show that no adsorption by the walls has taken place. The pressure calculated from Boyle's law, 4.3×10^6 mm/Hg, is higher than the values indicated by the Veeco gauge at the several emissions. The low reading on the Veeco is in agreement with observations of Barnes[2] ascribed to the high ratio of positive ions to neutral molecules in the space between the grid and the tube walls. This coincidence could be fortuitous, and no affirmative statement should be based on a single observation. However, the method of approach shows as possessing potentialities.

REFERENCES

1. Wayne B. Nottingham and Franklin M. Torney, Jr., Technical Report 379, MIT Research Laboratory of Electronics, AD248376.

2. George Barnes, "Erroneous Readings of Large Magnitude in a Bayard-Alpert Ionization Gauge, Review of Sci. Instruments, 31, 1121 (1960).

SECTION D

A SURVEY OF THE LITERATURE ON ADSORPTION OF COMMON GASES ON STEEL AND OTHER METALS

INTRODUCTION

Originally, in collecting these references, information was sought on the adsorption of gases at ultra-high vacuum, and at room temperatures or below, on steel and other structural metal surfaces. As satisfactory information of this type was not available, the scope of the search has been broadened. References in the appended bibliography will be discussed in relation to the following topics:

The magnitude of adsorption of common gases on steel and on metals going into steel; the nature of the "irreversible" adsorption observed on metals; experiments on the adsorption of gases at very low pressures.

ADSORPTION OF COMMON GASES ON STEEL AND SOME OF ITS COMPONENT ELEMENTS

Some direct measurements have been made of adsorption of gases on steel surfaces. M. H. Armbruster has contributed several articles on this subject (31-34). Measurements were made at -195 to 20°C at pressures ranging from 10^{-3} to 1 Torr, on both reduced and unreduced surfaces. Two types of adsorption were observed: a reversible adsorption which could be removed by pumping in a moderate (10^{-6} Torr) vacuum, and an "irreversible" adsorption which could not be thus removed without raising the temperature. The reversible adsorption was recognized to be held by physical (e.g., van der Waals) forces, and approached a limit at 0.1 to 1 Torr, comparable in magnitude to a monolayer.

Nitrogen and argon on reduced surfaces at -195°C, carbon dioxide at -78°C, and ethyl iodide at 20°C, were found to be held entirely by physical forces. Except when observed on unreduced surfaces, the "irreversible" adsorption was thought to be held by chemical forces (i.e., chemisorbed). Carbon monoxide, water vapor, argon, and nitrogen on unreduced surfaces were all observed to have at least partial irreversibility of about a monolayer or less. Oxygen on a reduced surface was found to be chemisorbed to the extent of at least 8 monolayers. It should be noted that temperatures used in reduction and

outgassing were no greater than 600°C, which may not have been great enough to produce clean surfaces.

Chessick et al (27) made a similar study on the physical adsorption of common gases at pressures greater than 10^{-5} Torr on molybdenum powder. Kavtaradze (20) has recentcently made adsorption measurements of H_2, CO, O_2, and C_2H_4 on metal films at pressures of 10^{-7} to 10^{-2} Torr at temperatures ranging from -195 to 250°C; he found adsorption to be either large and irreversible, or small and reversible. This is in agreement with what one would expect from Armbruster's data.

Several articles have been published on the adsorption of oxygen on iron and steel, especially in relation to passivity. One such article is that by Burshtein and Levina (77) on the adsorption of highly alloyed stainless steels. At 20°C, the magnitude is 1/5th the amount observed by Armbruster (surface measured by B.E.T. method), i.e., about 1.3 monolayers. Zettlemoyer and Chessick (76) found that water vapor was completely reversibly adsorbed on nickel and steel powders reduced at 25°C, indicating that the oxide layer was thick enough to prevent diffusion of water vapor to the metal surface. When elevated temperatures were used to "activate" the surface, 10 to 13 layers of water were adsorbed at room temperature. This is far in excess of the adsorption observed by Armbruster.

If temperatures are sufficiently high, dissociation will occur on adsorption. While Armbruster found only physical adsorption of CO_2 at -78°C, Takao Kwan (81) found evidence that CO_2 was dissociated into CO and O at 150°-200°C on reduced nickel. Wright and Ashmore (43) found that both ethane and methane were dissociated on adsorption by evaporated tungsten surfaces at 0-100°C. Ethane was found to adsorb in the same manner on nickel and on iron at temperatures greater than 70°C.

The adsorption on evaporated metal films seem qualitatively different from adsorption on powders or bulk metal surfaces; in particular, chemisorption appears to be more prevalent and pronounced on the evaporated films. A. S. Porter and F. C. Tomkins (28) measured the adsorption of CO and H_2 at 10^{-5} Torr on iron films. Most of the gas adsorbed at high pressures was found to remain to the low-pressure limit. The heat of adsorption for both carbon monoxide and hydrogen was calculated to be about 20 kcal/mole. Armbruster, in contrast, did not observe any adsorption of H_2, and calculated the average heat of adsorption for CO to be about 3.5 kcal/mole. While Armbruster found only physical adsorption for CO_2 on reduced steel at -78°C, Collins and Trapnell (65) found strong chemisorption of CO_2 on Fe, W, Mo, and Ni films at -78°C to 70°C. Mazumdar (50) found that ethane and methane were chemisorbed on Ni films at -195°C.

IRREVERSIBLE ADSORPTION AT LOW PRESSURE

No reference has been found which gives information on the evolution of irreversible adsorbed gases at pressures below 10^{-7} Torr. The data of Porter and Tomkins (28)

suggest that this evolution could be appreciable for CO and H_2 on evaporated iron films. Also, Armbruster thought that the irreversible adsorption of N_2 and A on unreduced surfaces of steel at -183°C might have been due to strong physical forces between the adsorbed molecules and an oxide layer. The reasons put forth for suspecting physical adsorption were (1) no adsorption for N_2 and A was observed at -78°C, indicating the weak nature of the forces involved; (2) argon, usually chemically inert, was irreversibly adsorbed to about the same extent as nitrogen. One might expect adsorption of this character to desorb at outgassing pressures lower than those used by Armbruster (10^{-6} Torr).

The heat of adsorption is one indication of the strength of the bonds holding an adsorbed substance. Heats of physical adsorption are usually less than 10 kcal/mole; heats of chemisorption, on the other hand, may be as great as 100 kcal/mole. Molecules adsorbed in a state characteristic of such high heat (adsorbed atoms, for example) have a negligible equilibrium pressure at room temperature or below; however, materials with intermediate heats of adsorption might evolve at a rate appreciable at very low pressures. Porter and Tomkin's data suggested this might be 20 kcal/mole.

SOME EXPERIMENTS ON ADSORPTION ON METALS IN HIGH VACUUM

Three references have been found which deal with the adsorption of gases at pressures of about 10^{-8} Torr. Ehrlich and Hudda (22) made a study of the adsorption of the rare gases on a tungsten field emitter at low temperatures, and found no detectable adsorption of He, Ne, or A below 10^{-7} Torr above 20°K. R. J. Hill (21) made a field-emission study of the adsorption of water vapor on tungsten at 80°K and 400°K; but the adsorption is only indicated qualitatively by photographs of the resulting patterns. P. Kisliuk (51) has determined the adsorption of nitrogen on tungsten to be from 10^{-8} to 10^{-5} Torr at 1100° to 1700°K. As might be expected, the nitrogen is dissociated into atoms, and adsorption is proportional to the square root of pressure.

A complete search of the literature on this topic is expected to yield more information of this nature. However, it seems that the literature is lacking in systematic equilibrium studies of adsorption in the pressure region below 10^{-6} Torr.

APPENDIX A

INTERCHANGE OF INFORMATION

From the interchange of information and ideas between members of the Summer Workshop and the permanent staff have crystallized the investigations and studies pursued by the Workshop. In the course of this interchange, a number of questions and problems have arisen which merit further discussion.

ANALYSIS OF RESIDUAL GASES

To improve cryogenic pumping and space simulation, it is essential to know the nature and partial quantities of the vapors and gases evolved from the components of the vacuum chamber and the spacecraft.

The mass spectrometer is an instrument that lends itself to analysis of the gases being evolved in a cryogenic pumping system at high vacuum. However, the gas analyzer capable of measuring minute quantities of gases or vapors over a range of molecules from 2 to 80 was constantly and continuously in a state of disrepair since the beginning of the Summer Workshop. Besides, the instrument is of limited molecular range, and some of the components given off by elastomers and plastics are of such high molecular weights that the instrument is not capable of detecting them.

It is therefore desirable to consider other methods of analysis. One such method is gas chromotography, which requires larger quantities of gas samples than can be obtained in vacuum test-chambers at high vacuum; this, however, can be overcome by collecting samples on the fore-pressure side, where the gases evolved are compressed from 10^4 to 10^6 times. It is essential to point out that samples of gases thus collected will also contain vapors of the diffusion oil, for which corrections could be determined. The application of this method to analysis of residual gases in high-vacuum chambers merits further investigation.

CONTAMINATION OF SPACECRAFT SURFACE

In addition to the common gases occurring in the atmosphere, which are given off in the course of evacuation by the different components of the chamber during a thermal-vacuum evaluation, gases and vapors are also being evolved which are characteristic of the components of the spacecraft and their histories. Steel, for instance, evolves–in

addition to the gases adsorbed from the atmosphere, such as water vapor, oxygen, nitrogen and carbon dioxide–also carbon monoxide and hydrogen formed and absorbed in the course of its manufacture. The elastomers and plastics evolve a variety of different organic substances related to the polymeric materials of which they are composed. Some of these gases, including hydrogen and carbon monoxide, may be irreversibly adsorbed on the metallized surface of the spacecraft and may change its properties.

In this connection, it is of interest to point out that surface potentials are sensitive to surface composition, and lend themselves to measurement under conditions prevailing during simulation testing. Surface potentials with respect to an inert electrode can be measured by using the vibrating-electrode technique, or by means of a radioactive electrode that is an alpha-emitter. Both techniques are described in the literature.

DETECTION OF LEAKS IN CRYOPANELS

There have been instances of leakage in cryopanels only when liquid nitrogen is circulating in them. This was the case with the cryoliner in the cryosorption experiment described elsewhere in this report.

One approach to detecting a low-temperature leak is to find a material that will dissolve in, or mix with, liquid nitrogen and will produce an imprint on the surface of the cryoliner at the point of leakage. If iodine could be dissolved to any appreciable extent in liquid nitrogen, it would leave an imprint on a starch-painted cryoliner.

There are perhaps to be found materials that fluoresce in ultraviolet.

Another more promising approach is the use of radio tracers. A radioactive isotope of nitrogen, oxygen, or tritium would be injected into the circulating liquid nitrogen, and the area of leakage detected with a Geiger-Muller counter or scintillator.

ORIENTATION OF SENSORS IN SPACE SIMULATORS

In a gaseous system where the molecular mean-free-path is very much less than the dimensions of the vessel, intermolecular collisions are the major factors in the consideration of the physical properties of the gas. In such a gas, the vacuum sensor would not depend on its orientation, because the number of collisions per unit volume in a given position in the vessel would be the same in all orientations.

However, in a region of pressure where the molecular mean-free-path is of the same magnitude as the dimensions of the vessel, or greater (the so-called region of free-molecular flow), the molecule-surface interaction is the governing factor. This condition prevails in space simulators. The kinetic energy of the molecules is characteristic of the temperature of the surface with which they interacted. Molecules originating from the surface of the spacecraft will generally be endowed with energies different than those

originating from the cryoliner, and will possess kinetic energies characteristic of the temperature of the spacecraft. For this reason, the orientation of the vacuum sensor is important.

To derive a relationship between the pressures and temperatures of free-flowing molecules in these two orientations, assume equilibrium between the sensor and the spacecraft at which it is looking. The number of collisions per second with unit surface is given by

$$\nu = \frac{1}{4} n v,$$

where n is the number of molecules per unit volume and v is the average velocity. The mass striking unit surface per second is

$$m\nu = \frac{1}{4} \rho v$$

where m is the mass of a molecule and ρ is the mass density. For the condition of equilibrium, the mass striking unit surface in either direction is the same, and therefore,

$$\rho_1 v_1 = \rho_2 v_2$$

where the subscript 1 refers to the molecules originating from the sensor and the subscript 2 refers to the molecules coming from the surface of the spacecraft. Substituting the kinetic expressions for ρ and v, we obtain

$$P_1 / \sqrt{T_1} = P_2 / \sqrt{T_2}$$

where T_1 and T_2 are the temperatures of the sensor and of the surface of the spacecraft, respectively, and P_1 and P_2 are the corresponding pressures.

APPENDIX B

BIBLIOGRAPHY

CRYOSORPTION AND CRYOGENIC PUMPING

1. B. B. Dayton: "Relations Between Size of Vacuum Chamber, Outgassing Rate and Required Pumping Speed," Transactions of Sixth National Symposium on Vacuum Technology 1960.

2. H. A. Steinhertz and P. A. Redhead; "Ultrahigh Vacuum."

3. E. E. Callaghan: "Hard Vacuums and Cryogenics," Machine Design, June 21, 1962.

4. J. D. Pinson, "Research for Space Simulation in Design of Ground Test Facilities," Third Annual Symposium on Space Environment Simulation, June 1962.

5. O. O. Haneldsen and A. Cohen: "Cryopumping Characteristics of Non-Condensible Gases."

6. F. C. Hurlbut and B. J. Mansfield: "Calculated and Observed Pumping Speeds of a Shielded Cryogenic Pumping Surface," Third Annual Symposium on Space Environment Simulation," June 1962.

7. A. D. Le Vantine: "Gas Evolution Rate Determination for Cat-A-Lac Flat Back Epoxy Paint," J. of Environmental Sci., June 1963.[2]

8. I. Farkass: "Ultra-high Vacuum Design for Large Space Simulation Systems," Institute of Environmental Sciences, April 1962.

9. R. B. Scott: "Cryogenic Engineering," D. Van Nostrand Co., 1959.

10. J. Yarwood: "High Vacuum Technique," Chapman and Hall Ltd., 3rd edition, 1956.

11. F. E. Hoare, L. C. Jackson, N. Kurti: "Experimental Cryophysics," Butterworth and Co., Ldt., London, 1961.

12. G. N. Patterson: "Molecular Flow of Gases," J. Wiley and Sons, Inc., 1956.

13. G. K. White: "Experimental Techniques in Low Temperature Physics," Oxford University Press, 1959.

14. S. Dushman: "Scientific Foundations of Vacuum Technique, "J. Wiley and Sons, Inc., 1949.

15. A. Guthrie and R. K. Wakerling: "Vacuum Equipment and Techniques," McGraw-Hill, 1949.

16. J. G. Aston: "Research and Development on Thermodynamics of Simple Gases Adsorbed on Solids," ORD Project No. TB2-0001 (1098), Penn State Univ., University Park, Pa., January 1962.

17. "Proposal for the Investigation of Adsorption Pumping Techniques," NRC, Cambridge Mass., Q41-1120, September 1961

18. L. A. Harris; "Trapping with Alumina in Vacuum Systems and its Effect on Cathode Activity," Rev. Sci. Instr., Vol. 31, p. 908, 1960.

19. "Research Study of New Techniques for Cryopumping Noncondensible Gases," Linde Co., Contract No. AF 40(600) - 944, 945, May 1962.

ADSORPTION OF GASES ON METALS

20. N. N. Kavtaradze, Zhur. Fiz. Kim. 36, 628-9 (1962). Topic, adsorption of gases on metals; 10^{-7}, -10^{-3} Torr.

21. R. J. Hill, "The Adsorption of Water on Tungsten," Vacuum 11, 260-71 (1961).

22. G. Ehrlich and F. G. Hudda, J. Chem Phys. 30, 493. Topic; interaction of rare gases with metal surfaces.

23. C. Hayashi, "Rate of Adsorption in Production and Measurement of High Vacuum," National Symp. on Vacuum. Technol. 4th., Boston, 1957, B, 26 (Pub. 1958).

24. M. I. Elinson, "The Influence of Gas Adsorption at the Emitter Surface Upon its Field Electron Emission," Radiotekh, i Elektron, 3, 433-5 (1958).

25. C. H. Rehfopf, "Sorption of Gases by Anodic Materials of Electron Tubes," Sylvania Technologist II, 114-16 (1958).

26. E. Waldschmidt, "Liberation of Gas and Gas Permeability of Metallic Structural Materials from Vacuum Apparatus," Metall. 8, 749-58 (1954).

27. J. J. Chessick, F. H. Heally, A. C. Zettlemoyer, "I. Adsorption Studies on Metals. II, Absolute Entropies of Adsorbed Molecules on Molybdenum," J. Phys. Chem. 57, 912-915 (1953).

28. A. S. Porter and F. C. Tomkins, "The Sorption of Hydrogen and Other Gases by Evaporated Iron Films," Proc. Roy. Soc. (London), A-217, 544-54 (1953).

29. Albert P. Crowell, "Adsorption of Gases by Metal Films and Single Crystals," Am. J. Phys. 20, 89-98 (1952).

30. R. M. Barrer, "Gas-Metal Equilibria, Interstitual Solutions, and Diffusion," Discussions Faraday Soc. 1948, No. 4, 68-81.

31. M. H. Armbruster, "The Sorption of Gases on a Plane Surface of Two Stainless Iron-Chromium - Nickel Alloys at 20°C, -78°C, -183°C," J. Am. Chem. Soc., 20, p. 1734 (1948).

32. M. H. Armbruster, "The Sorption of Water Vapor, at Low Pressure on the Surface of Some Cold-Rolled Steels at 20°C," J. Am. Chem. Soc., 68, 1324-7 (1946).

33. M. H. Armbruster and J. B. Austin, J. Am. Chem. Soc. 66, 159-71 (1944). Topic, "The Adsorption of Gases on Smooth Surfaces of Cold-Rolled Steel."

34. M. H. Armbruster, "The Adsorption of Ethyl Iodide on a Plane Surface of Iron at 20°C," J. Amer. Chem. Soc. 61, 1117 (1939).

35. Henry Lepp, "Gases in Metals and Their Influence, Adsorption, Absorption and Chemical Reactions," Metal Ind. (London) 53, 27-30, 59-63, 79-83, 103-107, 131-6 (1938).

36. I. E. Den Besten, et al., "The Mechanism of Chemisorption; Carbon Monoxide and Carbon Dioxide on Nickel," J. Phys. Chem. 66, 450-3 (1962).

37. Victor R. Deitz and Frank A. Carpenter, Advances in Chemistry Series 1961, 2-4, "The Rate of Physical Adsorption at Low Surface Coverages," pp. 146-59.

38. H. Dunken, et al., "Simple Model Concepts of the Chemisorption of Hydrogen, Oxygen, and Nitrogen on Metals," Z. Chem. 1, No. 9, 282-3 (1961).

39. H. Dunken and H. Mueller, "Simple Model Conception on the Chemisorption of H, O, and N on Metals," Z. Chem. I, 844-3 (1961).

40. V. M. Gryasnov and V. I. Shimuli, "Effect of the Adsorbed Hydrogen on the Electrical Conductivity of Transparent Films of Platinum," Eston, Mosk., Univ., Kim. Ser. II 16, No. 6, 23-7 (1961).

41. N. N. Kavtaradze and V. I. Lygin, "The Structure of Surface Compound of Carbon Monoxide and Palladium from the Evidence Obtained by Adsorption Measurement and Improved Spectra," Daklady Akad. Nauk. S.S.S.R. 138, 616 (1961).

42. N. N. Kavtaradze and Bores-kova Lygin, "Adsorption of CO on Palladium, and Properties of the Surface Compounds," Kine tika i Kataliz, 3, 378-85 (1961).

43. P. G. Wright and Ashmore, Trans. Faraday Soc. 54, 1692-1702 (1959), "Dissociation and Adsorption of Methane and Ethane on Metal Films," (C.A. 53-15698).

44. Farnsworth and Schlier, "Tests with Low-Energy Electron Diffraction for Adsorbed H_2 and Nickel Hydroxide Formed on the Surface of a Nickel Crystal at 25°C," Phys. and Chem. of Solids, 9, No. 1, 57-9 (1959).

45. Vayward and Gomer, J. Chem. Phys. 30, 1912 (1959). Topic: "Adsorption of CO_2 on Tungsten."

46. "Adsorption on Krypton on Metals; An Appraisal of Several Interaction Theories," J. Phys. Chem. 63, 680-686 (1959).

47. Shuppe and Zakirov, "Dependence of Adsorption on Monocrystalline Metals on Crystallographic Orientation," Trudy Sredeaciat Gosudarst Unit. in V. I. Lenin 148, Fiz. Mat. Nauki, No. 20, 45-80 (1959).

48. P. L. Walker, et al., J. Phys. Chem. 63, 133-140 (1959), "Dissociation of Chemisorbed CO on Fe into C and O."

49. Robert Gomer, J. Phys. Chem. 63, 468-72, "Adsorption of Argon on Tungsten."

50. Mazumdar, Bibhuti R., "Adsorption of Gases on Evaporated Metal Films and Oxidized Niclel Film," Univ. Microfilms (Ann Arbor, Mich.) L. C. Card No. Mic 58-3085, 70 pp.

51. P. Kisliuk, J. Chem. Phys., 30, 174-81, "Chemisorption of N_2 on W at very Low Pressures and High Temperatures."

52. Joseph Eisinger, "Adsorption of Oxygen on Tungsten," J. Chem. Phys. 30, 412-16 (1959).

53. S. J. Stephens, "Surface Reactions on Evaporated Palladium Films," J. Phys. Chem. 63, 188-99 (1959).

54. Hickmont and Ehrlich, Phys. and Chem. Solids 5, 47-77 (1958), "Surface Structure and Adsorption."

55. S. J. Stephens, National Symposium on Vacuum Technol., 4th, Boston, 1957, pp. 34-7, "Sorption of Gases by Au-Prd Alloy and Rd Films."

56. N. N. Kavtaradze, "Character of the Maximum of the Adsorption Isobars for the Sorption of Hydrogen on Nickel, Platinum, Iron, Chromium, and Other Metals," I Zvest. Akad. Nauk. S.S.S.R., Otd. I, Chim. Nauk., 1958, pp. 1045-53.

57. Joseph Eisinger, "Properties of Hydrogen Chemisorbed on Tungsten," J. Chem. Phys. 29, 1134-60 (1948).

58. Z. Elektrochem. 62, 707-16 (1958), "Stainless Steel Passivation and Adsorption."

59. W. M. H. Sachter, Bull. Soc. Chim. Belges, 67, 467-88 (1958) (in English), "Electrical Resistance of, and Adsorption on Nickel Films."

60. J. C. P. Mignolet, "Geometric Study of Adsorption on Some Simple Crystallographic Faces. Interpretation of the Two Adsorptions on Hydrogen on Bare Metallic Surfaces," Bull. Soc. Chim. Belges, 67, 358-72 (1958).

61. P. Kisliuk, Phys. and Chem. Solids 5, 78-84 (1958), "Sticking Probabilities in Surface Coverage and Chemisorption of Gases on Solids."

62. W. P. McKinnel, Jr., "Sorption of Some Diatomic Gases on Stainless Steel and Iron Surfaces, and Its Relation to Passivity," University Microfilms (Ann Arbor, Mich.), No. 21444, 83 pp., Dissertation Abstracts 17, 1329-30 (1957).

63. M. G. Fontana and W. P. McKinnel, "A New View to the Passivity of Stainless Steel," Werkstoffe Und Korrosion 8, 249-54 (1957).

64. N. N. Kavtaradze, Collection of papers given at the symposium on adsorption, 1957, pp. 73-81, "Adsorption of H, C_2H_4,O on pure Ni, Fe Cr and Other Metals."

65. A. C. Collins and B. M. W. Trapnell, "The Chemisorption of CO_2 on Evaporated Metal Films," Trans. Faraday Soc. 33, 1476-82 (1957).

66. E. G. Brock, Advances in Catalysis 9, 452-7 (1957), "Adsorption of N_2 on W."

67. Sahlier and Farnsworth, "Low Energy Electron-Diffraction Studies of Oxygen Adsorption and Oxide Formation on a (100) Crystal Face of Nickel Cleaned Under High Vacuum Conditions," Advances in Catalysis 9, 434-40 (1957).

68. M. A. Avdeenko et al., "Catalytic Activity of Metals in Relation to Homomolecular Isotope Exchange of Hydrogen," Problemy Kinetiki i Katalize Acad. Nauk., S.S.S.R. Ind. Fiz. Khim. Soveshchame, Moscow, 9, 61-75 (1956).

69. J. C. P. Mignolet, J. Chim. Phys. 54, 19-26 (1957), "Adsorption of Hydrogen Atoms and Molecules on Platinum."

70. B. M. W. Trapnell, "Mechanisms of Chemisorption," Chemisorption, Proc. Symposium Kiele, 1956, 101-105 (1957).

71. Gert Ehrlich, "Mechanisms of Chemisorption on Metals," Phys. and Chem. Solids 1, 1-13 (1956).

72. Gert Ehrlich, J. Chem. Phys. 24, 482 (1956), "State of Nitrogen Adsorbed on Tungsten."

73. E. Greenhalgh, et. al., "The Interaction of Nitrogen with Clean Metal Surfaces," Trans. Faraday. Soc., 52, 865-72 (1956).

74. Pickup and Trapnell, J. Chem. Phys. 25, 182, "Recombination of H atoms at Metal Surfaces."

75. M. A. H. Lanyon and B. M. W. Trapnell, Proc. Roy. Soc. A, 227, 387-99 (1955), "Chemisorption of Oxygen on Metal Films."

76. A. C. Zettlemoyer and J. J. Chessick, J. Phys. Chem. 58, 242-3 (1954), "Sorption of Water Vapor on Nickel Steel."

77. S. D. Levina and R. Kh. Burshtein, "Oxide Layers on Highly Alloyed Steels," Zhur. Fiz. Khim, 26, 555-9 (1952).

78. A. E. J. Eggleton and F. C. Tomkins, "Thermal Accommodation Coefficients of Gases and Their Adsorption on Iron," Trans. Faraday Soc., 48, 738-49 (1952).

79. Wang and Harman, J. Phys. Chem. 56, 771-4 (1952), "Sorption of Gases by Metal Powders and Metal Reactivity."

80. F. C. Tomkins, Z. Elektrochem. 56, 360-363 (1952) (In English), "Adsorption of Gases by Metal Films."

81. Takao Kwan and F. Yuzabro, Bull. Chem. Soc. Japan 24, 46-50 (1951), "Adsorption of CO_2 by Reduced Fe."

82. A. I. McClellan and Norman Hackerman, "The Sorption of Gases on Metals at Room Temperature," J. Phys. and Colloid Chem. 55, 374-82 (1951).

83. Norman Hackerman and Leland L. Antes, "Contact Potentials of Evaporated Iron Films in Air and in Nitrogen at Low Pressures," Science 112, 471 (1950).

84. "Adsorption of Gases on Metals," Lehigh Univ. Tech. Rept. No. 2, 46 pp., (1950), Nuclear Sci. Abstracts 4, No. 20.

85. Takao Kwan, J. Chem. Phys. 18, 1309-10 (1950), "Adsorption of Carbon Dioxide by Reduced Nickel."

86. J. A. Allen and J. W. Mitchel, Discussions Faraday Society 1950, No. 8, 309-314, "O_2 Adsorption on Cu."

87. O. Beeck and H. W. Ritchie, "Measurement of the Surface of Oriented and Unoriented Evaporated Porous Ni Films by the Brunauer-Emmett-Teller Method, Using Ne, Kr, Ch_4, C_4H_{10}," Discussions Faraday Soc. 1950, No. 8, 139-66.

88. S. Kruyer, "Numerical Calculation for the Adsorption of N on Fe," J. Chem. Phys. 18, 1112 (1950).

89. P. Crothwell and H. E. Farnsworth, "The Measurement of Gas Adsorption on Metals Using a Radioactive Tracer Method," Phys. Rev. 78-351.

90. R. Kh. Burshtein, J. Phys. Chem. (U.S.S.R.) 20, 789-801 (1946), "Adsorption of O_2 on Fe Wire and Powder."

91. Walter Van Dingenen, "Adsorption of Gases on Pure and Activated Metal Surfaces and its Relation to the General Physcial Properties of Metals," Verhandl. Kon Vlaamsch Acad. Wetensch, Letteren, Schoone Kunsten Belgie, Klasse Wetensch 4, No. 4 59. 49 pp. (1942).

92. Colin J. Smithels, "Gases and Metals," J. Roy. Soc. Art 86, 936-44 (1935).

93. Kimio Kawakita, "Adsorption of CO_2 on Reduced Fe, Rev." Phys. Chem. Japan, 14, 1-10 (1940); 13, 87-95, 12, 105-14 (1935), 11, 39-53 (1937); 8, 89-116 (1934).

94. A. F. Benton and T. H. White, "Sorption of Gases by Copper," J. Amer. Chem. Soc, 54, 1373-90 (1932).

95. A. F. Benton and T. A. White, "Sorption of Gases by Iron," J. Amer. Chem. Soc., 54, 1820-1830 (1932).

96. W. K. Lewis, E. R. Gilliland, B. Chertou, W. P. Cadogen, "Adsorption Equilibria—Pure Gas Isotherms," Ind. Eng. Chem. 42, 1326 (1960).

97. D. Basmadjian, "Adsorption Equilibria of Hydrogen, Deuterium and Their Mixtures, Part I," Canadian Journal of Chemistry 38, 141 (1961).

98. B. M. W. Trapnell, "Chemisorption," Butterworth Publications, Pergamon Press (1955).

99. A. W. Adamson, "Physical Chemistry of Surfaces," Interscience Publishers Inc., New York (1960).

IONIZATION GAUGES

100. D. H. Holkeboer and D. J. Santeler: "Ion Gauge Characteristics in a Space Simulation Chamber," Third Annual Symposium on Space Environment Simulation, June 1962.

101. "Study of Ultrahigh Vacuum Instrumentation, the Bendix Company Contract," AF 40(600)-955, Sept. 1961.

102. P.A. Redhead, "Errors in Measurement of Pressure with Ionization Gauges," Vacuum Technology Transactions, Proceedings of 7th National Symposium.

103. W. B. Nottingham and F. M. Torney, "A Detailed Examination of the Principles of Ion Gauge Calibration," ASTIA AD248376.

104. H. Schmart, "Forced Periodic Changes of Kinetic Energy of Gas Molecules as a Means of Vacuum Measurement," Rev. Sci. Instr., Vol. 31, pp. 433-438, 1960.

105. R. A. Redhead, "Modulated Bayard-Alpert Gauge," Rev. Sci. Instr., Vol. 31, pp. 343-344, 1960.

106. G. Barnes, "Erroneous Readings of Large Magnitude in a Bayard-Alpert Ionization Gauge and Their Probable Cause," Rev. Sci. Instr., Vol. 31, pp. 1121-1127, 1960.

107. J. J. Kinsella, "The Dependence of Ionization Gauge Sensitivity on Electrode Geometry," Vacuum Symposium Transactions, 1954.

108. W. B. Nottingham, "Design and Properties of the Modified Bayard-Alpert Gauge," Vacuum Symposium Transactions, 1954.

MISCELLANEOUS ARTICLES OF INTEREST

109. I. Farkass and E. J. Barry, "Mass Spectrometry Technique and the Gas Permeability of Solids," American Physcial Society, New England Section Meeting, April 1961.

110. D. W. Breck and J. V. Smith, "Molecular Sieves," Scientific American, January 1959.

111. M. L. Minges, "Current Vacuum Technology and Practice," ASTIA 271-969, Dec. 1961.

112. J. R. Jordan and R. Young, "Molecular Sealing," Parker Seal Company.

113. G. E. Trepus, R. S. Roper, W. R. Hickman, "Design Data for O-Rings and Similar Elastic Seals," WADC Tech. Report 56-272, March 1960.

114. M. D. Bunch and R. L. Powell, "Calibration of Thermocouples at Low Temperatures," Advances in Cryogenic Engineering, New York, Plenum Press, Vol. 3, 1960.

115. R. Stewart, "How to Handle the Problem of Measuring Low Temperature," Power, Vol. 104, (1960).

116. I. Farkass and E. J. Barry, "Improved Elastomer Seal Designs for Large Metal Ultra-High Vacuum Systems Permitting Ultimate Pressure in the Low 10^{-10} Torr Range," Seventh National Symposium on Vacuum Technology Transactions, 1960.

117. H. C. Wolfe, "Temperature, Its Measurement and Control in Science and Industry," Reinhold Publishing Corp., 1955.

118. D. C. Carman, "Flow of Gases Through Porous Media," Butterworths Sci. Publication, London 1956.

119. H. M. Abbott, "Space Environmental Effects on Seals, Gaskets, Adhesives and Other Elastomeric and Polymeric Materials," A Bibliography, ASTIA AD 267531, September 1961.

120. C. C. Minter, "Thermal Conductivity Leak Detector," Rev. of Sci. Instr., Vol. 29, pp. 793-794, 1958.

121. C. C. Minter, "Vacuum Leak Testing with Liquids," Rev. of Sci. Instr., Vol. 31, pp. 458-459.

122. F. J. Norton, "Permeation Problems in High Vacuum," Vacuum Symposium Transactions, 1954.

ACKNOWLEDGMENT

The authors wish to acknowledge gratefully the help and cooperation of Messrs. Hardgrove and Shapiro of the permanent staff. They also appreciate the contributions of Drs. Graham Gutsche, Christopher Wilson, and Paul Stamberger. Finally, they wish to thank Dr. Elias Klein, director of the Summer Workshop, for his untiring support given to the execution of this work.

PART IV

CORONA AND DISCHARGE EFFECTS INSIDE SPACECRAFT AT LOW EXTERNAL PRESSURE

CONTENTS

ILLUSTRATIONS

PART IV

CORONA AND DISCHARGE EFFECTS INSIDE SPACECRAFT AT LOW EXTERNAL PRESSURE

PRELIMINARY STATEMENT

(F. C. Yagerhofer, Space Power Technology Branch, Spacecraft Technology Division, GSFC)

The problem in corona will be discussed in three parts: The first will be a review of the background of the corona problem; the second will be a summary of present spacecraft corona problems; and the third, methods and techniques for the detection and suppression of corona.

First, let us glance into the background of the corona phenomenon. Corona can be defined as that ionization phenomenon which is produced when the ionization potential of a gas or air is exceeded. Corona forms small quantities of ozone, which attacks insulation materials, and oxides of nitrogen which corrode metals. This problem was first encountered years ago in the electrical distribution industry. Even nowadays, the engineers who design overhead-distribution lines will allow a value of about 1000 watts of power loss per mile for a fair-weather day. If the weather gets foul, in rainy or humid weather, for example, this power loss can readily go up by a full order of magnitude.

Another problem encountered years ago was in the aircraft electrical industry. During the war, it was found that dynamotors used aboard the aircraft to change 28 volts to over 400 volts as necessary to power the navigational and surveillance equipment on the airplane had a tendency to generate corona. This shortened the life of the insulation, and at the same time generated a high-frequency component which was reflected into the electronics aboard the aircraft.

Although a lot of vile things have been said about the corona, it can nevertheless be employed to a useful end. At the Naval Research Laboratory, we tried to use the corona-starting voltage as a method for studying the quality of insulation materials. We wanted to establish a nondestructive test to depict adequately the true condition of the insulation in, let's say, an aircraft generator. We found in our tests that the breakdown potential was approximately twice the corona-starting voltage (CSV). We determined that this corona-starting voltage test would be a valid nondestructive test for periodically testing the quality of insulation, if we could find some method or means to precisely detect the existence of corona. A number of major problem areas remain in the study of corona;

in fact, as far as can be determined, there really is no universally accepted definition for corona even today.

Item 2, a summary of our present spacecraft problems: A number of experimenters here at Goddard have encountered corona. Leo Davis, for example, in his rocket probes, encountered corona in a 2000-volt power supply. He figured, though, since this occurred at altitudes corresponding to 60,000 kilometers, the corona did not exist for a sufficient length of time to create a carbonized path, or anything of that sort. So, since it didn't occur at sea level, nor at the extremely high altitudes, the corona was tolerated. But in his equipment used aboard spacecraft, he encapsulated these critical components in a hard epoxy in order to minimize or eliminate this corona.

Another incident occurred during the thermal vacuum test in the UK-1 satellite, in a power supply that supplied 40,000 volts for the X-ray ionization chambers. This power supply used a plug-in connector to attach the external wiring into the power supply, and arc-over occurred right at the connector. Now, somehow or other, this gaseous discharge got into some of the transistors located in close proximity and damaged them. A puncture occurred from the emitter to the base in one of the transistors. The fix in this instance consisted in removing the entire connector and installing a solid conductor with a heavy insulation, plus an additional insulating sleeving, which eliminated the problem from this particular experiment.

Mr. Flanick encountered corona in his high-voltage power supplies for the Geiger-Muller as well as for the photomultiplier tubes. He employed the standard technique of encapsulating the critical components in a hard epoxy; in some instances, he used a rubberized silastic compound to eliminate corona.

In our own case we designed a 6,000-volt power supply to be used for the Redhead gauge in the S-6 atmospheric structure satellite. During vacuum tests, corona appeared in the transformer core. We increased the thicknesses of the Teflon insulation between the layers of this saturable core and potted it with a foster-cast polyester, which eliminated the corona.

This brings us now to our third item, the methods and techniques for corona suppression. There are three basic methods: one, by pressurization or evacuation. Pressurization, as you probably know, is employed for the wave guides used on high-powered radar equipment. A second way is to increase the radius of curvature of the current-carrying conductor. The voltage gradient at any point on the surface of a conductor varies approximately inversely with the radius of curvature. Thus, to eliminate discharge, increase the curvature of all points at high voltage. This system, by the way, is used in our high-voltage power-distribution lines. You find in a 500-kv line a 2-inch OD conductor; this is really a thin-walled tubing, with about a quarter-inch or an eighth of an inch wall. Now, this large diameter isn't necessarily for carrying heavy currents—it's to eliminate, or at least minimize, the corona power loss.

The third method which I mentioned earlier, is to encapsulate or to immerse the critical components in a high dielectric material such as an epoxy, rubberized silastic, or oil. Any of these methods can be used, but there must be no contaminants on the surface of the conductor, and no voids in which ionization can form between the wire and insulation.

I have briefly covered a few of the problems that we have had in the past. A number of problems remain to be solved, particularly an accurate means of detecting corona, as well as improved dielectric-strength materials capable of withstanding satellite environment.

ON THE BREAKDOWN VOLTAGES OF SOME ELECTRONEGATIVE GASES AT LOW PRESSURES

by

Stefan Schreier

ABSTRACT

The breakdown voltages of five Freon gases and SF_6 were determined at low pressures between parallel plates, with a view to determining their insulating properties under these conditions, and especially to find their minimum breakdown voltages. It was found that the advantages of these gases over air is much less at low pressures than at atmospheric pressure or higher, and that the use of these gases as insulators at lower pressures is therefore limited. Preliminary investigations reveal, however, that the vapors of compounds which are liquid at normal temperature and pressure, such as FC-75, maintain their dielectric strength much better than do electronegative gases as the pressure is reduced, and thus seem to hold promise as insulators at lower pressure.

INTRODUCTION

Certain artificial earth satellites, having direct-current power supplies in the range of 1,600 to 2,000 volts, were found to have difficulties caused by corona-type discharges when passing through altitudes in the vicinity of 100,000 feet. These difficulties occurred because the equivalent pd (p equals pressure and d equals distance between electrodes) in the satellites passes through the range of minimum breakdown voltage, which in air is about 350 volts. No difficulties occurred at either higher or lower altitudes, as might be expected from Paschen's Law, which states that the breakdown voltage between two electrodes is a function of the pressure times the distance between the electroces and decreases with this product down to a certain minimum, after which it rises again as pd decreases further.

The exact shape and location of the curve of pd versus breakdown voltage will depend on the shape of the electrodes, the material of which they are made, and the nature of the dielectric between them.

Various suggestions have been made for preventing corona-type discharges in satellites. The solution presently in use consists of imbedding all electrodes (charged conductors) in a solid dielectric, thus making gaseous discharges impossible. This has the disadvantage that, once conductors are so imbedded, they are difficult to remove. Other

suggestions include the use of electronegative gases as insulators (the subject of the present investigation), pressurizing high-voltage components, immersing them in oil, evacuation of the entire system, keeping the power off until the critical values of pd have been passed (delayed switching), and artificial suppression of free electrons in the gas. Some of these suggestions may well bear further investigation. Other possible avenues of investigation are the seeking of improved design criteria to delay corona, and the further study of the effects of electrode materials and configurations with a view not only to prevent, if possible, the onset of corona, but also to provide the designer with improved methods of predicting when corona may occur.

In order to solve the satellite problem, it was proposed to enclose the high-voltage components in an electronegative gas which would be allowed to leak out as the satellite rose, maintaining the pressure inside the satellite about the same as the pressure outside. This would eliminate the need for pressurization and the danger of unintentional leaks, and would prevent corona-type discharges as long as the minimum breakdown voltage of the gas was higher than the maximum voltage expected in the satellite. For this reason, a study was undertaken to find the minimum breakdown voltages of certain electronegative gases.

PREVIOUS WORK ON ELECTRONEGATIVE GASES

As is well-known, electronegative gases obtain their dielectric strength from the fact that their molecules have a tendency to absorb loose electrons, thus inhibiting the electron avalanches necessary for breakdown. This is already discussed briefly in Meek and Craggs.[1] A somewhat longer summary has been given by Devins and Sharbaugh.[2] The effect of pressure on the positive-point-to-plane discharge for some electronegative gases was investigated in 1939 by Pollack and Cooper.[3] After the war, further investigations were undertaken by Camilli and Chapman[4] and Wilson Simons and Brice.[5] Further work was done on fluorine-containing gases by Camilli and Plump in 1952.[6] Additional theoretical considerations were given by Geballe and Reeves in 1953.[7] The electric breakdown of perfluorocarbon vapors and their mixtures with nitrogen were discussed by Berberich, Works, and Lindsay in 1955;[8] the dielectric behavior of some fluorogases and their mixtures was also discussed in the same year by Camilli, Liao, and Plump.[9] Additional discussion of factors controlling electric strength of gaseous insulation was given by Narbut, Berg, Works and Dakin in 1959.[10] The advantages of gas insulated power transformers were discussed by Camilli in 1959.[11] In the same year, Blodgett evaluated some of the dielectric properties of octafluorocyclobutane.[12] A further discussion of fluorocarbons as electrical insulators was given by Reuther in 1961.[13]

The above is by no means a complete listing, but is merely given as an illustration of some of the things which had been done in this field. Further references may be found in AIEE Special Publication S-97.[14] The difficulty with most of the previous work is that it is concerned chiefly with the insulating properties of gases at atmospheric or higher

pressures; very little had been said about breakdown at lower pressures, and especially about minimum breakdown voltages.

GASES CONSIDERED IN THE PRESENT STUDY

The gases considered in the present study were Freons 14, 114, 115, 116, and C318. SF_6 was chosen because it is perhaps the best known and most used of the electronegative gases. The newer Freons were evaluated because little is as yet known about their properties, and it was hoped that they would prove superior to their older relatives.

FREON 14. Freon 14 is perfluoromethane, CF_4. It has a molecular weight of 88.01, boils at -128°C, and freezes at -168°C at one atmosphere pressure. Its dielectric strength at one atmosphere and 23°C relative to nitrogen is 1, and its dielectric constant is 1.0006 at 24.5°C and one atmosphere.

FREON 114. Freon 114 is $CClF_2$-$CClF_2$. It has a molecular weight of 170.93, boils at 3.55°C and freezes at -94°C at one atmosphere pressure. Its dielectric strength relative to nitrogen is 2.8 at one atmosphere and 23°C, and its dielectric constant is 1.0021 at 26.8°C and one atmosphere.

FREON 115. Freon 115 is chloropentafluoroethane, $CClF_2$-CF_3. It has a molecular weight of 154.48, boils at -38°C, and freezes at -106°C at one atmosphere pressure. Its dielectric strength relative to nitrogen is 2.8 at one atmosphere and 23°C, and its dielectric constant is 1.0018 at 27.4°C and one atmosphere.

FREON 116. Freon 116 is hexafluoroethane, C_2F_6. It has a molecular weight of 138.0, boils at -78.2°C and freezes at -100.6°C at one atmosphere pressure. Its dielectric strength relative to nitrogen is 1.96 at one atmosphere, and its dielectric constant is 1.00197 at 23°C and 711 mm/Hg.

FREON C318. Freon C318 is octafluorocyclobutane, C_4F_8 (cyclic). It has a molecular weight of 200, boils at -6.0°C and freezes at -41.4°C at one atmosphere pressure. Its dielectric strength relative to nitrogen is 2.63 at one atmosphere, and its dielectric constant is 1.0034 at 10°C and 760 mm/Hg.

The properties of sulfurhexafluoride, SF_6, are well-known. Its molecular weight is 146, it boils at -63.8°C at one atmosphere, and its dielectric strength relative to nitrogen is 2.5 at one atmosphere.

THE EQUIPMENT USED

The equipment used was a variant of that used by Dakin and Lim[15] of Westinghouse and that of Brancato* of the Naval Research Laboratory (Figures 4-1 and 4-2). Two

*Emanuel L. Brancato, Naval Research Laboratory, Washington, D.C.

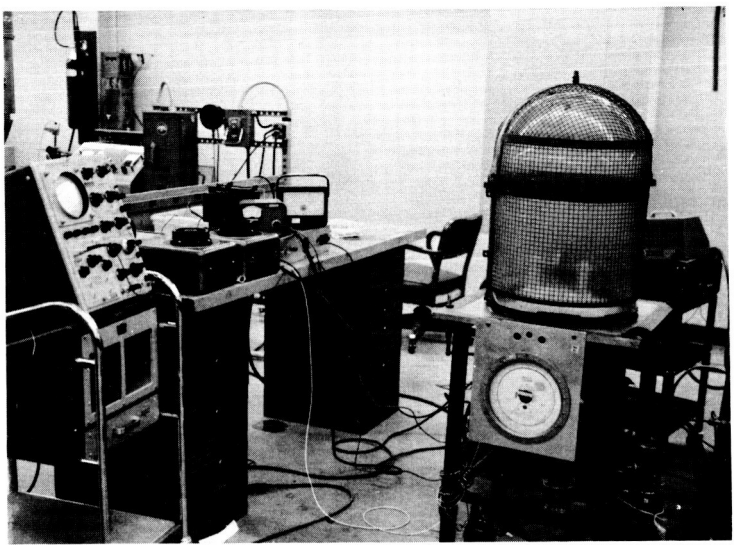

(a) Total setup, showing scope, variacs, vacuum gauge, voltmeter, bell jar, and pressure gauge

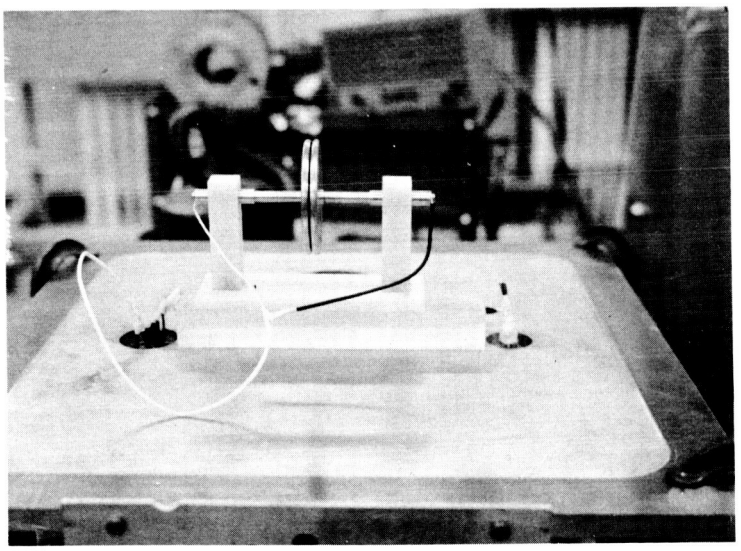

(b) The electrodes

Figure 4-1 - Experimental equipment for determining breakdown voltage of electro-negative gaser

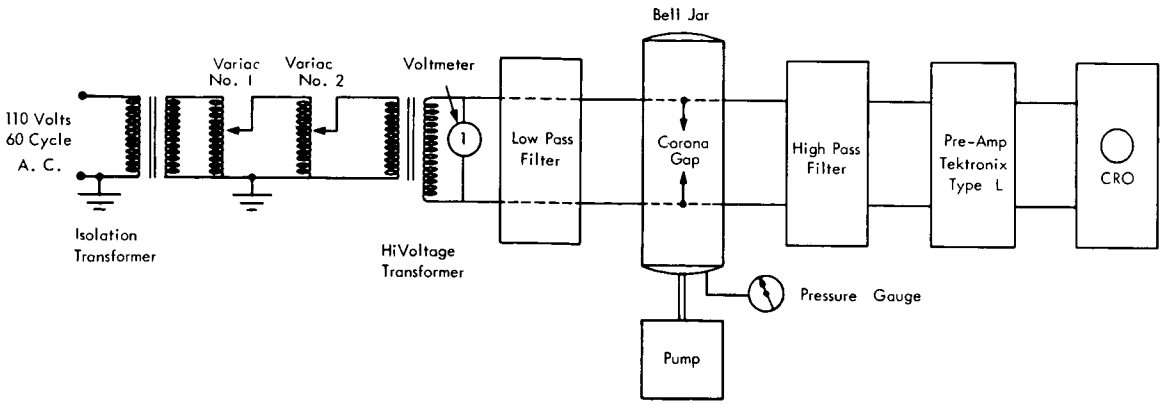

Figure 4-2 – Experimental equipment, block diagram

parallel circular brass plates, 4 inches in diameter and 1/4-inch thick with rounded edges of 1/8-inch radius, mounted on a teflon base, were used as electrodes. These were connected to a 3,000-volt transformer connected to an ordinary 60-cycle 110-volt power supply. 60-cycle alternating current has the advantage over direct current that, while it yields the same type of corona as direct current, because of its relatively slow oscillation, it triggers corona at each peak of the cycle on a regular basis at the proper voltage and thus makes it much easier to study the phenomenon (Figure 4-3). Filters were used both to suppress high-frequency noise from the power supply before it reached the electrodes, and to filter out the 60-cycle sine wave before feeding the signal to the oscilloscope. The presence of corona was determined by observing the signal from the electrodes on a Tektronix type 545A oscilloscope, using a type L plug in unit preamplifier with a fast rise time. The electrodes themselves were placed in a bell jar which was evacuated by means of a mechanical pump capable of reducing the pressure in the bell jar to 45 microns of mercury. Voltages across the electrodes were read from a carefully calibrated Simpson vacuum-tube voltmeter. The pressure inside the bell jar was read from a Wallace and Tierney absolute-pressure gauge calibrated to read NACA 1956 standard atmosphere to 200,000 feet; from 1 mm/Hg on down, the pressure was also read from a Consolidated Vacuum Corporation thermocouple vacuum gauge, giving a double check in the range of equivalent altitude from about 150,000 to 200,000 feet. The filters were immersed in transformer oil to prevent the possibility of local discharges occuring in the circuit.

THE EXPERIMENTAL PROCEDURE

The equipment was first tested in air (Figure 4-4) to make sure it was operating properly and to provide a basis for comparison with subsequent readings, as it is well-known that the exact shape of the Paschen curve tends to depend on the particular configuration and equipment being used. To test other gases, the bell jar was first evacuated to a pressure of 60 microns of mercury; enough gas was then introduced to raise the

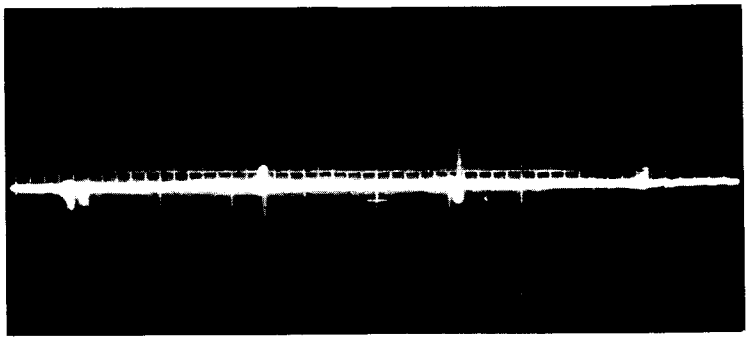

(a) Corona discharges being triggered by 60-cycle sine wave

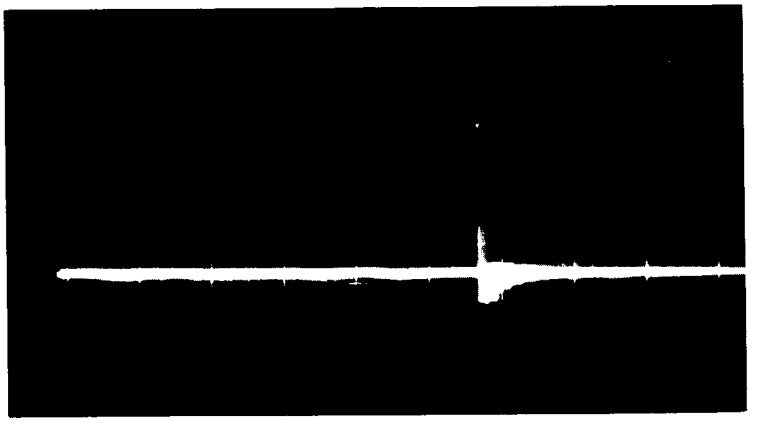

(b) Single corona pulse, showing initial spike (double exposure) followed by reverberation

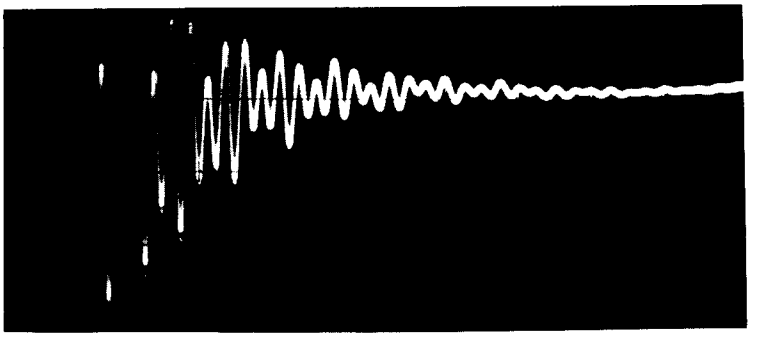

(c) Detail of reverberation following corona pulse (about 1 millisecond)

Figure 4-3 - Phenomenon of corona discharge

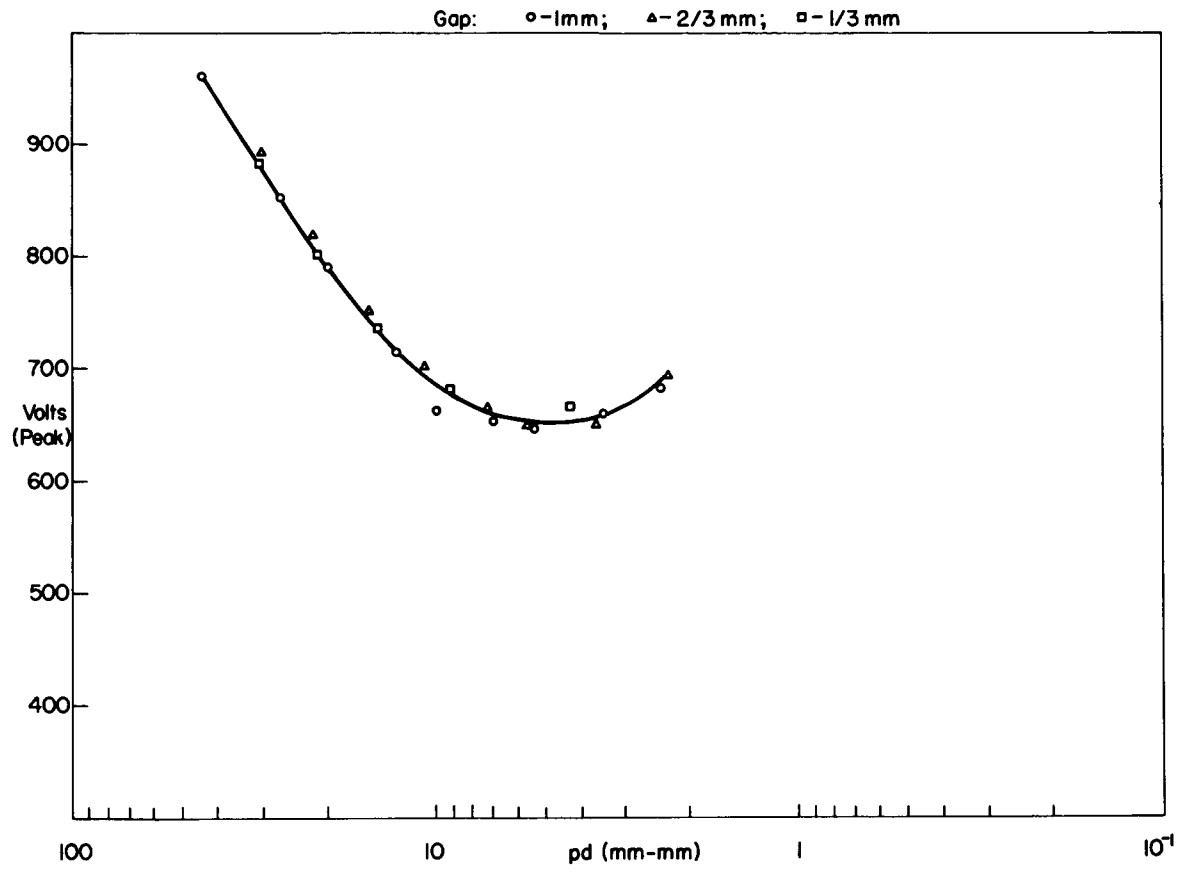

Figure 4-4 - Paschen curve, air test

pressure to 60 mm/Hg or more, thus guaranteeing a purity of 99.9% in the gas being tested. After the pressure was recorded, the voltage was raised across the electrodes until breakdown was observed on the oscilloscope. The voltage was then backed off until the discharge ceased and then raised again in small increments until corona was again observed. This procedure was followed to prevent errors due to time-lag effects. For each reading, the entire procedure was followed twice to make sure the reading was correct. Once the reading was obtained for a given pressure, enough gas was pumped out to lower the pressure by about 10,000 feet equivalent altitude (around 5,000 feet near the minimum voltage), and the next breakdown voltage was obtained. Three runs were made for each gas, using a gapwidth between the electrodes of 1 mm, 2/3 mm, and 1/3 mm.

CONCLUSION

The results show that the electronegative gases tested lose most of their advantage over air as insulators at lower pressures. Freon 114, which has one of the highest dielectric strengths of any of the Freons at atmospheric pressure, was found to have the lowest minimum breakdown voltage of any of the gases tested (about 435 volts). SF_6 was

found to have the highest minimum breakdown voltage (520 volts) as compared to a minimum for air of 353 volts, in the present configuration. Note that the relation between breakdown voltage and molecular weight mentioned by Camilli[11] ceases to hold for the minimum breakdown voltage.

The results of these tests, shown in Figures 4-5 through 4-10, indicate that gases of the type tested are not too promising as insulators at lower pressures in satellites. On the other hand, preliminary tests indicate that vapors of such liquids as FC-75 seem to keep their dielectric properties much better than gases at lower pressures. Two new Freon compounds currently under development, which are liquid at normal temperature and pressure, also hold promise; they are 1,1,1,3-tetrachlorofluoropropane, and 1,1,1-trichloropentafluoropropane. The former especially is claimed by the manufacturer to have a dielectric strength in vapor form 4.7 times that of FC-75. These vapors would seem to merit further investigation.

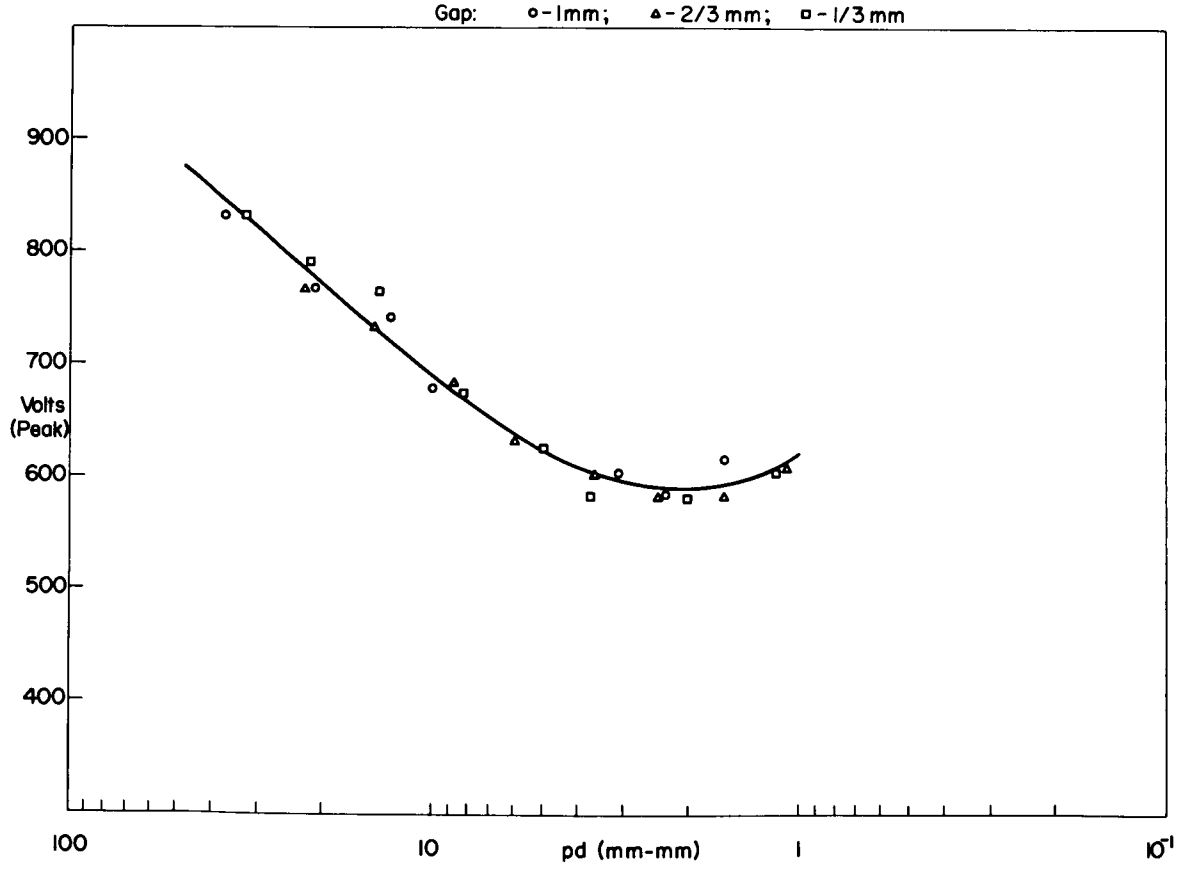

Figure 4-5 - Paschen curve, Freon 14

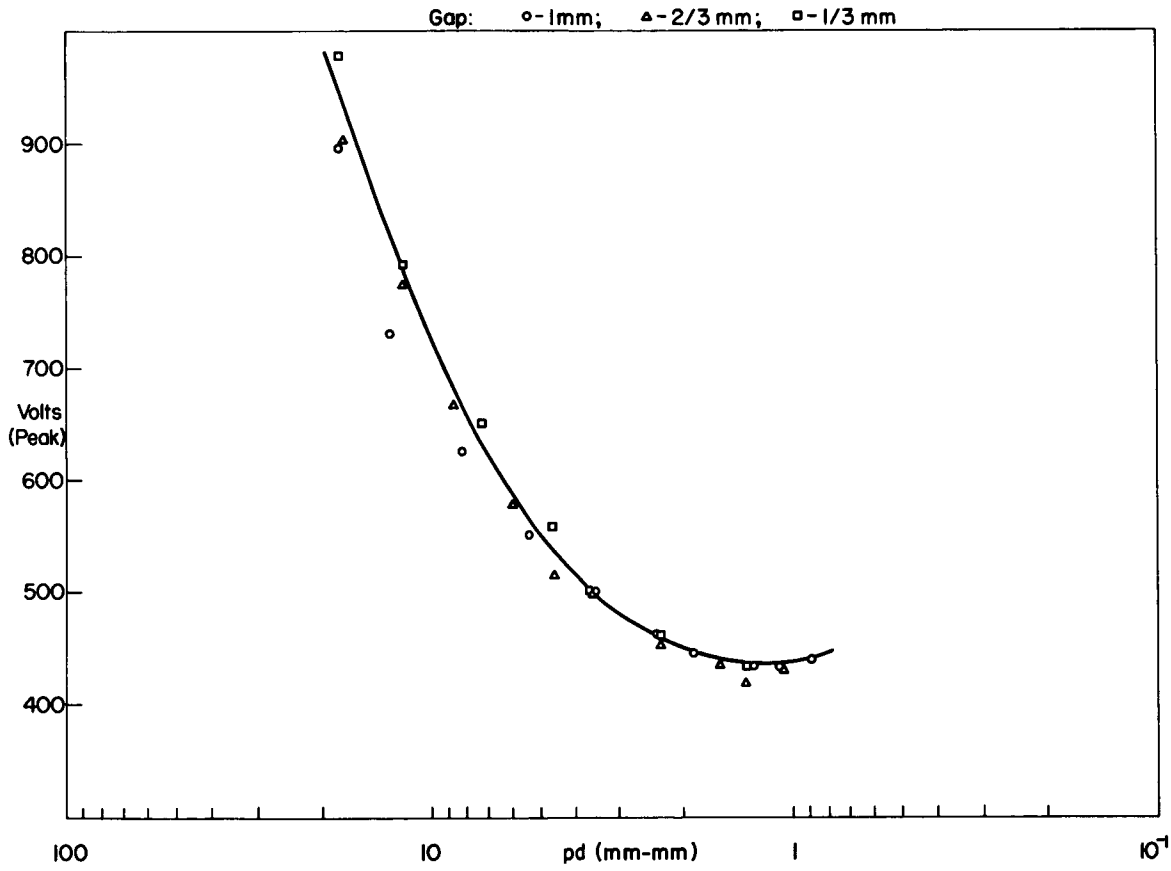

Figure 4-6 - Paschen curve, Freon 114

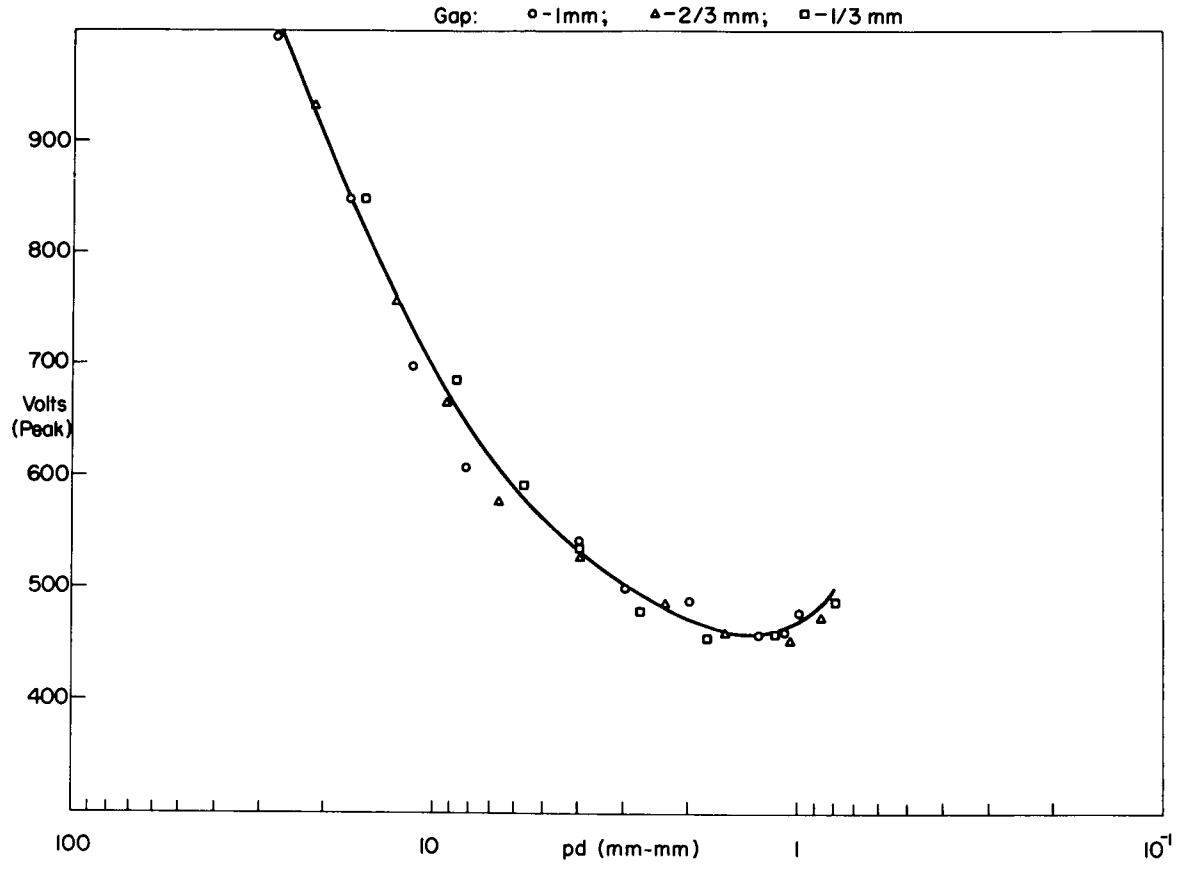

Figure 4-7 - Paschen curve, Freon 115

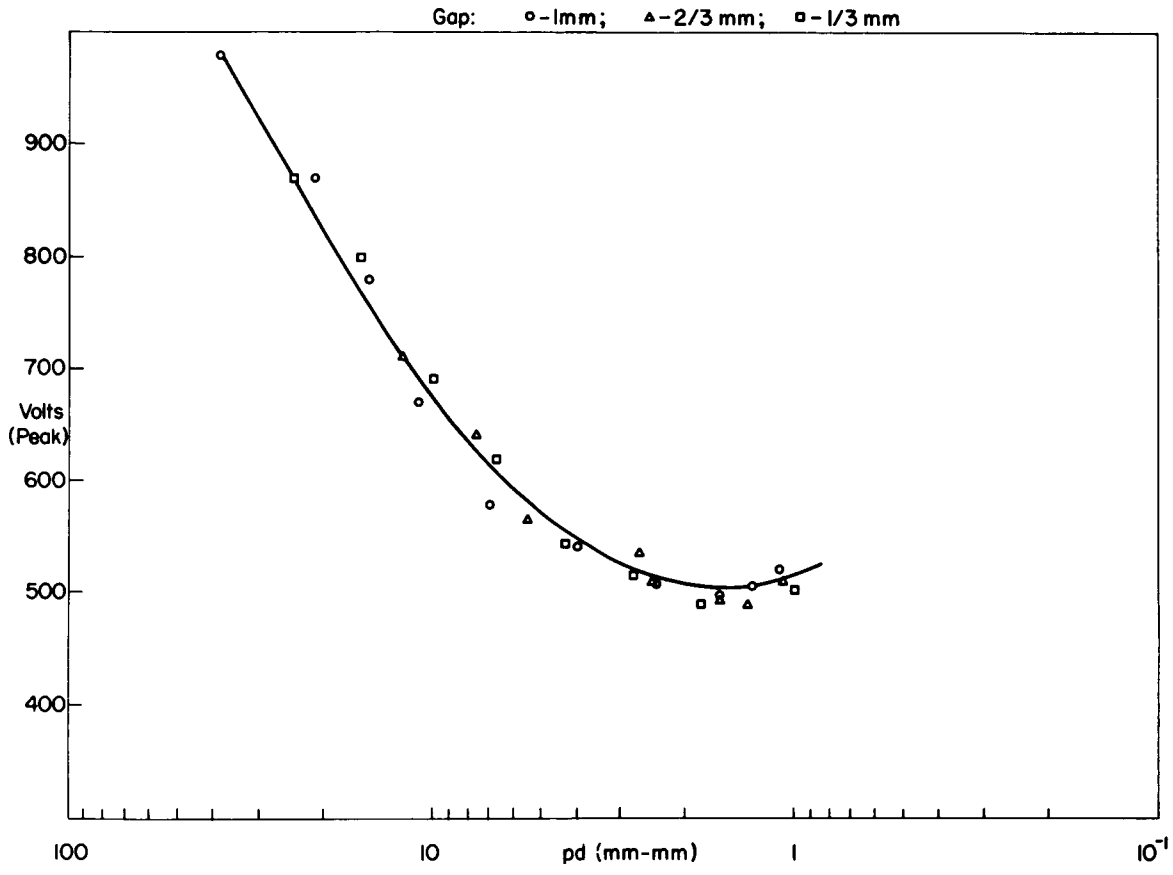

Figure 4-8 - Paschen curve, Freon 116

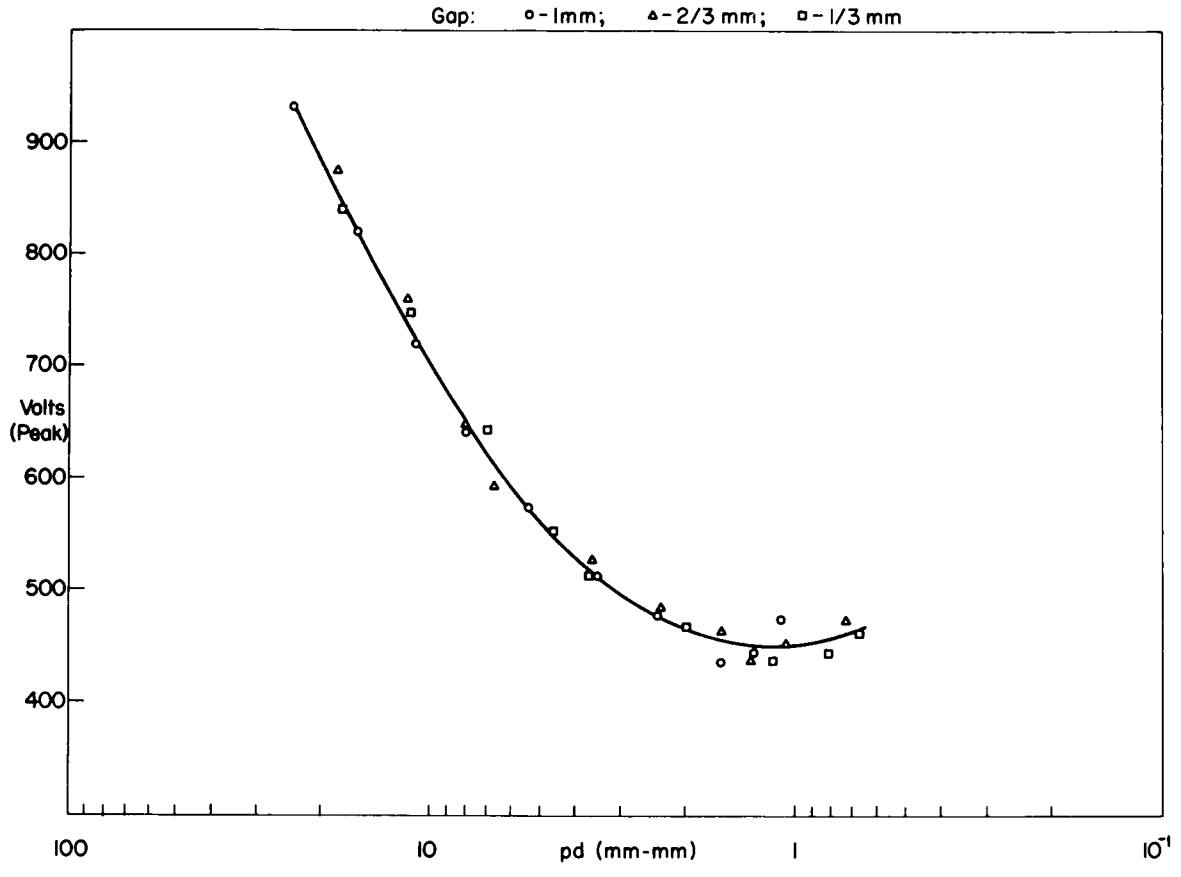

Figure 4-9 - Paschen curve, Freon C-318

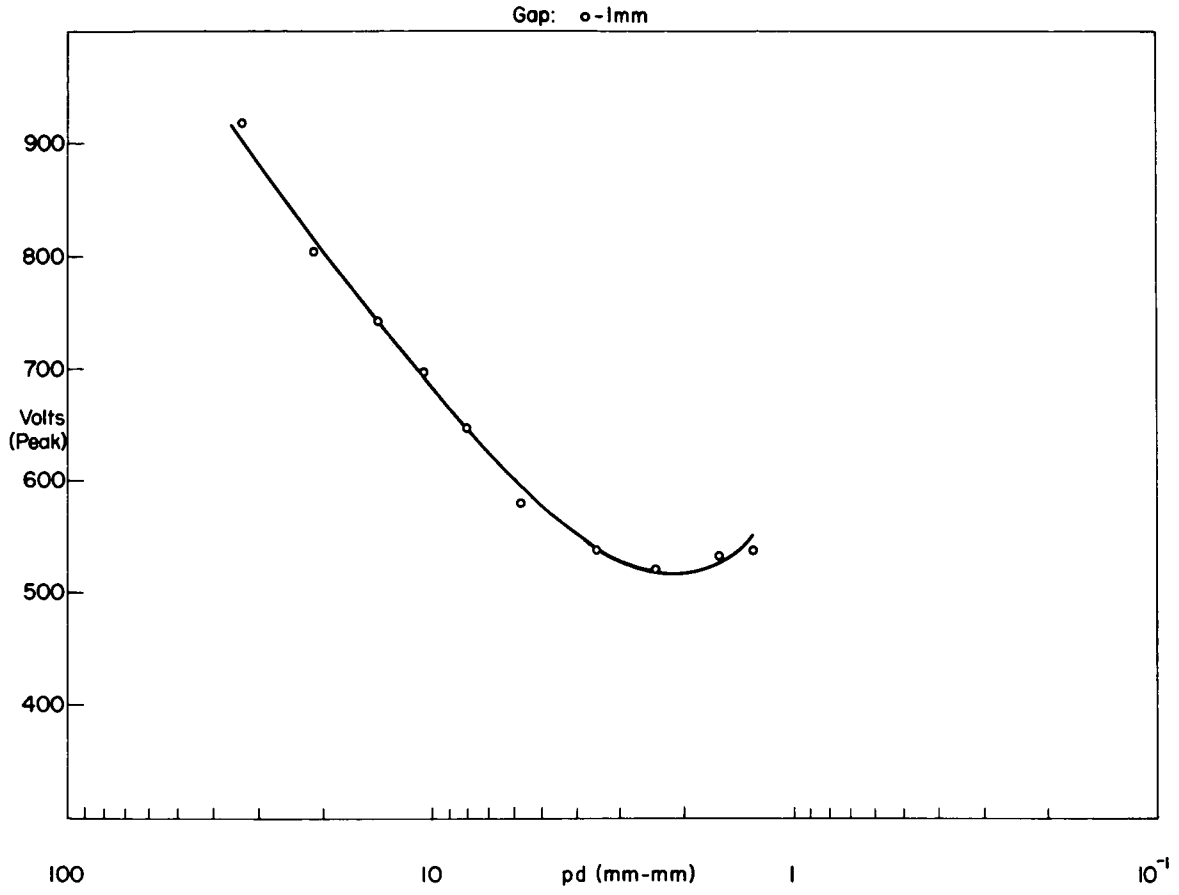

Figure 4-10 - Paschen curve, SF_6

REFERENCES

1. "Electrical Breakdown of Gases," J. M. Meek and J. D. Craggs, Oxford at the Clarenden Press, 1953.

2. "The Fundamental Nature of Electrical Breakdown," J. C. Devins and A. H. Sharbaugh, Electro Technology, Science and Engineering Series, February, 1961.

3. "The Effect of Pressure in the Positive Point to Plane Discharge in N_2, O_2, CO_2, SO_2, SF_6, CCl_2F_2, A, He, and H_2," H. C. Pollack and F. S. Cooper, Physical Review, July 15, 1939.

4. AIEE Technical Paper 47-240 (September 1947), G. Camilli and J. J. Chapman.

5. "The Dielectric Strength of Gaseous Fluorocarbons," W. A. Wilson, J. H. Simons, and T. J. Brice, Journal of Applied Physics, March 1950.

6. "Flourine-Containing Gaseous Dielectrics," G. Camilli and R. E. Plump, Transactions of the AIEE, May 1953.

7. "A Condition on Uniform Field Breakdown in Electron-Attaching Gases," R. Gabelle and M. L. Reeves, Physical Review, November 1953.

8. "Electric Breakdown of Perfluorocarbon Vapors and Their Mixtures with Nitrogen," L. J. Berberich, C. N. Works, E. W. Lindsay, Transactions of the AIEE, October 1955.

9. "The Dielectric Behavior of Some Fluorogases and Their Mixtures," G. Camilli, T. W. Liao, and R. E. Plump, Transactions of the AIEE, November 1955.

10. "Factors Controlling Electric Strength of Gaseous Insulation," P. Narbut, D. Berg, C. N. Works, and T. W. Dakin, Transactions of the AIEE, August 1959.

11. "Gas-Insulated Power Transformers," G. Camilli, The Institution of Electrical Engineers, August 1960.

12. "Properties of Octafluorocyclobutane, a Dielectric Gas," F. W. Blodgett, Transactions of the AIEE, March 1959.

13. "Fluorokarbone als Elektrische Isolierstoffe," H. Reuther, Elektrie, June 1961.

14. "Bibliography on Gaseous Dielectric Phenomena," AIEE Special Publication S-97, April 1957.

15. "Corona Measurement and Interpretation," T. W. Dakin and J. Lim, Transactions of the AIEE, December 1957.

ACKNOWLEDGMENT

This work was performed at the Goddard Space Flight Center of the National Aeronautics and Space Administration, Greenbelt, Maryland, whose generous support the author wishes to gratefully acknowledge.

The author is especially indebted to Dr. Elias Klein of NASA and to Dr. Donald L. Waidelich of the University of Missouri for their constant assistance and advice during the course of this work. He would also like to express his appreciation to Dr. Thomas W. Dakin of Westinghouse, and to Mr. G. Camilli, formerly of General Electric, for their helpful advice so unstintingly given, and to Dr. Eugene C. Coyner of E. I. Du Pont de Nemours and Company who supplied the freon gases used and who gave generously of his time and counsel.

Last but not least, the author would like to express his appreciation for the assistance given him by the many technicians and machinists of the Goddard Space Flight Center, without whose assistance this work would not have been possible.

PART V

MAGNETIC FIELD SIMULATION

CONTENTS

ILLUSTRATION

TABLE

PART V

MAGNETIC FIELD SIMULATION

PRELIMINARY STATEMENT

(By Dr. J. Heppner, Fields and Particles Branch, Space Sciences Division, GSFC)

As is well-known, the earth's field is roughly a dipole, and some of the principal areas of investigation in space science are the magnetic field, the radiation belts, and so forth, so that quite a bit of emphasis goes into measuring the magnetic field. If we consider the requirements, say, of a satellite instrumented with magnetometer, we'll hit on problems encountered in almost all other satellites.

Under the category of magnetometer test, it is desired to map the magnetic field at the surface of the earth, where it ranges from around 31,000 gammas (1 gamma = 10^{-5} gauss) at the equator to about 65,000 gammas at the poles. On the other hand, at great distances from the earth, the fields may interfere with and cancel each other. Hence, in order to be sure that magnetometers will operate under such conditions, magnetic-field simulation must be capable of ranging anywhere from one gamma up to, say, 65,000 gammas.

To calibrate these various types of magnetometers and to determine their frequency response, they must have a very homogeneous field in which to operate, certainly much better than the field existing in the air around us.

Since a magnetometer generally must be located some distance away from the spacecraft, as on a boom, so that the fields may not be severely distorted by the spacecraft itself, additional problems arise. At this distance, it will have thermal problems all its own; it is not part of the overall heat balance of the system, and its thermal condition fluctuates wildly due to its very small heat capacity. This would require that it be tested in a nonmagnetic thermal-vacuum chamber.

After a magnetometer has been placed in a certain position, it must stay there. Components of the rest of the spacecraft (and even the whole package) must be tested to make certain they do not interfere with the operation of the magnetometer. If interference does occur, the magnetic materials and current loops within the spacecraft must be eliminated.

As the spacecrafts grow larger, a very large volume must be sought over which there is a controlled homogeneous magnetic field; this leads to rather large coil systems, with very precise controls and very fine tolerances in the coils.

These same considerations apply to a lesser degree to practically all payloads, one reason being that many satellites–sounding rockets especially–use small magnetometers as an inexpensive method of determining orientation up to a few degrees of accuracy. This isn't too bad, as long as the rocket is going up only a few thousand kilometers or less. Nevertheless, magnetometers still must be located properly for proper operation.

There is another category, namely, satellite orientation control, that is, using the magnetic field to control the orientation of the vehicle. When you put in a large magnet, which then locks into the magnetic field, such as in TRANSIT, one will want to know how well it's going to lock in. One must also know beforehand the moment of the payload, etc. This is control in the passive sense.

Semiactive systems, like TIROS, are designed to change the orientation of the spacecraft. A large current is put through a coil and the torque between that field and the earth's field produces a transient change in the position of the satellite. In this way it can be reoriented, and pictures can be taken over more of the orbit. In these last two cases one must be able to take measurements on the variability of the magnetic torque.

Then there are systems, such as the OAO, where the magnetic field is used in an active sense; measurements of the magnetic field are made, and that information is used to operate gas jets, etc., to orient the vehicle.

One of the important things is to know the variability of the field and how this affects the payload. The magnetic properties of the materials inside haven't changed, but their position on a B-H curve has changed, and measurements must be made to find the whole range of variation to determine its limits.

The spinning of a satellite, especially if it is small and metallic, introduces new problems. When a satellite spins in a magnetic field, the spin damps out rather fast if there is much of a surface. In fact, fields of 5,000 gammas or so can be generated inside a metal ball like a typical Vanguard satellite, just due to the fact that there is a conducting surface spinning in a magnetic field. So spin damping becomes another of these problems.

MAGNETIC FIELD SIMULATION

by

D. L. Waidelich and M. E. Pittman

ABSTRACT

Several new and, in some respects, better solutions have been obtained relating to the production of homogeneous magnetic fields by the use of circular coil systems.

Previous work exists in many forms, mainly giving particular solutions in which the author is interested, such as setting all currents equal or setting the radii equal.

The work deals with the calculation leading to two particular types of optimal systems: the optimum for the largest coil radius and the optimum for the mean coil radius.

One calculation is presented on the tolerances necessary when one coil is moved from its optimum position.

INTRODUCTION

In testing the magnetic properties and instruments of spacecraft, there is a need to cancel the earth's magnetic field and then to produce a very homogeneous controlled magnetic field. It is desired to produce a magnetic field homogeneous to 1 part in 10^5, such that there is ample access to the working volume. The electrical design and construction should be simple, and the largest possible mechanical tolerances should exist. It is the purpose of this report to review briefly some of the previous work on circular coil systems, and to present the results of calculations made on these systems during the Summer Workshop. In addition, some work on tolerances will be given.

THEORY OF IDEAL COIL SYSTEMS

In his paper, McKeehan[1] reviews many of the more important particular solutions for producing a homogeneous magnetic field using two, three, four, six and eight loops, and also gives several new solutions. Our equations and terminology are the same as

his. In some cases the distances to the periphery of the coils are kept constant. This was done by Maxwell[2] for 3 coils, by McKeehan[1] and Garrett[3] for 4 coils and by Williams and Cain[4] for six and eight coils. Fanselau[5,6] and Braunbek[7] held the currents equal. McKeehan[1] used equal currents in a six-coil solution. Barker[8,9] solved for 3 and 4 identical coils. Additional work on these systems is given in Sauter.[10]

Two methods of attack were considered; one[11,12] used the idea of making the field the same at a number of points along the axis, but did not control the magnetic gradients that exist. The second[1] used the idea of making as many terms zero as possible in the series for the magnetic field on the axis of the system. This method, which afforded some control of the magnetic gradients, was the one used here. Both circular[1] and rectangular[11] coil systems were considered, but it was decided to work on the circular coils because more work had been done on these and there is more symmetry present; in addition, rectangular systems are more difficult to calculate. The problem of calculating the circular coil system may be worked by the use of elliptic functions, or by an infinite series of Legendre functions; the use of the elliptic functions proved to be quite difficult, and the method using Legendre polynomial expansions was adopted.

One other method of obtaining a uniform field was considered: this was the use of a spherical current sheet[13,14] in which the current density varies as the sine of the angle that the radius vector makes with the axis. This method, while giving a theoretically perfectly uniform field, would allow an extremely limited access or would require the use of many connections to permit access. It was felt that the disadvantage of poor access ruled out further consideration of this method.

The scalar potential due to a single coil, whose periphery is described in polar coordinates as r_p and θ_p at a point r and θ is given by:

$$V_p = \frac{2\pi i_p}{C} \left\{ 1 + u_p - (1 - u_p^2) \sum_{n=1}^{\infty} \frac{1}{n} (r/r_p)^n P'_n(u_p) P_n(u) \right\}, \qquad (1)$$

FOR $r < r_p$.

Here V_p is expressed in Gaussian units, i_p is the current in the pth coil, c is the velocity of light, and u and u_p are used in place of $\cos\theta$ and $\cos\theta_p$, respectively. $P_n(x)$ and $P'_n(x)$ are the nth Legendre polynomial and its first derivative, respectively. This is illustrated in Figure 5-1. The total potential V equals $\sum_p V_p$.

Since $|P_n(u)| \leq 1$ and equals one if and only if $u = 1$, it is felt that, if the main inhomogeneities on the axis are eliminated, then the rest of the field will be at least as well off as points on the axis. It now becomes easier to work with the field itself on the axis. If x is the distance (on axis) from the origin, then

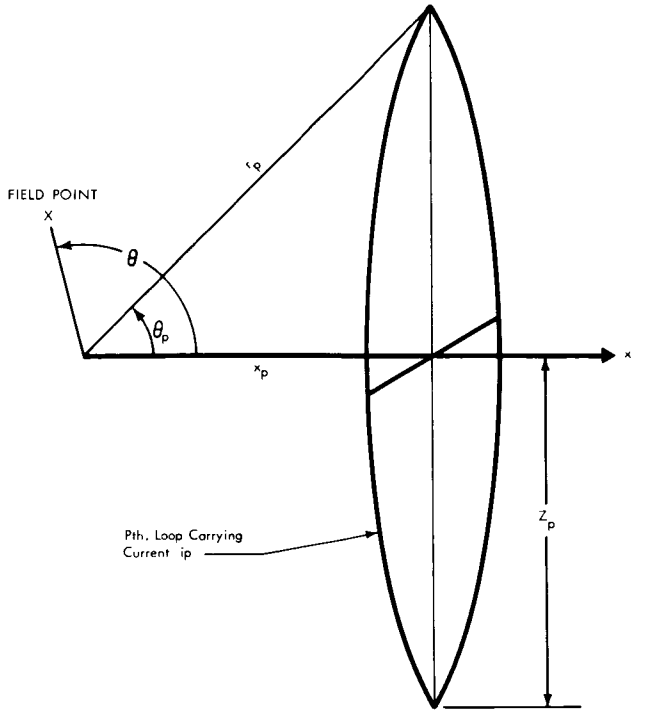

Figure 5-1.

$$H(x) = \frac{2\pi}{c} \sum_{n=0}^{\infty} x^n \left\{ \sum_p i_p (1 - u_p^2)\, P'_{n+1}(u_p) / r_p^{n+1} \right\} \tag{2}$$

where H is the component of the field parallel to the axis.

As long as the coils occur in pairs, symmetric about the origin, then the parity of the Legendre polynomials will eliminate the inner brackets for n odd, and the sum need be taken only over even terms. The field will be of the form:

$$H(x) = \sum_{n=0}^{\infty} a_{2n} x^{2n} = a_o + a_2 x^2 + a_4 x^4 + \cdots \tag{3}$$

Perfect homogeneity is obtained if a_2, a_4, etc., are all identically zero, as in the case of the so-called sine-windings on a sphere.

Approximations can be made here so that a finite number of terms, a_2, a_4, . . . a_{n-2} are zero. To find the volume of homogeneity, rewrite the equation as:

$$H(x) = a_o \left(1 + \bar{r}\, \frac{a_n}{a_o} \left(\frac{x}{\bar{r}}\right)^n + \cdots\right), \tag{4}$$

where $\bar{r}$ = mean coil radius = $\sqrt[n]{r_1 \cdot r_2 \cdots r_n}$

Neglecting higher order terms, we see that (for .001%)

$$\left| \bar{r}^n \frac{a_n}{a_o} \left(\frac{x}{\bar{r}}\right)^n \right| \leq 10^{-5}, \text{ or } \frac{x}{\bar{r}} \leq \left| \bar{r}^{-n} \frac{a_o}{a_n} \cdot 10^{-5} \right|^{1/n}. \tag{5}$$

Such an expression as $x/\bar{r}$ must be used rather than x/r_1, etc., to prevent the ratio from going from infinity to zero, as r_1 goes from zero to infinity leaving the other coils constant.

The specification for which $x/\bar{r}$ is a maximum for a particular number of coils, is called the optimum for the mean-coil radius.

Another useful quantity to consider is x/r_{max} where r_{max} is the largest r_p of the system. The point at which this quantity is a maximum is called the optimum for the largest-coil radius. If one is limited to a certain largest volume in which to operate, then obviously this would be the better of the two to use. Unfortunately, this involves changing functions as the ratio of radii crosses unity. It is possible to define other optima as well, but it is believed that the two mentioned above are the most useful and practical.

PARTICULAR CASES

For specifications of all coils mentioned, consult Table 5-1.

EXPLANATION OF TABLE 5-1

The name "efficiency optimum" represents the optimum for the mean-coil radius. The ratios of the currents and radii are given in the table, whereas the magnitudes are determined by the amount of field desired and the volume of workroom desired respectively. The field at the center is given by:

$$H(o) = \frac{2\pi}{c} \sum_p i_p \, (1 - u_p^2) / r_p .$$

As mentioned previously, $\bar{r} = (r_1 \cdot r_2 \cdots r_n)^{1/n}$, noting especially that, for three coils, $\bar{r} = (r_1 \cdot r_2^2)^{1/3}$. Furthermore, i_p is actually equal to the number of turns in each winding time the current in each turn, so that if the same current flows in all wires, $i_2/i_1 = N_2/N_1$, etc.

To determine $H(x)$ at any point on the axis, the table is sufficient. As an example, consider the Helmholtz coil, with a_2 equal to zero. $H(x)$ is then proportional to $(1 - 1.8\,(x/\bar{r})^4)$.

Table 5-1
Specifications of Various Coil Systems

Name and Number of Coils	Ampere (1)	Helmholtz (2)	Barker (3)*	Maxwell (3)*	Efficiency Opt. (3)*
Assumptions	none	none	$z_1 = z_2$	$r_1 = r_2$	none
Which a's are zero	none	a_2	a_2, a_4	a_2, a_4	a_2, a_4
Coefficient of next derivative	-1.5	-1.8	-5.0695298	-2.0428571	-2.036426
u_1	0	±.447214	0	0	0
u_2	-	-	±.760051	±.6546537	±.61627
r_2/r_1	-	-	.796143	1.	1.19697
i_2/i_1	-	-	2.2604	1.53125	3.075846
$x/\bar{r}$	.26%†	4.86%	11.30%	13.031%	13.037%
x/r_{max}	.26%	4.86%	9.71%	13.031%⊕	11.564%

Name and Number of Coils	Fanselau (4)	Braunbek (4)	Barker (4)	McKeehan (4)	Efficiency Opt. (4)
Assumptions	$i_1 = i_2$	$i_1 = i_2$	$z_1 = z_2$	$r_1 = r_2$	none
Which a's are zero	a_2, a_4	a_2, a_4, a_6	a_2, a_4, a_6	a_2, a_4, a_6	a_2, a_4, a_6
Coefficient of next derivative	-1.289	-2.23448	-2.4725	-2.255102	-2.2219679
u_1	±.285232	±.26789	±.243186	±.2852315	±.2723547
u_2	±.765055	±.74213	±.940731	±.7650553	±.7484183
r_2/r_1	1.136009	1.098	1.336	1.	1.0712777
i_2/i_1	1.	1.	2.2604	.6821109	.9040608
$x/\bar{r}$	14.07%	21.682%	21.480%	21.607%	21.677%
x/r_{max}	13.20%	20.682%	18.583%	21.607⊕	20.944%

Name and Number of Coils	Neumann (6)	Braunbek-McKeehan (6)	Cain-Williams (6)	Neumann McKeehan (8)	Cain-Williams (8)
Which a's are zero	a_2, a_4, a_6	a_2 to a_{10}	a_2 to a_{10}	a_2 to a_8	a_2 to a_{14}
u_1	±.20929922⊕	±.190655	±.20929922	±.1652754♦	±.1652754
u_2	±.59170018	±.550274	±.59170018	±.4779250	±.4779250
u_3	±.87174003	±.843307	±.87174003	±.7387739	±.7387739
u_4	-	-	-	±.9195342	±.9195342
r_2/r_1	1.071723	1.046147	1.	1.0222398	1.
r_3/r_1	1.242359	1.157907	1.	1.1827288	1.
r_4/r_1	-	-	-	1.2382935	1.
i_2/i_1	1.	1.	.8270469	1.	.891626
i_3/i_1	1.	1.	.5108492	1.	.686604
i_4/i_1	-	-	-	1.	.406992
x/r_{max}	31%	34%	36%	16%	47%

*Current in middle coil = $2i_1$.
†Where inhomogeneity = 10^{-5}.
⊕Volume optimum, the optimum for the largest coil radius.
⊛Zeroes of $P_7'(u)$.
♦Zeroes of $P_9'(u)$.

A convenient way to find $x/\bar{r}$ (or x/r_{max}) for inhomogeneities other than .001% is to multiply the figures given by $10^{(5+a)/b}$ where a is the logarithm of the desired inohomgeneity, and b is the subscript of the first nonvanishing a.

To find where $x/\bar{r}$ crosses .1% for the Helmholtz coil, $a = \log 10^{-3} = -3$, and $b = 4$. Therefore, $x/\bar{r} = 4.86\% \cdot 10^{1/2} = 15.37\%$.

For convenience:

$$10^{1/2} = 3.1622777$$
$$10^{1/4} = 1.7782794$$
$$10^{1/6} = 1.4677990$$
$$10^{1/8} = 1.3335214$$
$$10^{1/12} = 1.2115275$$

TWO COILS. Since only one variable is free, only one term can be made to vanish, and that is a_2. The criterion, due to Helmholtz, is that $u_p^2 = 0.2$. For such a system, $x/\bar{r} = 4.9\%$.

THREE COILS. The third coil is placed at $u = 0$ to maintain symmetry. a_2 and a_4 can be set equal to zero, as does Maxwell[2] and Barker.[5] If, however, the term $|a_6|\bar{r}^6/a_o$ is determined in terms of one of the variables and minimized analytically, a slightly better system results.

$$f(y) = |a_6|\bar{r}^6/a_o \propto (15y^3 - 9y^2 + 5y + 5)/(y + 1), \tag{6}$$

where $y = u_2^2$.

Then $f'(y) = 0$, yields $u_2^2 = .4\sqrt{6} - .6$,
or $u_2 \simeq .61627$
$x/\bar{r}$ then equals 13.037% as compared with 13.031% of Maxwell's coil and 11.30% as calculated from Barker's.

In studying the optimum for the largest coil radius, x/r_{max}, it was found to coincide with Maxwell's solution to within six decimal places. It should be mentioned that the knowledge gained in solving the three-coil problem was very useful in planning the four-coil solution.

FOUR COILS. With the aid of an IBM 7090 computer, again slightly better results were obtained than previously found. a_2, a_4, and a_6 all vanish. After an unsuccessful attempt to make a_8 vanish, the following scheme was undertaken:

$$a_2 = 0 = P'_3(u_1) - k\,P'_3(u_2)$$

$$a_4 = 0 = P'_5(u_1) - k/r^2\,P'_5(u_2)$$

$$a_6 = 0 = P'_7(u_1) - k/r^4\,P'_7(u_3)$$

where $r = r_2/r_1$ and $k = i_2(1 - u_2^2)/i_1 r^3 (1 - u_1^2)$. (7)

Eliminating k and r yields:

$$\frac{P'_3(u_1)\,P'_7(u_1)}{[P'_5(u_1)]^2} = \frac{P'_3(u_1)\,P'_7(u_2)}{[P'_5(u_2)]^2} = F(u_2)$$

or

$$P'_3(u_1)\,P'_7(u_1) - F(u_2)\,[P'_5(u_1)]^2 = 0. \tag{8}$$

Over the entire range of u_2, this equation was solved for u_1, and then k and r were calculated. Literally hundreds of different solutions were obtained. These solutions included the old ones of McKeehan, Braungek, and Barker, as well as many new ones. It was then decided to minimize the next two terms in the series for added accuracy.

$$H = a_o\,(1 + \bar{r}^{-8} a_8/a_o\,(x/\bar{r})^8 + \bar{r}^{10}\,a_{10}/a_o\,(x/\bar{r})^{10})$$

and

$$(x/\bar{r})^{-8} = \bar{r}^8/a_o\,|a_8 + \bar{r}^2\,a_{10}\,(x/\bar{r})^2|. \tag{9}$$

Iteration procedures yield that

$$x/\bar{r} = 21.677\%.$$

This compares to 21.607% as calculated from McKeehan's[1] data; 21.671% of Braunbek;[7] 21.480% of Barker;[8] and 14.07% of Fanselau.[5] Fanselau's solution makes a_2 and a_4 zero, a_6 is not zero. The other solutions make all three a's zero.

Again the optimum for the largest-coil radius coincides with the solution for equal radii, that of McKeehan.

Another interesting result is that of Fanselau[6] in which the two coils to the one side of the center of the system are placed in one plane, while the other two coils are placed in another parallel plane. This arrangement may have considerable advantages in structural design and accessibility to the object being tested. The disadvantage would be a smaller $x/\bar{r}$ or x/r_{max} than that of the other solution of Fanselau[5] given in Table 5-1. The results for this solution are $u_1 = \pm 0.285232$, $u_2 = \pm 0.765045$, $r_2/r_1 = \pm 0.372820$, $i_2/i_1 = 28.2897$. Scott[17] may have a similar solution. The solutions of Fanselau[6] and Scott[17] appear to make a_2 and a_4 zero. It is believed that, among the many four-coil solutions obtained by use of the computer, there is one that will place two coils in the same plane and the other two coils in another parallel plane. This solution would have the advantage of making a_2, a_4, and a_6 zero, and thus should have a larger volume of uniformity than the solutions of Fanselau[6] or Scott[17], although smaller volume than the optimum four-coil solution given in Table 5-1. It is hoped to pick out this solution and add it to Table 5-1 later.

SIX COILS. A computer program was also set up to solve the six-coil problem. Since seven variables are available (three angles, two current ratios, and two radii ratios), an attempt was made to set six of the derivatives equal to zero. Previous efforts[1,4,16] have made a maximum of five vanish.

Three of the variables can be easily eliminated from the first three equations, and substituted into the remaining derivatives. This leaves the problem as three equations in three unknowns, plus one more which could be set at an arbitrary value. If u_1^2 is less than u_2^2 and u_3^2, then its range is limited between 0 and .2. u_1^2 was to be taken over this range in steps of .001.

Upon meeting an equation such as: $f(x, y, z) = 0$, and guessing approximate solutions: x_o, y_o, z_o; a correction to the variable $\underline{x}$ could be obtained by letting $f(x_o + \Delta x, y_o, z_o) = 0$

$$0 = f(x_o + \Delta x, y_o, z_o) = f(x_o, y_o, z_o) + f'(x_o, y_o, z_o)\,\Delta x + \cdots,$$

where the prime denotes derivatives with respect to $\underline{x}$.

This gives us the first order correction to x_o:

$$\Delta x = -f(x_o, y_o, z_o)/f'(x_o, y_o, z_o)$$

The next approximation to be used is $x_1 = x_o + \Delta x$. Various loops were designed into the program, for all three variables to zero in on the correct values. When the criterion was met that the corrections to the three variables were all less than 10^{-7}, the computer would calculate the seventh derivative with the eventual hope of minimizing it.

RESULTS

In this particular program, numbers frequently arose which were too large or too small for the computer to handle. As a result, traps were built into the program to eliminate these particular values of u_1^2. This happened in 44 of the 200 values. In another 21 cases, the ratios of the radii went imaginary, so these values were eliminated. 132 values did not register, because they were apparently diverging. This was previously taken care of by setting a maximum to the number of times each variable could be incremented. In the remaining three cases, "solutions" were obtained. Here current ratios were on the order of 10^{25}, and radii ratios were about 10^3.

An example is the following set of data:

$$u_1^2 = .02900$$
$$u_2^2 = .67269$$
$$u_3^2 = .71167$$
$$r_1/r_2 = .0003897$$
$$r_1/r_3 = .0004642$$
$$i_2/i_1 = 1.05 \cdot 10^{24}$$
$$i_3/i_1 = -1.64 \cdot 10^{24}$$

As a result, these also should be thrown out, due purely to the ridiculous orders of magnitude.

Despite the very pessimistic results obtained, it is still felt that a much more carefully planned program could be devised without the need for such traps, possibly by some sort of compensation for these large orders of magnitude.

The available solutions of Neumann,[16] and Braunbek-McKeehan[1] for equal currents, and of Cain and Williams[4] for equal radii are listed in the Table.

EIGHT COILS. Solutions for eight coils have also been made. The Neumann-McKeehan[1] solution held the currents equal, and only made four coefficients vanish. Cain and Williams[4] were able to set seven of them zero by holding the radii equal. These solutions are also in Table 1.

TOLERANCES. Raff[15] has discussed the effect of displacing one coil of a particular system, first parallel to the coil system axis and then perpendicular to the system axis. A similar solution was made for the optimum four-coil system, assuming that one of the inner coils is moved slightly parallel to the axis of the system. For the optimum system

$$H(x) = a_o + a_1 x + a_2 x^2 + \cdots , \tag{10}$$

where the odd a's are zero because of the symmetry, and a_2, a_4 and a_6 are zero because of the choice of dimensions and current ratios. Suppose now that one of the inner coils is moved a distance $\Delta\zeta_1$ in the direction of its axis. Then a given a_ℓ which is initially zero has a Taylor's series, two terms of which are

$$a_\ell = a_\ell\Big|_{\Delta\zeta_1=0} + \frac{\partial a_\ell}{\partial\zeta_1}\Big|_{\Delta\zeta_1=0}\Delta\zeta_1 = \frac{\partial a_\ell}{\partial\zeta_1}\Big|_{\Delta\zeta_1=0}\Delta\zeta_1 \tag{11}$$

where

$$\frac{\partial a_\ell}{\partial\zeta_1} = -\frac{i_1(1-u_1^2)\,P'_{\ell+2}(u_1)\,(\ell+1)}{2r_1^{\ell+2}}. \tag{12}$$

From (11) and (12)

$$a_\ell = \frac{-(\ell+1)\,i_1(1-u_1^2)\,P'_{\ell+2}(u_1)}{2r_1^{\ell+2}}\Delta\zeta_1. \tag{13}$$

Now

$$a_o = \frac{i_1}{r_1}\left[(1-u_1^2) + i\,(1-u_2^2)/r\right] \tag{14}$$

where $i = i_2/i_1$ and $r = r_2/r_1$.

From (13) and (14),

$$r_1^\ell\, a_\ell/a_o = -\frac{(\ell+1)\,P'_{\ell+2}(u_2)}{2\left[1+\dfrac{i(1-u_2^2)}{r(1-u_1^2)}\right]}\left(\frac{\Delta\zeta_1}{r_1}\right) \tag{15}$$

Using (10):

$$H = a_o\left[1 + r_1\,a_1/a_o\,(x/r_1) + \cdots + r_1^\ell\,a_\ell/a_o\,(x/r_1)^\ell + \cdots\right] \tag{16}$$

If the results for the optimum four coil system are used

$$H = a_o \left[1 + 0.674 \left(\frac{\Delta\zeta_1}{r_1} \right) \left(\frac{x}{r_1} \right) + 1.81 \left(\frac{\Delta\zeta_1}{r_1} \right) \left(\frac{x}{r_1} \right)^2 + \cdots \right.$$
$$\left. - 1.69 \, (x/r_1)^8 + 2.58 \, (x/r_1)^{10} + \cdots \right].$$

The terms involving $\Delta\zeta_1$, are caused by moving one coil from its optimum position, while the terms involving $(x/r_1)^8$ and $(x/r_1)^{10}$ are the residual terms after the optimum positions have been assumed. The latter two terms are used to obtain the optimum value of $x/\bar{r} = 21.677\%$ given previously. The effect of the terms involving $\Delta\zeta_1$ is to shift the center of uniformity a distance D where

$$D = - \frac{0.674 \left(\frac{\Delta\zeta_1}{r_1} \right) \frac{1}{r_1}}{2 \left[1.81 \left(\frac{\Delta\zeta_1}{r_1} \right) \frac{1}{r_1^2} \right]} = -0.187 \, r_1 \qquad (18)$$

If the coil which is shifted is to the right of the center of the system, the center of uniformity is shifted to the left of the center of the system by an amount given by (18). Furthermore, if $\Delta\zeta_1$ is positive (the coil is shifted to the right), H increases as the distance from the center of uniformity increases. Similarly, if the coil is shifted to the left, H decreases as the distance increases. The length L of the uniform region is given approximately by

$$L = 2 \sqrt{\left| \frac{a_o \delta}{a_2} \right|} = 2 r_1 \sqrt{\frac{0.554 \delta}{(\Delta\zeta_1 / r_1)}}, \qquad (19)$$

where $\delta = 10^{-5}$ for 0.001% uniformity.

Suppose that $\Delta\zeta_1 = 1/32$ inch and $r_1 = 10$ feet, then $\Delta\zeta_1 / r_1 = 2.6 \times 10^{-4}$, L = 2.92 feet and D = 1.87 feet. Hence, the effect of moving a coil 1/32 inch from its optimum position is to produce a region of uniformity approximately that of a sphere 2.92 feet in diameter, and to shift the center of this sphere approximately 1.87 feet to the left. If the field along the axis of an actual coil system could be measured, it might be possible to determine which coil must be shifted, and how much and in which direction it should be shifted.

CONCLUSIONS

The optimum four-coil solution has been found, while other solutions obtained include those of various earlier investogators. The best six-coil solutions known at this time are also given. The effect of moving one coil out of position in a four-coil system is calculated. This one calculation seems to indicate that the position must be held well within 1/32 inch if 0.001% uniformity in a three-foot sphere is required.

It is recommended that:

1. Additional work on tolerances be done, particularly on moving the coil perpendicular to the system axis and on deforming the coil. Work on the coil-winding depth and breadth would also be useful.

2. The six-coil system solution should be finished.

3. A study should be made of rectangular coil systems, because these might be easier to construct than circular ones.

4. A model of a four-coil system, say five feet in diameter, would be helpful in checking the conclusions, particularly those of the tolerance study.

NOTE: Further work on the calculations of the six-coil system is now under way. The complete manuscript with all computations will be submitted for publication as a Goddard Technical Note.

ACKNOWLEDGMENTS

The authors wish to express their gratitude to the staff of the Test and Evaluation Division, with special thanks to Dr. Elias Klein for his many services, and to the Data Systems Division, in particular to S. M. Rosenthal, for his many patient hours of programming assistance.

BIBLIOGRAPHY

1. L. W. McKeehan, Review of Scientific Instruments, 7, 150-3, 1936.
2. J. C. Maxwell, "A Tretise on Electricity and Magnetism," Vol. 2, pp. 331-8 and 353-9 (1904).
3. M. W. Garrett, Journal of Applied Physics, 22, 1091-1107, 1951.
4. V. L. Williams and J. C. Cain, "Homogeneous Magnetic Fields Produced by Circular Current Loops," unpublished memorandum, Goddard Space Flight Center.
5. G. Fanselau, Zeitschrift fur physik, 54, 260-9, 1929.
6. G. Fansealu, Zeitschrift fur Geophysik, 9, 236-7, 1933.
7. W. Braunbek, Zeitschrift fur Physik, 88, 399-402, 1934.

8. J. R. Barker, Journal of Scientific Instruments, 26, 273-5, 1949.

9. J. R. Barker, Journal of Scientific Instruments, 27, 197-9, 1950.

10. A. Sauter and F. Sauter, Zeitschrift fur Physik, 122, 120-36, 1944.

11. S. M. Rubens, Review of Scientific Instruments, 16, 243-5, 1945.

12. F. W. Warburton, Navord Report 3768, U.S. Naval Ordnance Laboratory, White Oak, Md., June 18, 1955.

13. J. P. Blewett, Journal of Applied Physics, 18, 968-76, 1947.

14. J. W. Clark, Review of Scientific Instruments, 9, 320-2, 1938.

15. M. S. Raff, NOLM 6081, U.S. Naval Ordnance Laboratory, October 18, 1944.

16. F. Neumann, "Vorlesungen uber elektrische Strome," (B. G. Teuber, Leipzig, 1884), from notes by K. Vondermuhl taken in 1864 and 1865.

17. G. G. Scott, Review of Scientific Instruments, 28, 270-3, 1957.

PART VI

RESPONSE OF VEHICLE STRUCTURES TO ACOUSTIC FIELDS

CONTENTS

PART VI

RESPONSE OF VEHICLE STRUCTURES TO ACOUSTIC FIELDS

PRELIMINARY STATEMENT

(Dr. J. E. Greenspon, Contract Consultant)

During certain phases of spacecraft flight, the structure is subjected to intense jet noise and thrust reactions which can cause violent vibrations. The payload can receive vibrations through many paths: Vibrations of the engines can be transmitted directly through the structure to the payload attachment points; also, a certain portion of the acoustic load can be transmitted to the payload through the air. Part of the acoustic energy will excite vibrations of the casing. One aspect of Goddard's program in this field is an attempt to predict the response of the structural shell and the payload when subjected to this intense acoustic environment. Internal pressurization, temperature of the fuel inside, and structural damping of the casing are a few of the factors affecting the response of the shell.

The response of structures to these intense acoustic fields has been studied by a number of investigators. In particular, the writer has developed certain expressions for the response of unstiffened cylindrical shells in terms of the sum of complex frequency-response functions for sinusoidal-loading conditions. These response functions have been extended to cover random loading, and are programmed for the electronic computer. Results of this analysis have been correlated with experiment.

Thus far, only the response of unstiffened shells has been computed; the next logical step is to consider the shell with ring stiffeners. That is the purpose of the present work in the Summer Workshop Program.

EFFECTS OF RESIDUAL STRESS ON THE VIBRATION OF RING-STIFFENED THIN CYLINDRICAL SHELLS

by

D. F. Haskell

ABSTRACT

In this investigation, expressions are presented for the total potential and kinetic energies of one bay of a ring-stiffened, circularly cylindrical, thin shell subjected to internal hydrostatic pressure. A procedure is explained for determination of the natural frequencies and modes of vibration, from the equations of motion which may be formulated by means of Lagrange's equations. In addition, a method is presented which may be used to determine the effect of residual stress upon the vibration characteristics of the system.

The equations presented in this report are general equations which may be employed for analysis of axial excitation of the structure as well as of the radial excitation considered here. An extension of the present theories is required before a comprehensive method can be obtained for theoretical prediction of launch vehicle and satellite response to the various vibration excitations. The response excitation is not yet available. The vibration characteristics of longitudinally stiffened shells should be studied as well as those of cross-stiffened shells. The response of a bulkhead to excitation from various shell configurations, the effect of residual stress on longitudinally and cross-stiffened shells, the response of a satellite to bulkhead- and shroud-vibration inputs, and the response of satellites to various vibrations of solid-fuel launch vehicles are some of the areas that require future study.

INTRODUCTION

A satellite launch vehicle system is a complicated structure. During various stages in its flight, this structure is subjected to severe vibrations which can cause direct physical damage to the system. Two examples of deleterious effects of the vibration environment are malfunction of electronic and mechanical equipment due to induced oscillatory motions, and generation of oscillatory stresses leading to fatigue failure (actual fracture or fretting fracture wear).[1] Such effects can damage both the launch vehicle and the satellite.

The vibration arises from various sources, some of which are combustion oscillations in rocket motors, aerodynamic flutter, and noise from the rocket exhaust. The combustion oscillations in the rocket motor can be transmitted up through the fuel-storage section or casing of the launch vehicle to the satellite in the form of axial vibrations. On the other hand, noise from the exhaust transmitted through the surrounding air can impinge on the external surface of the launch vehicle and satellite shroud in the form of radial vibratory motion.

Of central importance in the test and evaluation of satellites is the development of a theory to enable prediction of satellite response to this external acoustical excitation. Preliminary studies in this area have been conducted by A. Powell,[2] I. Dyer,[3] S. H. Crandall and A. Yildiz,[4] and J. E. Greenspon.[5] Greenspon has presented theoretical analysis of the random excitation of unstiffened cylindrical shells due to jet noise, and has compared the results of his theoretical analysis with experiment. The next step in the development of a theory to predict satellite response to external loading is to consider the random response of stiffened cylindrical shells. Therefore, the present investigation is concerned with the development of a theory to predict vibration characteristics of ring-stiffened, thin cylindrical shells. The energy method used in the analysis is extended to include the effects of residual stresses in the shell which would arise if the stiffened rings were welded to the shell. The latter study may be useful in design because, if the effects of residual stress on the characteristics of the vehicle could be predicted, then stiffened rings could be welded to the shell, rather than chemically milled, which is the present procedure. This would serve to reduce the fabrication costs of the vehicle.

THEORETICAL ANALYSIS

RING-STIFFENED THIN SHELL WITHOUT CONSIDERATION OF RESIDUAL STRESS. For purposes of this analysis, the structure of a launch vehicle is considered to be a multiple-bay, ring-stiffened, thin cylindrical shell which is subjected to internal* hydrostatic pressure. The method used is formulation of the equation of motion of one bay of the system, by means of Lagrange's equations for continuous motions.

The total potential of one bay of the system is taken as the sum of the change in extensional bending, plus the shear-strain energies of the shell, total potential of the finite rigidity stiffening rings, and total work done by external forces acting on the shell. The sum of these expressions, equations (1),** was developed by Nash[6] and is written in terms of displacement components of a point in the middle surface of the shell. The kinetic energy of the system consists of the kinetic energy of the shell and of the stiffening rings. The shell kinetic energy, T_s , is given by equation (2), and the kinetic energy of the stiffening rings, T_{sr} , is given by equation (3); these expressions are also written in terms of

* This presentation will hold either for internal or external pressure. The equations presented in this report are for positive external pressure.

** Equations are given in the Appendices

the displacement of a point in the midsurface of the shell. The elasticity of the stiffening rings is taken into account by assumption of enough terms in the displacement functions, equation (4), to allow the rings to translate, dilate, bend in their plane, and deform in the circumferential direction.

By substitution of the displacement configuration (4) into equations (1), (2), and (3), the general expressions for total potential of one bay, shell kinetic energy, and stiffening-ring kinetic energy—equations (7), (5), and (6) respectively—are obtained in terms of the system constants, generalized coordinates, A, B ---- N, and the time functions U, V, and W. To obtain the equations of motion, equations (5), (6), and (7) must next be substituted into Lagrange's equations (12). The natural frequencies of vibration may then be calculated from the equations of motion by assuming suitable time functions.

RESIDUAL-STRESS CONSIDERATIONS. The previous development may be extended to include the effect of residual stress upon the vibration characteristics, by adding an equivalent residual-strain energy term to the total potential energy expression. To do this, it is assumed that an "equivalent residual-stress load" may be determined. By this procedure may be calculated the external hydrostatic pressure required to produce the same deflection as that which would be caused when stiffeners are welded to a cylindrical shell.

It has been found[7] that a cylindrical shell acquires an initial measurable deflection between stiffening rings where the rings are welded to the shell; if a static external-pressure distribution can be determined which produces the same deflected shape as would the actual residual-stress distribution, then the change in potential due to the actual residual-stress distribution may be replaced by the change in potential due to this "equivalent residual-stress load."

In Appendix B, the static external-pressure distribution and initial displacement configuration are assumed to have the same form as the second-degree curve measured by Lunchick and Short.[8] These distributions are substituted into Flugge's equations of motion,[9] and the "equivalent residual-stress load" is determined in terms of the shell parameters and assumed maximum initial shell deflection—this maximum initial shell deflection may be either assumed or taken from experimental evidence. This calculated "equivalent residual-stress load" (p_o) is then added to the applied hydrostatic stress (p) as a sort of correction factor for residual stress. In this manner, the effect of residual stress is introduced to the change in total potential of the system through the pressure, P. After this is accomplished, the equations for kinetic and total potential energies presented in Appendix A (which excludes the effect of residual stress) may be extended to include the effects of residual stress, by including in the total pressure term, P (which only included the applied hydrostatic pressure, p, in Appendix A), the "equivalent residual-stress load," p_o ; i.e., instead of $P = p$, P is set equal to the sum of p_o and p for the case where residual stress is considered.

REFERENCES

1. Jones, C. D., E. O. Doebelin, L. S. Hau, J. H. Shaw, N. T. Bobrovnififf, E. L. Jasseni, and V. A. Lunardini, "Preliminary Investigation of Interplanetary Lunar and Near Planet Environments and Methods of Simulation," ASD TR 61-267 (July 1961), pp. 146-156.

2. Powell, A., "On the Response of Structures to Random Pressures and to Jet Noise in Particular," Random Vibration, edited by S. H. Crandall, J. Wiley and Sons, Inc. (1958) p. 187.

3. Dyer, D., Ibid., p. 231.

4. Crandall, S. H. and A. Yildiz, "Random Vibration of Beams," ASME paper No. 61-WA-149.

5. Greenspon, J. E., "Random Excitation of Cylindrical Shells Due to Jet Noise," Contract NAS 5-1515, Tech Rep. No. 1, May 1962 (also Addendum July 1962), work sponsored by Goddard Space Flight Center.

6. Nast, W., "Buckling of Multiple-Bay Ring-Reinforced Cylindrical Shells Subject to Hydrostatic Pressure," J. Appl. Mech., 20, 4, 469-474, December 1953.

7. Krenzke, M., David Taylor Model Basin Report No. 1327 (April 1960).

8. Lunchick, M. E., and Short, R. D.,

9. Flugge, W., "Stresses in Shells," Springer Verlag (1960).

ADDITIONAL BIBLIOGRAPHY

VIBRATION AND IMPULSIVE LOADING

Nardo, S. V. and Erickson, B., "Buckling of a Column Under Dynamic Loading in the Inelastic Range," ONR PIBAL Rep. 197 (May 1952).

Fung, Y. C., Sechler, E. E., and Kaplan, A., J. Aero. Sci. V. 24 (1960) pp. 650-660.

Farrow, J. H., Jewell, R. E., and Wilhold, G. A., "Structural Response to the Noise Input of the Saturn Engines," Symposium on Structural Dynamics of High Speed Flight, (April 24-26, 1961) p. 710.

Greenspon, J. E., "Vibrations of Thick and Thin Shells Surrounded by Water," J. G. Engineering Research Associates, Baltimore, Maryland, Contract No. NOnr-2733 (00), Tech. Rep. No. 4, (Sept. 1960).

RESIDUAL STRESS

Huber, A. W., "The Influence of Residual Stress on the Instability of Columns," Ph.D. Dissertation, Lehigh University (1956).

Huber, A. W., and Beedle, L. S., "Residual Stress and the Compressive Strength of Steel," Welding Journal, V. 33, No. 12 (1954).

Yang, C. H., Beedle, L. S., and Johnston, B. G., "Residual Stress and the Yield Strength of Steel Beams," Welding Journal, V. 31, No. 4 (1952).

Ketter, R. L., "The Influence of Residual Stress on the Strength of Structural Members," Proceedings, Seventh Technical Session, Column Research Council (1957).

Anderson, R. J., and Tahlman, E. G., "A Method for Measuring Internal Stresses in Brass Tubes," Inst. Metlr. J. V. 32 (1924) pp. 367-383 (1925) pp. 271-300.

Landau, H. G. and Weiner, J. H., "Transient and Residual Stresses in Heat-Treated Plates," J. App. Mech., V. 25, No. 4 (Dec. 1958) pp. 459-465.

Weiner, J. H. and Huddleston, J. V., "Transient and Residual Stresses in Heat-Treated Cylinders," ASME Trans., V. 81E (J. App. Mech.), 1, March 1959, p. 31-39.

Krenzke, M. A., "Effect of Initial Deflections and Residual Welding Stresses on Elastic Behavior and Collapse Pressure of Stiffened Cylinders Subjected to External Hydrostatic Pressure," DTMB Rep. 1327 (Apr. 1960).

BUCKLING

Lunchick, M. E., and Overby, J. A., "An Experimental Investigation of the Yield Strength of a Machined Ring-Stiffened Cylindrical Shell (model BR-7M) Under Hydrostatic Pressure," David W. Taylor Model Basin Report No. 1255 (Nov. 1958).

Lunchick, M. E., "Plastic Axisymmetric Buckling of Ring-Stiffened Cylindrical Shells Fabricated from Strain-Hardening Materials and Subjected to External Hydrostatic Pressure," DTMB Rep. 1393 (Jan. 1961).

Lunchick, M. E., "Graphical Methods for Determining the Plastic Shell-Buckling Pressures of Ring-Stiffened Cylinders Subjected to External Hydrostatic Pressure," DTMB Rep. 1437 (Mar. 1961).

Bijlaard, P. P. "Buckling Under External Pressure of Cylindrical Shells Evenly Stiffened by Rings Only," J. Aero. Sci. V. 24, No. 6 (June 1957), pp. 436-447.

Slankard, R. C., "Tests of the Elastic Stability of a Ring-Stiffened Cylindrical Shell, Model BR-4, Subjected to Hydrostatic Pressure," DTMB Rep. 876 (Feb. 1955).

Hoff, N. J., "Buckling of Thin Shells," AFOSR TN 61-1422 (Stanford Univ., Dept. of Aero. Engng. Rep. 114), August 1961.

Johnson, E. E., "Pressure Tank and Instrumentation Facilities for Studying the Strength of Vessels Subjected to External Hydrostatic Loading," DTMB Rep. 979 (Apr. 1956).

Van Sauden, K. and Gunther, K., "The Strength of Cylindrical Shells, Stiffened by Frames and Bulkheads, Under Uniform External Pressure on all Sides," DTMB Translation 38 (Mar. 1952).

Keefe, R. F. and Overby, J. A., "An Experimental Investigation of Effect of End Conditions on Strength of Stiffened Cylindrical Shells," DTMB Rep. (1326) (1959).

Paul, B., "Carrying Capacity of Elastic-Plastic Shells With Various End Conditions Under Hudrostatic Compression," Polytechnic Institute of Brooklyn, Aeronautical Lab. Rep. 420 (Apr. 1958).

Galletly, G. D. and Bart, R., J. App. Mech. Trans. ASME, V. 78 (1956) pp. 351-358.

Tinoshenko, S., "The Theory of Plates and Shells," McGraw Hill Book Company, Inc. (1940).

Gerard, G., "Elastic Stability of Orthotropic Shells," J. Aerospace Sci. (1960).

Hoff, N. J., and Vincenti, W. G., "Aeronautics and Astronautics," (Chapter on Nonlinear Buckling of Thin Shells), Pergamon Press, Inc., New York (1960).

Battdorf, S. B., "A Simplified Method of Elastic-Stability Analysis for Thin Cylindrical Shells. II - Modified Equilibrium Equation," NACA TN 1342 (1947).

Tsien, Hsue-Shen, "A Theory for the Buckling of Thin Shells," J. Aero. Sci., V. 9, No. 10, (August 1942) pp. 373-384.

Sauders, J. L., Jr., "Nonlinear Theories for Thin Shells," Harvard Univ. Div. Engng. and App. Phys. Tech Rep. 10 (Feb. 1961).

APPENDIX A

KINETIC AND TOTAL POTENTIAL ENERGY EXPRESSIONS

The total potential of one bay of the system, which includes elastic extension, bending, and shear strain energies, work done by the external load and the ring strain energy, may takes the form

$$U_T = K_1 \int_0^{2\pi R} \int_0^L \left[\left(\frac{\partial u}{\partial x}\right)^2 + \left(\frac{\partial v}{\partial s}\right)^2 + \left(\frac{\omega}{R}\right)^2 + 2\nu \frac{\partial u}{\partial x}\frac{\partial v}{\partial s} - \frac{2}{R}\frac{\partial v}{\partial s}\omega \right] dxds$$

$$+ K_2 \int_0^{2\pi R} \int_0^L \left[\left(\frac{\partial^2 \omega}{\partial x^2}\right)^2 + \left(\frac{\partial^2 \omega}{\partial s^2}\right)^2 + 2\nu \frac{\partial^2 \omega}{\partial x^2}\frac{\partial^2 \omega}{\partial s^2} + 2(1-\nu)\left(\frac{\partial^2 \omega}{\partial x \partial s}\right)^2 \right.$$

$$\left. + \left(\frac{\omega}{R^2}\right)^2 + \frac{2}{R^2}\frac{\partial^2 \omega}{\partial s^2}\omega \right] dxds$$

$$+ K_3 \int_0^{2\pi R} \int_0^L \left(\frac{\partial u}{\partial s} + \frac{\partial v}{\partial x}\right)^2 dxds$$

$$+ PR \int_0^{2\pi R} \int_0^L \left[-\frac{1}{2}\left(\frac{\partial \omega}{\partial s}\right)^2 + \frac{1}{2}\left(\frac{\omega}{R}\right)^2 - \frac{\partial u}{\partial x}\frac{\omega}{R} - \frac{1}{4}\left(\frac{\partial \omega}{\partial x}\right)^2 \right] dxds$$

$$+ \frac{bh_o E}{2} \int_0^{2\pi R_1} \left[\left(\frac{\partial v}{\partial s}\frac{R_1}{R}\right)^2 + \left(\frac{\omega}{R_1}\right)^2 - \frac{2}{R}\frac{\partial v}{\partial s}\omega \right]_{x=0} ds$$

$$+ PbR_1 \int_0^{2\pi R_1} \frac{1}{2}\left(\frac{\omega}{R_1}\right)_{x=0}^2 ds + \frac{EI_{zo}}{2} \int_0^{2\pi R_1} \left(\frac{\partial^2 u}{\partial s^2}\right)_{x=0}^2 ds. \qquad (1)$$

The kinetic energy of the shell, T_s, and of the stiffening rings, T_{SR}, may be given by

$$T_S = \frac{\rho t}{2} \int_0^{2\pi R} \int_0^{L} (\dot{u}^2 + \dot{v}^2 + \dot{\omega}^2)\, dx\, ds \tag{2}$$

and

$$T_{SR} = \frac{b(h_o - t)\rho}{2} \int_0^{2\pi R_2} (\dot{u}^2 + \dot{v}^2 + \dot{\omega}^2)_{x=0}\, ds. \tag{3}$$

The displacements during vibration to be used in these kinetic energy and total potential expressions are taken as

$$\begin{cases} u = \left[A \sin\frac{ms}{R} \sin 2\delta x + B \sin\frac{ms}{R} \cos \delta x + C \cos\frac{ms}{R} \sin 2\delta x + D \cos\frac{ms}{R} \cos \delta x + F\frac{x}{L}\right]U \\ v = \left[\sin\frac{ms}{R} (G + H \sin 2\delta x + J \cos 2\delta x)\right]V \\ \omega = \left[\left(K \sin\frac{ms}{R} + M \cos\frac{ms}{R}\right) (1 - \cos 2\delta x) + N\right]W. \end{cases} \tag{4}$$

After the displacement configuration (4) is substituted into equations (2), (3), and (1), the shell kinetic energy, ring kinetic energy, and total potential of one bay of the system take the following forms:

$$T_S = K_4 (k_{10} \dot{U}^2 + k_{11} \dot{V}^2 + k_{12} \dot{W}^2), \tag{5}$$

$$T_{SR} = K_5 (k_{13} \dot{U}^2 + k_{14} \dot{V}^2 + k_{15} \dot{W}^2), \tag{6}$$

$$U_T = [(k_{16} + k_{17} + k_{18})U^2 + (k_{19} + k_{20} + k_{21})V^2 + (k_{34} + Pk_{35})W^2] + [(k_{36} + k_{37})\, UV + (k_{38} - k_{39})VW + (k_{40} + Pk_{41})WU], \tag{7}$$

where

$$K_4 = \pi K L \rho t \qquad K_5 = \frac{\pi}{2} \rho b R (h_o - t)$$

$$k_{34} = (k_{22} + k_{23} + k_{24} + k_{25} + k_{26} + k_{27} - k_{28} + k_{32})$$

$$k_{35} = (-k_{29} + k_{30} - k_{31} + k_{33})$$

$$k_{10} = \frac{1}{12}(3A^2 + 3B^2 + 3C^2 + 3D^2 + 4F^2) + \frac{2}{3n\pi}(1 - \cos n\pi)(AB + CD)$$

$$k_{11} = \frac{1}{4}(G^2 + J^2)$$

$$k_{12} = (3K^2 + 2M^2 + 4N^2)$$

$$k_{13} = B^2 + 2D^2$$

$$k_{14} = (G + J)^2$$

$$k_{15} = 2N^2$$

$$k_{16} = \frac{\pi}{6}\frac{RK_1}{L}\left[3n^2\pi^2(4A^2 + B^2 + 4C^2 + D^2) + 4n\pi(2 + \cos 3n\pi - 3\cos n\pi)(AB + CD) + 12F^2\right]$$

$$k_{17} = \frac{m^2\pi LK_3}{2R}\left[A^2 + B^2 + C^2 + D^2 + \frac{4}{3n\pi}(1 - \cos n\pi)AB\right]$$

$$k_{18} = \frac{EI_{zo}}{2}\left(\frac{m}{R}\right)^4\left[\pi R_1(B^2 + D^2) + \frac{R}{2m}\left(1 - \cos\frac{4m\pi R_1}{R}\right)BD\right]$$

$$k_{19} = \frac{m^2\pi LK_1}{2R}\left[2G^2 + H^2 + J^2\right]$$

$$k_{20}\frac{2n^2\pi^3 RK_3}{L}\left[H^2 + J^2\right]$$

$$k_{21} = \frac{mbh_oER_1^2}{2R^3}\left(\frac{m\pi R_1}{R} + \frac{1}{4}\sin\frac{4m\pi R_1}{R}\right)\left[G + J\right]^2$$

$$k_{22} = \frac{2\pi LK_1}{R}\left[3K^2 + 4N^2 + 2M^2\right]$$

$$k_{23} = \frac{8n^4\pi^5 RK_2}{L^3} [K^2 + KM + M^2]$$

$$k_{24} = \frac{3m^4\pi LK_2}{2R^3} [K^2 + M^2]$$

$$k_{25} = \frac{4m^2n^2\pi^3\nu K_2}{RL} [K^2 + M^2]$$

$$k_{26} = \frac{2m^2n^2\pi^3(1-\nu)K_2}{LR} [K^2 - KM + M^2]$$

$$k_{27} = \frac{2\pi LK_2}{R^3} [3K^2 + 4N^2 + 2M^2]$$

$$k_{28} = \frac{3m^2L\pi K_2}{R^3} [K^2 + M^2]$$

$$k_{29} = \frac{3m^2\pi L}{4} [K^2 + M^2]$$

$$k_{30} = \pi L [3K^2 + 4N^2 + 2M^2]$$

$$k_{31} = \frac{n^2\pi^2R^2}{2L} [K^2 + M^2]$$

$$k_{32} = \frac{\pi bh_oE}{R_1} [N^2]$$

$$k_{33} = \pi b [N^2]$$

$$k_{36} = 2m\pi\nu K_1 [(\pi n) CJ - (1 - \cos n\pi) DG + 6(2 + \cos 3\pi n - 3 \cos n\pi) DJ]$$

$$k_{37} = 2mn\pi^2K_3 \left[JC + \frac{2}{3n\pi}(1 - \cos n\pi) DJ\right]$$

$$k_{38} = \frac{4m\pi LK_1}{R} \left[JM - 2GM\right]$$

$$k_{39} = \frac{bh_o E}{R} \sin\left(\frac{2m\pi R_1}{R}\right) \left[N(G + J)\right]$$

$$k_{40} = \frac{4\pi\nu K_1}{3} \left[3n\pi AK + 6n\pi CM + (1 - \cos n\pi)\,BK + (1 - \cos n\pi)\,DM\right]$$

$$k_{41} = 6\pi R \left[3n\pi AK + 6n\pi CM + (1 - \cos n\pi)\,(BK + DM)\right],$$

and

$$k_{34} = \frac{2\pi L}{R} \left(K_1 + \frac{K_2}{R^2}\right) \left[3K^2 + 4N^2 + 2M^2\right]$$

$$+ \frac{m^2\pi K_2}{2R^3 L} \left(3m^2L^2 + 8n^2\pi^2\nu R^2 - 6L^2\right) \left[K^2 + M^2\right]$$

$$+ k_{23} + k_{26} + k_{32}.$$

APPENDIX B

DETERMINATION OF THE EQUIVALENT RESIDUAL-STRESS LOAD

The displacement configuration caused by residual stress and external pressure distribution is assumed to be of the form

$$\omega = \frac{4\Delta}{L}\left(x - \frac{x^2}{L}\right) \tag{8}$$

$$P_i = -\frac{4P_o}{L}\left(x - \frac{x^2}{L}\right), \tag{9}$$

and are to be substituted into Flugge's equations of motion, (5) which are

$$\begin{cases} a^2\dfrac{\partial^2 u}{\partial x^2} + \left(\dfrac{1-\nu}{2}\right)\dfrac{\partial^2 u}{\partial \phi^2} + \left(\dfrac{1+\nu}{2}\right)a\dfrac{\partial^2 v}{\partial x \partial \phi} + a\nu\dfrac{\partial \omega}{\partial x} \\ \qquad + k\left[\dfrac{1-\nu}{2}\dfrac{\partial^2 u}{\partial \phi^2} - a^3\dfrac{\partial^3 \omega}{\partial x^3} + \dfrac{1-\nu}{2}a\dfrac{\partial^3 \omega}{\partial x \partial \phi^2}\right] = -\dfrac{P_x a^2}{S} \\ \dfrac{1+\nu}{2}a\dfrac{\partial^2 u}{\partial x \partial \phi} + \dfrac{\partial^2 v}{\partial \phi^2} + \dfrac{1-\nu}{2}a^2\dfrac{\partial^2 v}{\partial x^2} + \dfrac{\partial \omega}{\partial \phi} \\ \qquad + k\left[\dfrac{3}{2}(1-\nu)a^2\dfrac{\partial^2 v}{\partial x^2} - \left(\dfrac{3-\nu}{2}\right)a^2\dfrac{\partial^3 \omega}{\partial x^2 \partial \phi}\right] = -\dfrac{P_\phi a^2}{S} \\ \nu a\dfrac{\partial u}{\partial x} + \dfrac{\partial v}{\partial \phi} + \omega + k\left[\dfrac{1-\nu}{2}a\dfrac{\partial^3 u}{\partial x \partial \phi^2} - a^3\dfrac{\partial^3 u}{\partial x^3} - \dfrac{3-\nu}{2}a^2\dfrac{\partial^3 v}{\partial x^2 \partial \phi}\right. \\ \qquad \left. + a^4\dfrac{\partial^4 \omega}{\partial x^4} + 2a^2\dfrac{\partial^4 \omega}{\partial x^2 \partial \phi^2} + \dfrac{\partial^4 \omega}{\partial \phi^4} + 2\dfrac{\partial^2 \omega}{\partial \phi^2} + \omega\right] = -\dfrac{P_r a^2}{S}, \end{cases} \tag{10}$$

where

$$k = \frac{t^2}{12a^2}$$

$$S = \frac{Et}{(1 - \nu^2)} .$$

If the maximum deflection caused by residual stress is written in terms of a fraction, n, of the shell radius

$$\Delta = \eta a$$

and it is assumed that

$$Px = P\phi = 0$$

$$Pr = Pi ,$$

then, after substitution of (8) and (9) into Flugge's equations (10), it is found that the "equivalent residual-stress load" is given by

$$Po = \left[\frac{Et(12a^2 + t^2)}{12a^3(1 - \nu^2)}\right]\eta . \qquad (11)$$

As indicated, this "equivalent residual-stress load" is a direct function of the magnitude of the residual stress, which is represented by the factor n.

APPENDIX C

EQUATIONS OF MOTION FOR RING-STIFFENED THIN SHELLS

The equations of motion for the ring-stiffened thin shell, with or without the consideration of residual stress, are formulated by means of Lagrange's equation of motion:

$$\frac{d}{dt}\left(\frac{\partial T}{\partial \dot{q}_i}\right) - \frac{\partial T}{\partial q_i} + \frac{\partial U}{\partial q_i} = Q_i, \quad (i = 1, 2, 3 \ldots), \tag{12}$$

where q_i are the generalized coordinates and Q_i are the generalized forces. The sum of the kinetic energy terms, equations (5) and (6), and the total potential energy, (7), are substituted into (12), and the number of equations obtained is equal to the number of generalized coordinates used in the kinetic-energy and potential-energy expressions. To determine the natural frequencies of motion, Q_i is set equal to zero.

For those cases in which the effect of residual stress is to be considered, the external pressure, P, is set equal to the sum of the "equivalent residual-stress load" and the actual applied hydrostatic pressure:

$$P = p_o + p.$$

For those cases in which residual stress is not a factor, the external pressure term is only equal to the actual applied pressure:

$$P = p.$$

PART VII

RELATING DAMAGE AND RELIABILITY TO ENVIROMENTAL DATA

CONTENTS

ILLUSTRATIONS

TABLE

PART VII

RELATING DAMAGE AND RELIABILITY TO ENVIRONMENTAL DATA

PRELIMINARY STATEMENT

(R. E. Dorrell, Quality Assurance Branch, Test and Evaluation Division, GSFC)

The environmental effects on systems elements, be they minimal or extreme, may cause severe damage, resulting in catastrophic failure to the entire spacecraft system. This is the type of "hard-nosed" problem which Goddard is facing and which Goddard must solve. The Quality Assurance Branch is responsible for making sure that, for every ground and spacecraft application, the proper material is used and that this material is used properly. Two recent occurrences will illustrate some of the problems that the Quality Assurance Branch encounters.

The first will exemplify the case of minimal environment and maximum damage. A failure was reported involving the IN 461 and IN 252 diodes made by the Sylvania Electric Company. The first indication of failure was a complaint that several of the diodes broke apart as their leads were straightened out upon being taken from the card in which they were shipped. Also, when they were put on printed circuit boards or otherwise soldered in place, a good many open diodes were encountered.

In order to determine just what was causing these failures, the opaque coating covering the diode to prevent any penetration of light photons was removed with a chemical. The first thing noticed was that, as soon as the leads were straightened out, failure of the glass resulted. This was no doubt due to a lack of annealing of the glass. During manufacture, although the semiconductor wafer itself must be kept relatively cool, the glass should be hot in order to provide a good seal. If the glass were not annealed, failure due to cracking of the glass would and evidently did result. Next, as soon as the diodes were put in circuits and cutting pliers were used to trim off the leads, open diodes resulted. Apparently the slightest of mechanical shocks, such as the action of cutting the lead wires, was sufficient to open-circuit the diode. Finally, the diode was examined under a microscope. To briefly describe the construction, an aluminum rod is pressed against the silicon wafer, heat is applied, the aluminum rod is cut off, and a pressure contact made with an S-shaped ribbon. However, under a microscope, the contact appeared to be almost completely severed, a factor which again might easily have led to failure.

The ideal method of relating all this to environmental parameters would be a vibration or shock test to determine whether or not failures of this type are present. However, when these poorly constructed diodes were placed in competition with others superior in design, on the same vibration test, they showed up every bit as well. In this vibration test, the forward characteristic was measured first; then the vibration test was conducted; then the forward characteristic was measured again–the two coincided very well. However, if this diode were used in a compter, any transient that the diode generated would give false indication or false signals. To perform a valid test, therefore, a current is passed through the diode and the forward current characteristic is displayed on an oscillograph; a vibration test is then conducted, and any discontinuities in this curve indicate a poor diode.

This was a case involving minimal environment because the diodes were not mistreated at all. Now, we shall discuss a problem in which the environment is more extreme. It is this problem toward which the Summer Workshop people will be contributing.

While the UK-1 satellite was being tested, particularly in thermal vacuum, a problem arose concerning a transistor used in a regulator circuit to govern the amount of energy put into the battery from the solar paddles. The regulator circuit consisted of a detector and power transistor, the transistor being used solely to dissipate excess power from the solar paddles. The system worked well in room temperature, but in thermal vacuum the transistor junction and case temperatures rose tremendously and the transistor eventually failed due to "thermal runaway." The transistor was rated for 50 watts while on a heat sink, yet it was only handling a maximum of 5 watts for this application, so the question arose of why this thermal runaway occurred.

The transistor without a heat sink was rated for only 3 watts, so one of the first things to be looked into was the matter of heat sinking. A power transistor generally is constructed by mounting the wafer on top of a stud or to the header that forms the base or lower end of the case. Now, the energy to be dissipated in the form of heat must be conducted away from the stud at the bottom to a metallic sheet or heat sink. However, it is very inconvenient to electrically connect the transistor collector power supply to the spacecraft ground or the frame. Therefore, an electrical insulator must be interposed between the transistor base and the heat sink, but must nevertheless provide a good heat-conductive path between transistor and heat sink. The interposed material takes the form of a washer, made of beryllium oxide or aluminum oxide or some other material which has high electrical resistance combined with high thermal conductivity.

Now, while the regulator was working in air, apparently there was enough convective cooling to alleviate the difficulty. However, since no convection is possible in a vacuum, the system must depend on cooling by conduction to the heat sink. The difficulty here, and probably the source of the problem, is the number of interfaces through which the heat must go to be conducted away from the transistor: first, between the wafer and the

stud; then between stud and can; another between can and washer; and another between washer and heat sink. Each interface contributes a certain resistance to heat flow, so that the sum of all the interface resistances may be sufficient to reduce heat dissipation to a dangerously low level.

One possible solution, tried by some transistor manufacturers, is to electrically insulate the transistor with a beryllium oxide or aluminum oxide tab placed inside the transistor case. This would help the situation by removing the necessity for so many external interfaces. However, this unit must undergo vibration exposure and thermal analysis before its effectiveness can be determined.

In summary, I think we have pointed out the area where we hope that the Summer Workshop will be able to give us some assistance. We are looking forward to seeing what can be evolved.

HEAT-SINKING TECHNIQUES FOR POWER TRANSISTORS IN A SPACE ENVIROMENT

by

J. John and J. Hilliard

ABSTRACT

An investigation was made of the cooling of power transistors in a space environment, where the only available mode of heat transfer is that of conduction to a heat sink and radiation from the heat sink to space. An attempt was made to minimize the thermal resistance between transistor case and heat sink, allowing the transistor to dissipate as much power as possible while maintaining its temperature within the maximum tolerable level to prevent thermal runaway. Further, it was necessary to electrically insulate the transistor from the heat sink. The use of beryllium oxide washers provided electrical insulation, while adding very little to the thermal resistance between case and sink, the BeO being a good heat conductor. However, the problem of contact thermal resistance at each interface arose, especially in vacuum—this contact resistance providing practically all the thermal resistance between case and sink. The effect on the contact resistance of surface pressure, insertion of foils, and soldering was examined. It was concluded that, for most efficient heat sinking, indium foil should be inserted at each interface, the indium foil having the effect of reducing the contact resistance in vacuum by a factor of 10.

INTRODUCTION

The problem of maintaining the junction temperature of a transistor within certain limits to prevent runaway and failure is well-known. The work performed to date has been concerned with transistor cooling in an atmospheric environment, either by free or forced convection. Typical of the work in this area is that performed by Abel[1] and others.[2] The investigation performed here, however, had the purpose of extending present knowledge to cover transistor cooling in a space environment.

The only mode of heat transfer available in space is radiation, either directly from the transistor or else from a heat sink to which the transistor is thermally coupled. Calculations show that the surface area of the transistor is too small to provide more than a few milliwatts of direct radiative heat dissipation, whereas several watts may have to be dissipated. So, the problem resolves itself into an investigation of the thermal path

between the transistor junction and the heat sink with the goal of making the thermal conductance as high as possible.

Figures 7-1 and 7-2 show how a typical power transistor is mounted on a heat sink. Two thermal paths are available: one from the case, through the top washer to the heat sink; and another from the case, through the stud and nut, through the bottom washer and to the sink. Essentially, then, we have the case of thermal resistances in parallel.

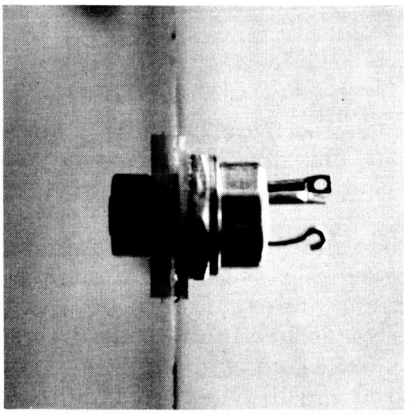

Figure 7-1 - Mounting of 2N1724 Transistor on anodized aluminum heat sink, using two BeO washers

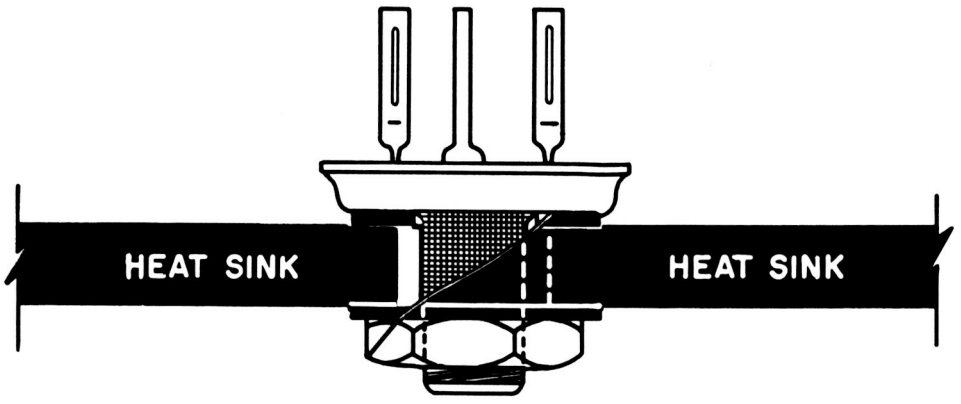

Figure 7-2 - Mounting of a typical pawn transistor, diagram

It is desired that the net thermal resistance be as low as possible. However, it is often necessary that the transistor also be electrically insulated from the sink. This means that some sort of device such as a washer, must be used that will provide good thermal conductivity while serving as an electrical insulator. Further, if washers are to be used, they must have good mechanical properties to resist cracking when the nut on the transistor is tightened during mounting. Materials satisfying these specifications to a greater or lesser degree are beryllium oxide,[3] mica, and aluminum oxide.

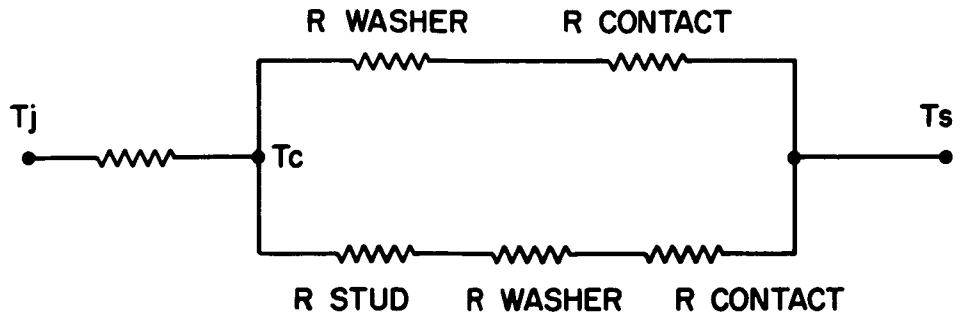

Figure 7-3 - Thermal network

Figure 7-3 is a schematic diagram of the thermal network. It can be seen that all quantities are readily determinable with the exception of contact resistance (the thermal resistance at the interface of two different materials).

Contact resistance is due to improper thermal contact between the two materials. Since no surfaces are perfectly smooth, they only touch at a limited number of points; the remainder of the space being filled with a nonconducting vacuum. Variables affecting the contact resistance would include the pressure between the two surfaces, the smoothness of the surfaces, the materials themselves, and the possible addition of greases, solders, or some soft material to fill the empty regions between the surfaces.

Several theoretical and experimental investigations have been made in the general area of thermal contact resistance. Theoretical considerations must necessarily assume an idealized shape of contact point and a distribution of contact points. An analysis carried out by Fenech and Rohsenow[4] attempted to predict, with some degree of success, the thermal conductance of metallic surfaces in contact. It is felt, however, that an analysis of this type can only be at best a fair approximation, and that experimental values should be determined. Several investigators have worked on the experimental side of the problem.[5,6,7] Their results are not considered applicable to this problem, because their data were obtained in air, not in vacuum; also, their data necessarily depended on the configurations of the surfaces they employed, somewhat different from the ones to be dealt with here.

Tests were run to determine the thermal resistance from transistor case to heat sink as a function of the previously mentioned variables. It was hoped to minimize this thermal resistance so as to provide a practical means of heat sinking in a space environment.

EXPERIMENTAL APPARATUS AND PROCEDURE

In this experiment, the junction temperature, case temperature, sink temperature, and energy dissipated per unit time were measured for each test. Variations in contact resistance were introduced by applying different torques on the transistor nut with a

torque wrench, and by employing various interface materials such as foils and solders. Variation in the smoothness of the surfaces was not undertaken because of the difficulty of measuring and controlling this parameter; in any case, it was felt that this could offer only limited improvement.

Case and sink temperatures were measured with copper-constantan thermocouples and a potentiometer. The thermocouples were fastened to the surfaces with aluminum tape, as shown in Figure 7-4. Two thermocouples were used on the heat sink, one at the base of the transistor and the other at the extreme edge of the heat sink.

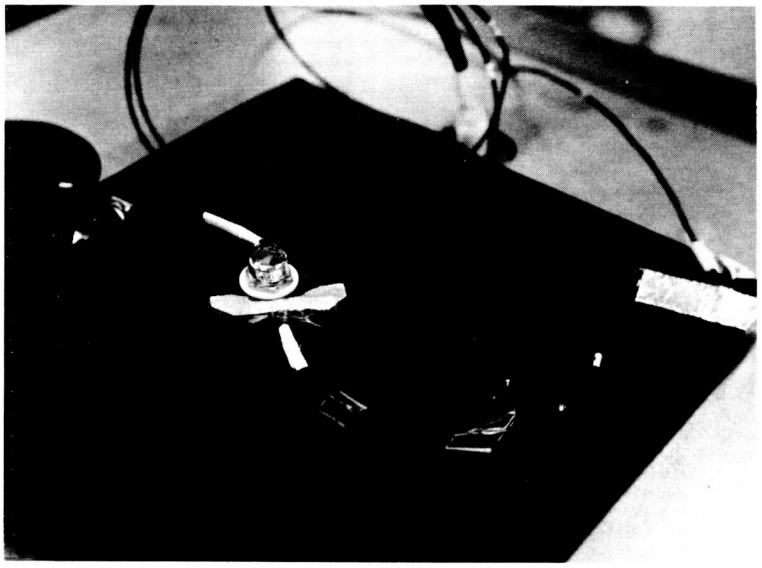

Figure 7-4 - Location of Thermocouples on anodized aluminum heat sink

As the collector junction was inaccessible to a thermocouple, its temperature had to be measured indirectly. Junction temperature (T_j) was determined by measuring the forward voltage drop (V_{CBO}) from collector to base with emitter open, since this voltage is directly dependent on junction temperature. The appendix contains an explanation of the technique employed and a schematic of the circuit used to make this measurement.

Figure 7-1 shows a typical power transistor (2N1724, which was used for all tests) mounted on a $10 \times 10 \times 1/16$-inch black anodized aluminum plate which served as a heat sink. In this configuration, beryllia washers were placed between the transistor case and the plate, and also between the nut and the bottom of the plate. The stud of the transistor was 1/4 in. in diameter and the hole through the plate was 5/16 in. The base of the transistor had a diameter of 3/4 in. All the beryllia washers employed were of the same thickness, 1/16 in.

An environmental pressure of approximately 10^{-5} mm Hg was obtained by the use of a bell-jar vacuum system employing a mechanical fore pump and an oil diffusion pump. In the tests made under both atmospheric and vacuum conditions, the measuring procedure was the same. Power was applied to the transistor from a constant-voltage power supply and all temperatures were allowed to stabilize for approximately 30 minutes. The junction, case, and heat-sink temperatures were then measured, and the temperature difference between the case and sink was calculated. The thermal resistance was obtained by dividing the temperature difference by the input power. The input power was set at several different levels and the procedure was repeated at each level.

RESULTS

Table 7-1 is a compilation of the experimental data obtained in this investigation, both in air and in vacuum.

TABLE 7-1
Experimental Data Obtained in Air and in Vacuum

Configuration	Vac. or Atm.	Torque (in. lb.)	(°C/watt)
2 BeO washers	Vac.	6	4.79
2 BeO washers	Air	6	1.19
2 BeO washers + 3 indium foil	Vac.	6	.61
2 BeO washers + 3 indium foil	Air	6	.50
2 BeO washers + 3 aluminum foil	Vac.	6	1.59
2 BeO washers + 3 aluminum foil	Air	6	.81
2 BeO washers + 3 copper foil	Vac.	6	3.15
2 BeO washers + 3 copper foil	Air	6	1.04
2 BeO metallized washers + 3 indium foil	Vac.	3	.71
2 BeO metallized washers + 3 indium foil	Air	3	.54
2 BeO metallized washers + 3 indium foil	Vac.	6	.66
2 BeO metallized washers + 3 indium foil	Air	6	.50
2 BeO metallized washers + 3 indium foil	Vac.	9	.61
2 BeO metallized washers + 3 indium foil	Air	9	.43
2 BeO metallized washers + 3 indium foil	Vac.	12	.55
2 BeO metallized washers + 3 indium foil	Air	12	.42
2 BeO metallized washers	Vac.	6	4.40
2 BeO metallized washers	Air	6	1.12

Table 7-1 (Continued)

Configuration	Vac. or Atm.	Torque (in. lb.)	(°C/watt)
2 BeO metallized washers + 2 indium foil + transistor soldered to washer (indium solder)	Vac.	6	.49
2 BeO metallized washers + 2 indium foil + transistor soldered to washer (indium solder)	Air	6	.40
Transistor soldered to metallized washer (indium solder), washer soldered to plate; 1 BeO washer + indium foil on bottom	Vac.	6	.56
Transistor soldered to metallized washer (indium solder), washer soldered to plate; 1 BeO washer + indium foil on bottom	Air	6	.43
1 BeO washer + 2 indium foil; stud insulated	Vac.	6	.70
1 BeO washer + 2 indium foil; stud insulated	Air	6	.49
2 BeO washers + 2 indium foil + Apiezon grease on threads	Vac.	6	.57
2 BeO washers + 2 indium foil + Apiezon grease on threads	Air	6	.47
No washers	Vac.	6	5.16
No washers	Air	6	1.36

*Washer dimensions - O.D. - .90"
I. D. - .26"

Early in the program it became apparent that the thermal resistance of the beryllium oxide washer ($R = L/Ak = .02°C/watt$) was much lower than the thermal contact resistances. Hence, instead of testing the effects of different washer materials, it was decided to use beryllium oxide exclusively, since little improvement over it could be expected.

EFFECT OF ENVIRONMENT. Figure 7-5 illustrates the increase in thermal resistance between the transistor case and sink due to the vacuum environment, as compared to the resistance in air. In a vacuum, the only mode of heat flow between the surfaces is conduction through the few discrete contact points; in air, there is also the possibility of heat convection between the surfaces or heat conduction across the narrow air layer. The presence of a vacuum thus tends to amplify the problem of heat sinking.

USE OF FOILS. Figure 7-6 illustrates the effect of using foils along the interfaces of the beryllia washers in a vacuum environment. In each case, a foil washer with the same surface dimensions as the beryllia washer was placed between the transistor case and top washer, between the top washer and the heat sink, and between the bottom washer and heat sink. The graph shows that the use of any of the three interface materials lowered the thermal resistance from case to heat sink. Indium foil, however, proved most

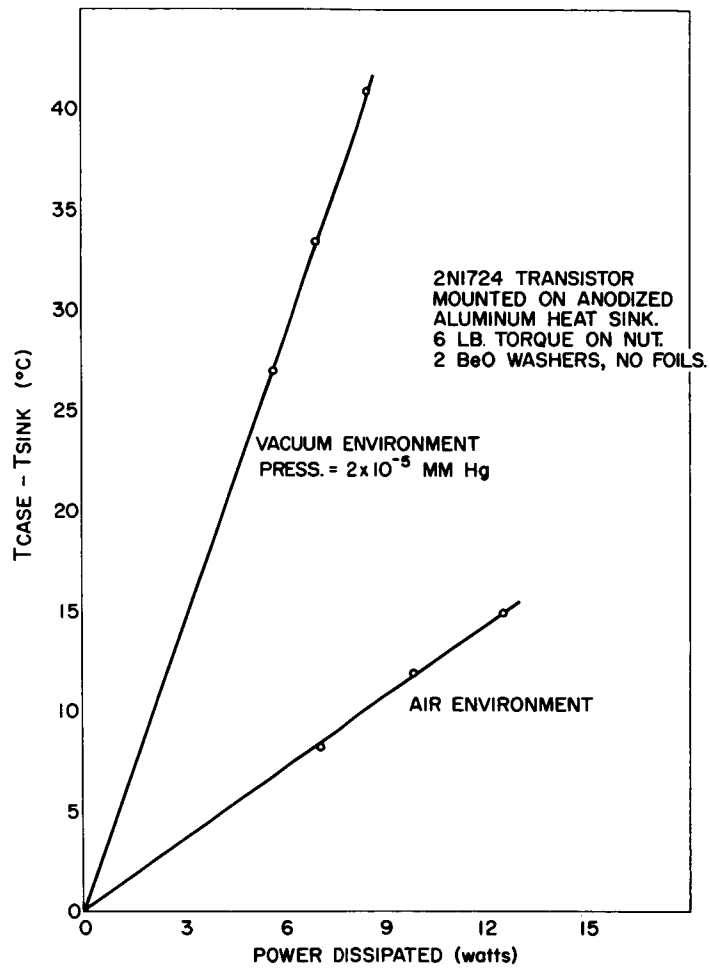

Figure 7-5 - Effect of environment on thermal resistance

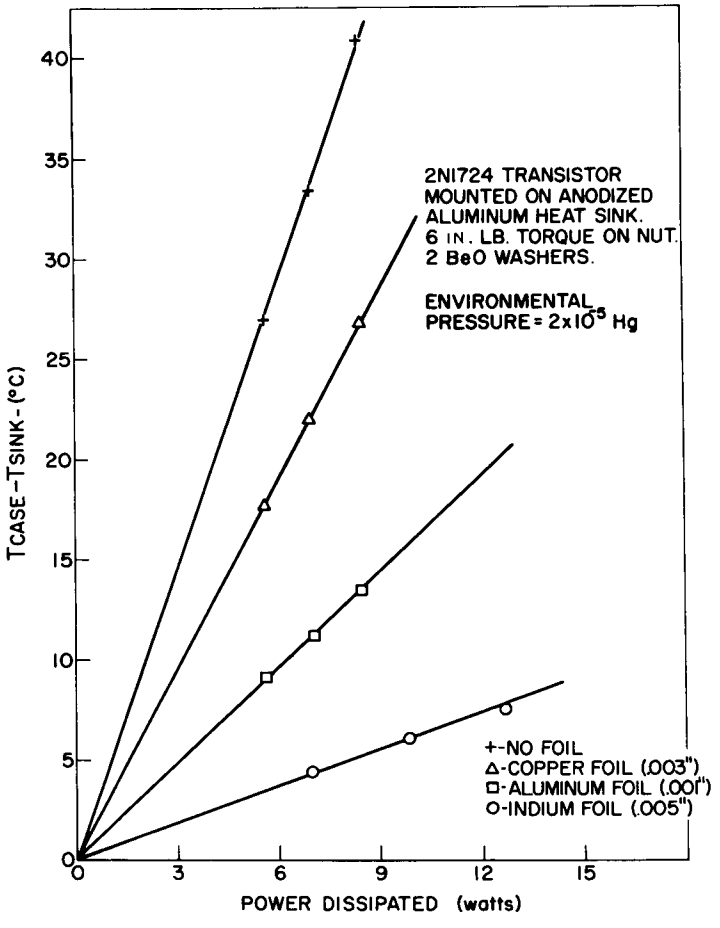

Figure 7-6 - Effect of interface foil on thermal resistance in a vacuum environment

effective, lowering the thermal resistance to .63 °C/watt, approximately 1/8 of its value without interface material.

The effect of the foil is to fill the void between the surfaces with heat-conducting material. The softness of the foil seems very critical in determining its effectiveness. Indium, by far the softest of the foils, in most cases was found to adhere to the contact surfaces due to the penetration of contact points into the foil.

SURFACE PRESSURE. The effect of surface pressure on thermal resistance is shown in Figure 7-7. The transistor was mounted with two beryllia washers and three indium washers as interface material, and torque on the nut was varied from 3 to 12 in. lb. in 3 in. lb. steps. As the graph illustrates, thermal resistance decreases linearly with an increase in surface pressure. Greater pressures probably would result in a still smaller thermal resistance; however, the cracking of the washer limits further tightening of the nut.

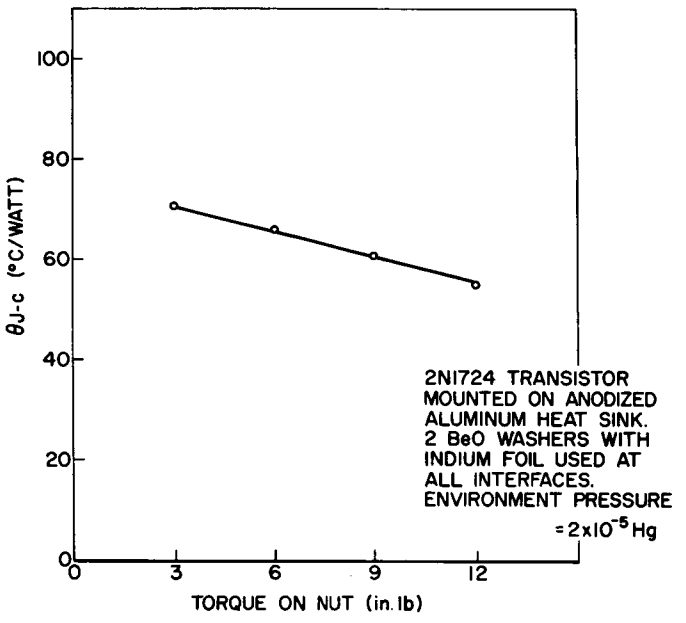

Figure 7-7 - Effect of surface pressure on thermal contact resistance in a vacuum environment

This increase in conductivity is thought to be due to further penetration of the indium into the voids as the surfaces are further compressed.

EFFECT OF SOLDERING ON CONTACT RESISTANCE. One way of reducing thermal contact resistance is to solder the surfaces together, in this case, soldering transistor to washer and then washer to heat sink. As the ceramic washer material cannot be directly soldered, the beryllium oxide must be metallized and then copper- or silver-plated. The metallizing is accomplished by depositing on the washer surface a

molybdenum manganese compound, a process carried out by the National Beryllia Corporation or the Brush Beryllia Company. The first tests made were for the purpose of investigating any change in thermal contact resistance due to the plated washers over those not plated. Using the same configurations, plated and unplated washers gave the same value for contact resistance. Next, the plated washer was soldered to the transistor and also soldered to the aluminum heat sink, the heat sink being nickel-plated to hold the solder more easily. A low-melting-point indium-alloy solder was used on the transistor to avoid any possible damage to it. Results showed that the soldering reduced the thermal resistance to roughly the same level as that achieved using indium foil in the interfaces.

To determine the magnitude of heat conduction through the stud, nut, and bottom washer in relation to that path through the top washer, the stud was insulated with teflon and paper, and conduction was allowed only through the upper path. The change in thermal resistance was so small that the lower path might almost be neglected when using a good conductive configuration such as the indium-beryllia washer method for the upper path. The high resistance of the lower path is thought to be caused mostly by ineffective contact between the screw threads and the nut, and between the nut and beryllia washer. An attempt was made to improve thermal conduction through the lower path by applying a film of Apiezon vacuum grease along the threads and putting indium between the nut and the beryllia washer; however, this made no appreciable change in overall thermal resistance.

Several power transistor manufacturers have attempted to combine the necessary thermal conduction and electrical insulation by insulating the collector from the transistor case internally, as in the 2N1724/I (which is identical to the 2N1724 except for this modification): this transistor therefore may be mounted directly on the heat sink. A test run in vacuum showed that direct contact between the two metal surfaces still gave a high thermal resistance, 5.16 °C/watt. This could be lowered considerably by the addition of indium foil to the interface. However, measurements made with the 2N1724/I transistor showed it to have a thermal resistance from collector junction to case of 1.17 °C/watt, while that of the 2N1724 transistor was .36 °C/watt. If the latter transistor is provided with the indium-beryllia washer method of heat sinking, the total resistance from junction to heat sink is .98 °C/watt, which is less than the junction-to-case resistance alone of the modified 2N1724/I transistor.

CONCLUSIONS

In summarizing, several facts stand out as important in the problem of heat-sinking a power transistor in a space environment. The use of a soft interface foil is highly effective. Indium foil, used as an interface material, reduces interface resistance to almost 1/10 of its normal value, and the ease with which it may be shaped to the required

geometry makes it very desirable. Aluminum and copper foils which offer some reduction in interface resistance, could be used depending on the amount of thermal conductivity desired.

The effect of surface pressure, although critical when no interface material is used, is not of too much importance when indium is employed. At very high pressures, the effect could probably be made appreciable; however, the cracking of the beryllia washers prevents this. It might be noted that the use of indium along the faces of the washers allows a sizeable increase in the amount of torque that may be applied to the transistor nut before the washers crack.

The process of soldering the transistor to the BeO washer and the washer to the heat sink provided effective heat sinking. The indium eutectic solder used between the case and washer proved very satisfactory, not only because of its conductive properties, but also because of its low melting point, which decreases the danger of harming the transistor.

RECOMMENDATIONS

As a result of this investigation, recommendations can be made concerning the most efficient methods of heat-sinking a power transistor in a vacuum. First, the insertion of indium foil at the interface between beryllium oxide washer and heat sink and between the beryllia washer and transistor base is sufficient to reduce the thermal resistance between case and heat sink to a very low level, and thus to aid in maintaining the junction temperature within its maximum permissible value, while the transistor is able to dissipate a fairly large amount of power. The use of indium in space will necessarily depend on its rate of sublimation and consequent deterioration. One reference,[8] however, indicates that, even at a temperature of 400°C, the rate of sublimation of indium in space is only 10^{-5} centimeters per year, which is less that that of lead or zinc, for example. Thus, since the temperature encountered by the indium in this application is less than 100°C, it is felt that sublimation will be no problem.

A second recommended procedure for heat sinking in vacuum is to metallize the BeO washer and to solder the transistor to washer and the washer to the case. This method provided roughly the same thermal resistance from case to sink as the previous method involving indium foil.

The first procedure recommended appears more advantageous, mainly because of its ease in assembly and adaptability. Once the joints have been soldered, it would be impossible to easily remove the transistor from the heat sink. Further, it is felt that the former method gives a more reliable joint, which would better tolerate vibration and shock.

APPENDIX

MEASUREMENT OF THE JUNCTION TEMPERATURES

The transistor junction temperature, T_j, can be determined by measuring electrical parameters of the transistors which are functions of T_j. The parameter used in this experiment was the forward voltage drop, V_{CBO}, from collector to base with emitter open. A schematic of the circuit to make this measurement is included as Figure 7-8 (also see Reference 9).

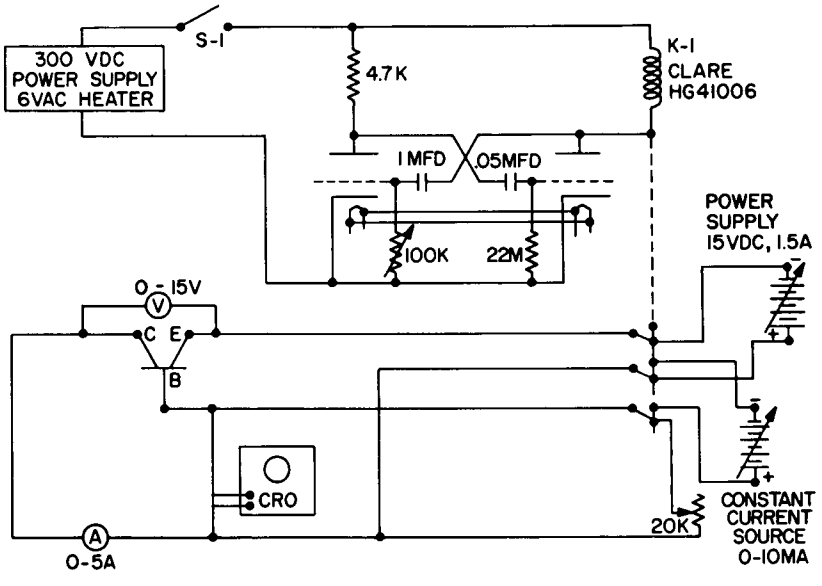

Figure 7-8 - Circuit for measuring heat dissipation and V_{CBO} of a transistor, schematic diagram

To determine the relationship between V_{CBO} and T for each transistor, the transistor, in a nonoperating condition, was placed in an oven and heated to temperatures in the transistor's operating region (between room temperature and 100°C). At each temperature, the transistor was allowed to reach a constant temperature throughout its structure. The switch (S-1 of Figure 7-8) was then closed, causing the relay, D-1, to energize momentarily at set intervals, permitting V_{CBO} to be measured on the oscilloscope and the calibration curve to be plotted (Figure 7-9).

In the actual tests, the transistor was mounted on a metallic plate serving as a heat sink, and placed in a bell jar, which was then evacuated to a vacuum of 10^{-5} mm Hg (Figure 7-10). Electrical connection was provided between the transistor and the circuit of

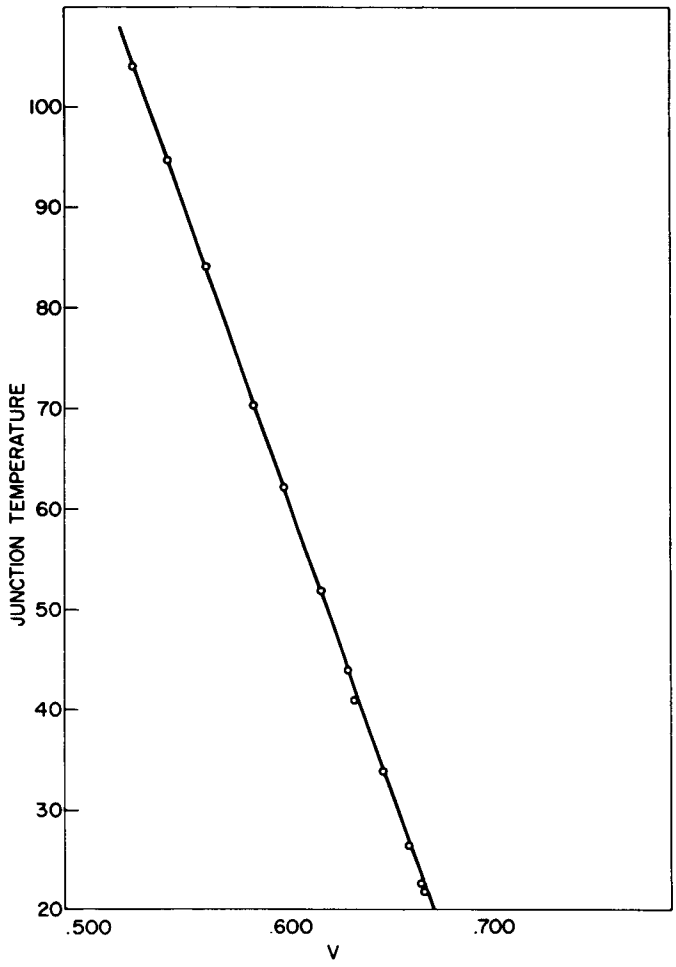

Figure 7-9 - Junction temperature vs V_{CBO}, 2N1724 transistor

Figure 7-3. Power into the transistor was varied by means of the rheostat in the base lead of the transistor; the emitter-to-collector voltage, V_{EC}, was kept constant at 14 volts while the emitter current, I_E, was varied. At each power level, the transistor temperature was allowed to stabilize, assuming that the input power would be equal to the heat dissipated per unit time. For each configuration of heat sinking, three or four different power levels were used. Switch S-1 was then closed causing the multivibrator to be activated; subsequently, power was switched from the power circuit to the V_{CBO} measuring circuit and back. The transistor remained in an operating condition for intervals of 2.25 seconds and was in the measuring circuit for 100 milliseconds. Since the switching time was in the order of 2 milliseconds, it was possible to read V_{CBO} before the junction temperature had decreased from its operating value. V_{CBO} was then measured, converted to degrees centigrade, and recorded.

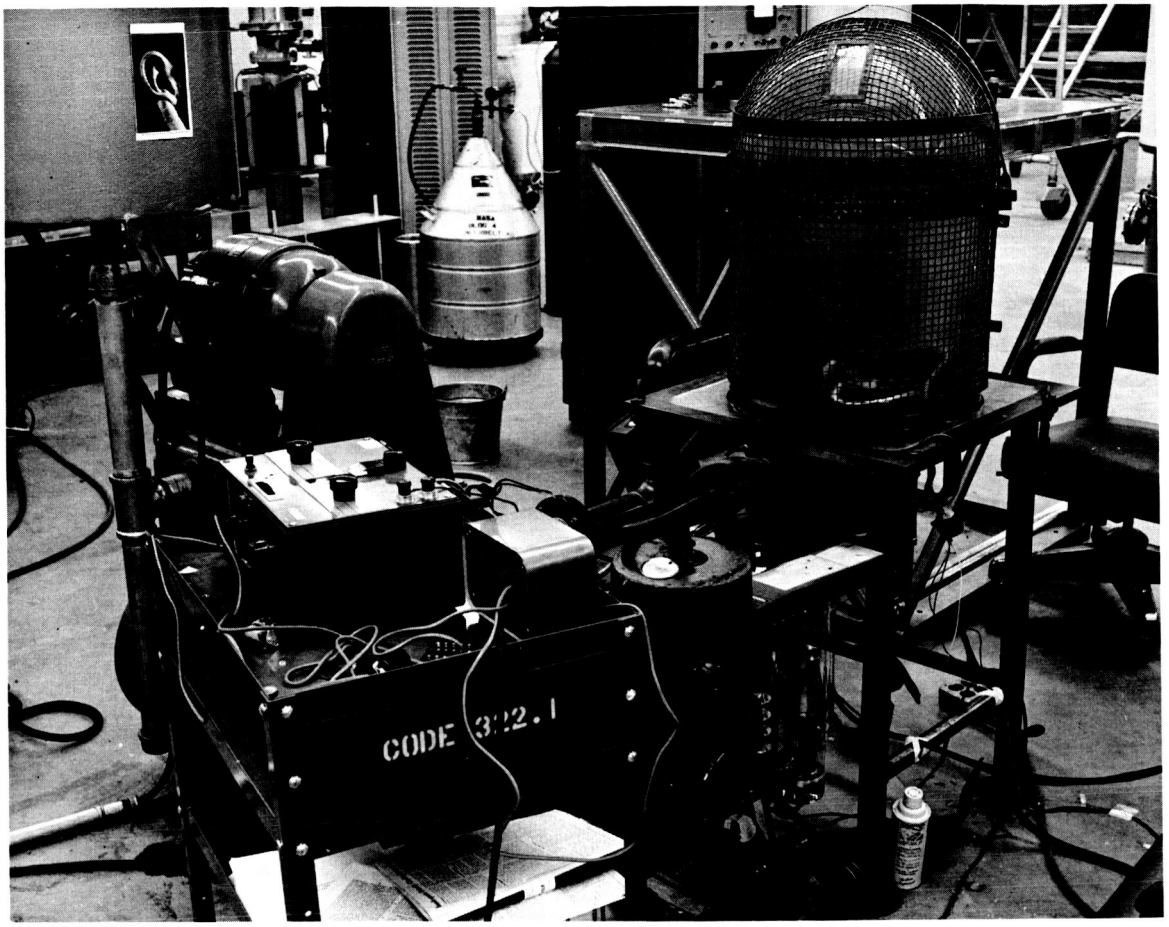

Figure 7-10 - Experimental equipment for measurement of junction temperatures

REFERENCES

1. Abel, A. D., "Power Transistor Cooling," Honeywell, Semiconductor Products Division, Applications Lab Report ALR-3, March 1961.

2. Tung-Sol Electric Inc., Semiconductor Division, Application Note 2-62, July 1962.

3. McPhee, K. H., "Cooling Transistors with Beryllia Heat Sinks," Electronics, May 5, 1961.

4. Fenech, H., and Rohsenow, W. M., "Prediction of Thermal Conductance of Metallic Surfaces in Contact," ASME-AIChE Heat Transfer Conference and Exhibit, Houston, Texas, August 5-8, 1962, ASME Paper No. 62-HT-32.

5. Weills, N. D., and Ryder, E. A., "Thermal Resistance Measurements of Joints Formed Between Stationary Metal Surfaces," ASME, Vol. 71, April 1949.

6. Barzelay, M. E., Tong, K. N., and Holloway, G. F., "Thermal Conductance of Contacts in Aircraft Joints," NACA TN 3167, March 1954.

7. Barzelay, M. E., Tong, K. N., and Holloway, G. F., "Effect of Pressure on Thermal Conductance of Contact Joints," NACA TN 3295, May 1955.

8. Jaffe, L. D., and Rittenhouse, J. B., "Evaporation Effects on Materials in Space," JPL Technical Report No. 32-161, Caltech, October 1961.

9. Laffin, J. P., "Evaluation of IERC - U-P Type Transistor Heat Dissipators," IERC Test Report No. 172A, July 1961.